ACT and Simons Observatory

Thibaut Louis

- 3 dichroic detector arrays for DR6: PA4, PA5 and PA6
- 3750 working detectors (70% yield) at 100 mK
- 3 broad bands: f090 (77 – 112 GHz),
  f150 (124 – 172 GHz) and f220 (182 – 277 GHz)
- Combined sensitivity of 6.2 μK√s,
  and 1.4’ FWHM @ f150

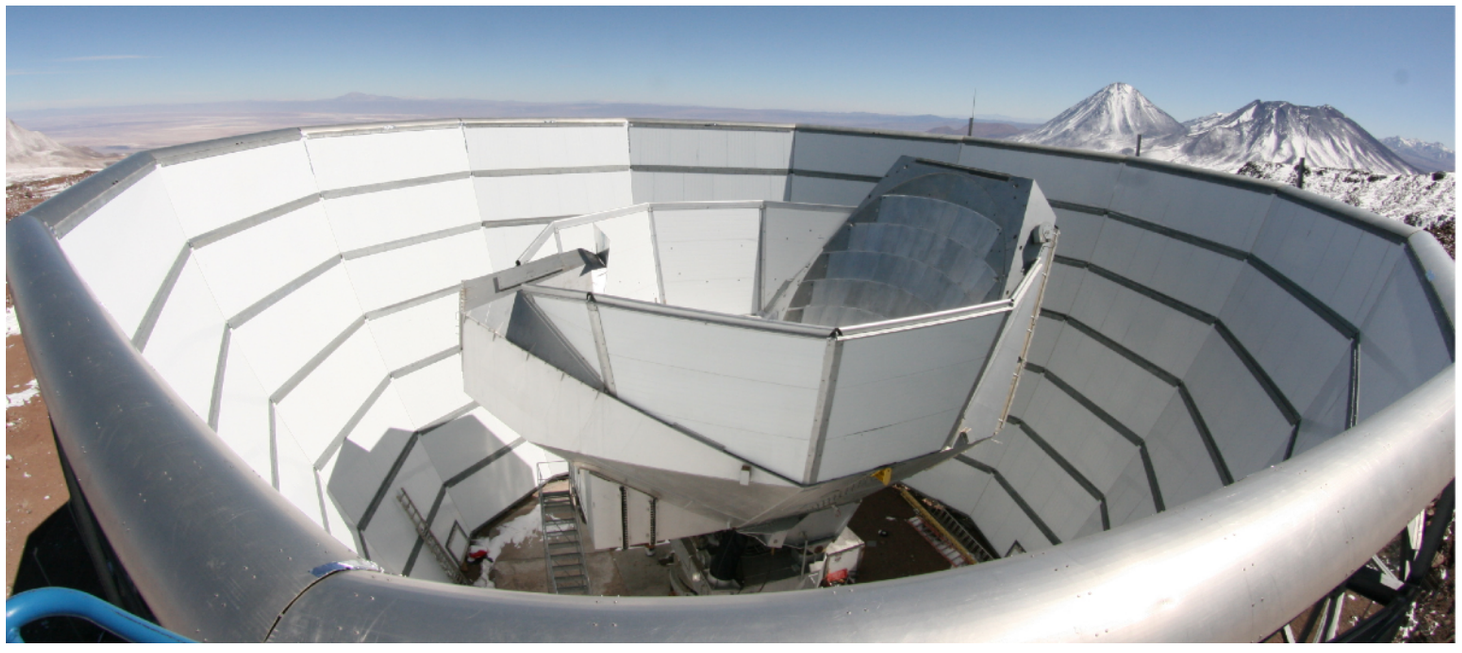

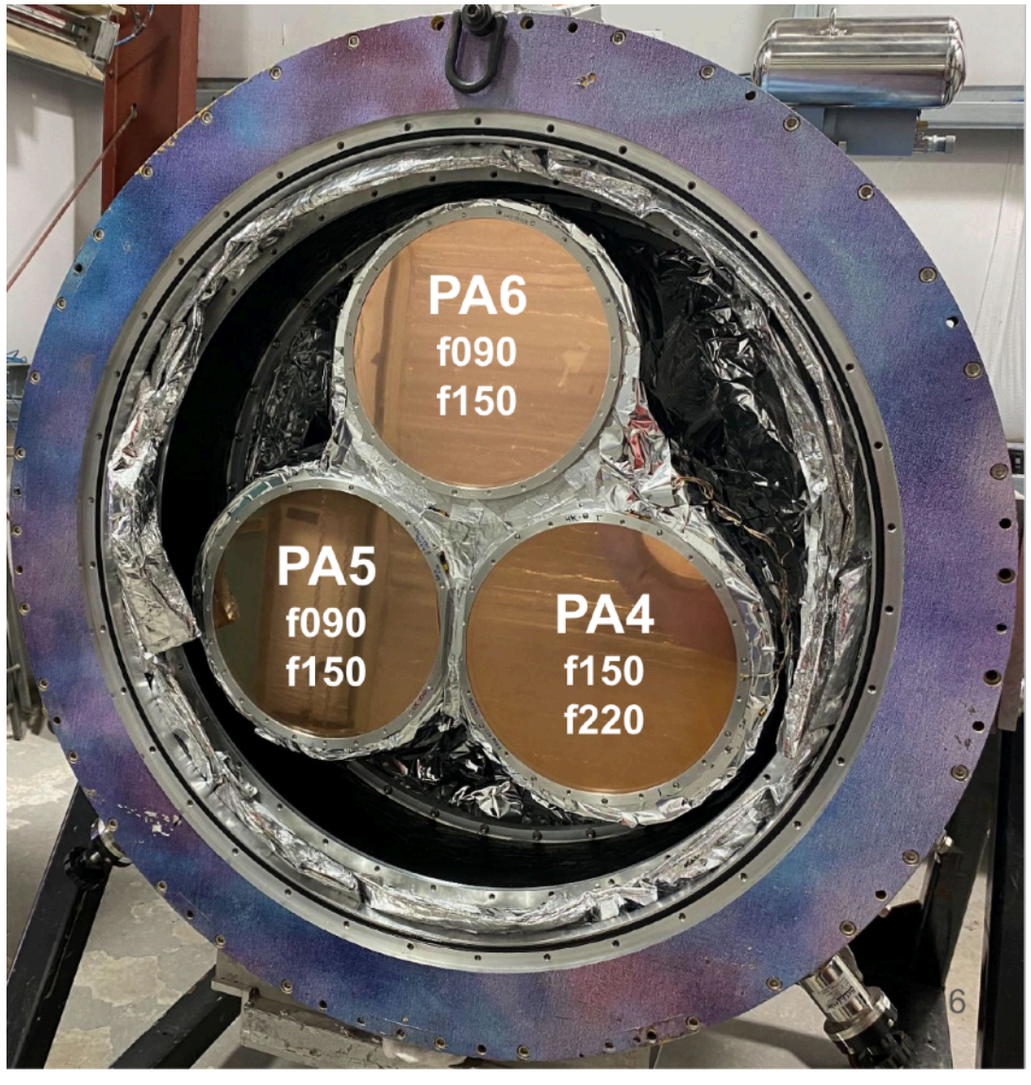

ACT survey: approx. 40% of the sky

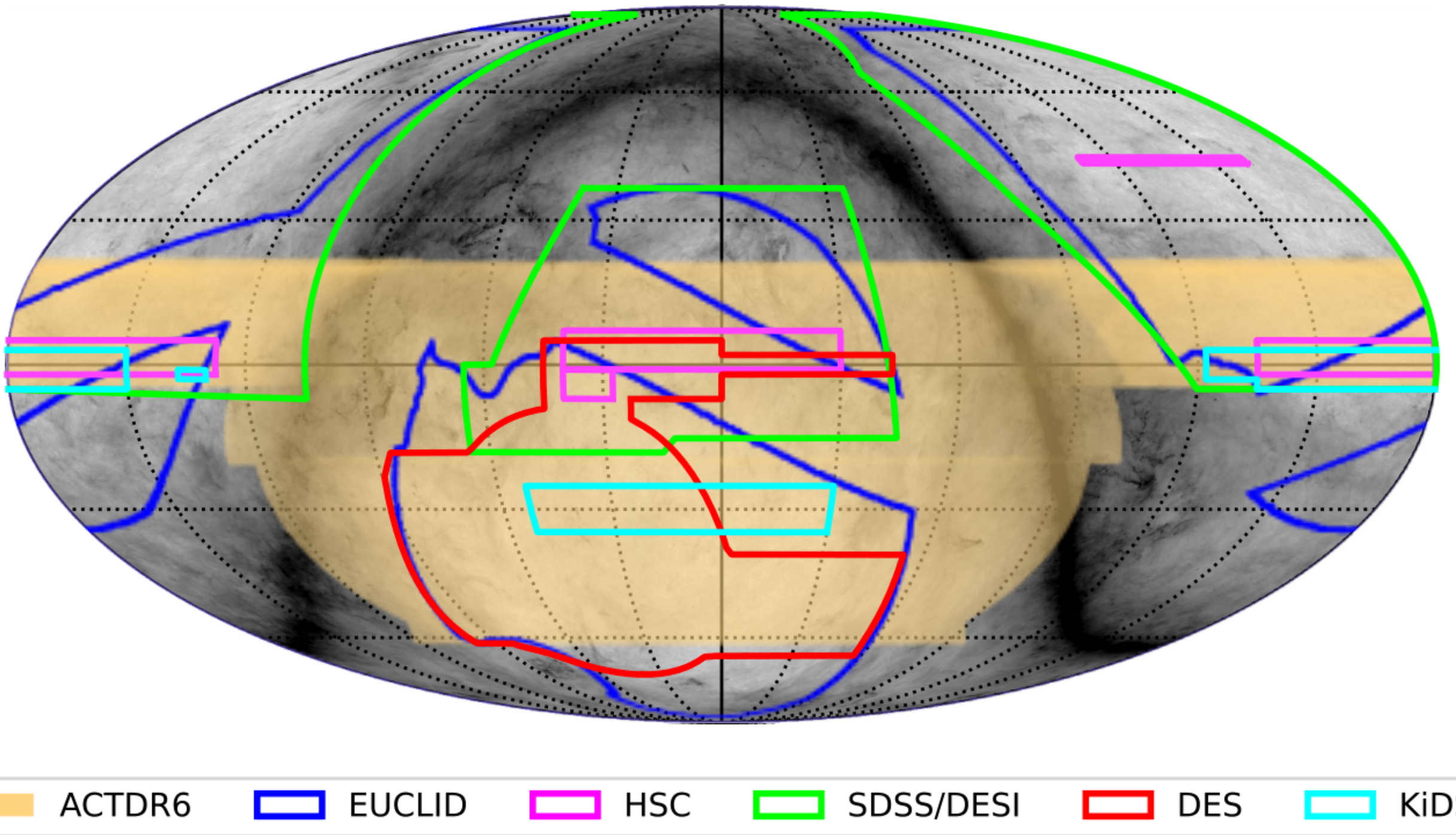

ACT Final Data Release: Three main papers

Draft version January 24, 2025
Typeset using LaTeX **twocolumn** style in AASTeX63

The Atacama Cosmology Telescope: DR6 maps

Sigurd Naess,[1] Yilun Guan,[2] Adriaan J. Duivenvoorden,[3] Matthew Hasselfield,[4] Yuhan Wang,[5] and et al, ACT collaboration

[1] *Institute of Theoretical Astrophysics, University of Oslo, Norway*
[2] *Dunlap Institute for Astronomy and Astrophysics, University of Toronto, 50 St. George Street, Toronto, ON M5S 3H4, Canada*
[3] *Joseph Henry Laboratories of Physics, Jadwin Hall, Princeton University, Princeton, NJ, USA 08544*
[4] *Center for Computational Astrophysics, Flatiron Institute, New York, NY, USA 10010*
[5] *Department of Physics, Cornell University, Ithaca, NY 14853, USA*

The Atacama Cosmology Telescope: DR6 Power spectra, Likelihood and ΛCDM parameters

Thibaut Louis,[1] Adrien La Posta,[2] Zachary Atkins,[3] Hidde T. Jense,[4] and ACT Collaboration

[1] *Université Paris-Saclay, CNRS/IN2P3, IJCLab, 91405 Orsay, France*
[2] *Department of Physics, University of Oxford, Denys Wilkinson Building, Keble Road, Oxford OX1 3RH, United Kingdom*
[3] *Joseph Henry Laboratories of Physics, Jadwin Hall, Princeton University, Princeton, NJ, USA 08544*
[4] *School of Physics and Astronomy, Cardiff University, The Parade, Cardiff, Wales, UK CF24 3AA*

The Atacama Cosmology Telescope: DR6 Constraints on Extended Cosmological Models

Erminia Calabrese,[1] J. Colin Hill,[2] Hidde T. Jense,[1] Adrien La Posta,[3] and ACT Collaboration

[1] *School of Physics and Astronomy, Cardiff University, The Parade, Cardiff, Wales, UK CF24 3AA*
[2] *Department of Physics, Columbia University, New York, NY 10027, USA*
[3] *Department of Physics, University of Oxford, Denys Wilkinson Building, Keble Road, Oxford OX1 3RH, United Kingdom*

esa

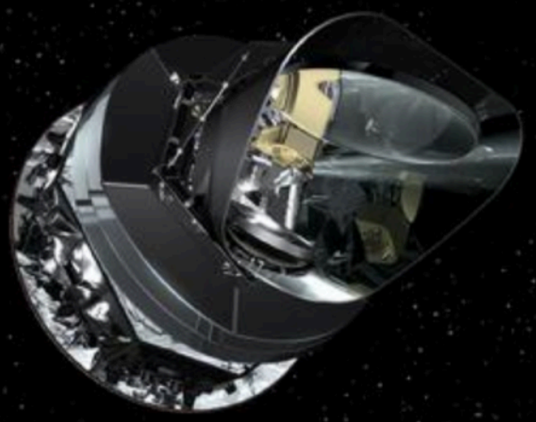

Planck f150 T

13°×7°

ACT+Planck f150 T

13°×7°

PLANCK E modes

Planck + ACT E-modes

First high S/N E-modes map ever made over a large portion of the sky

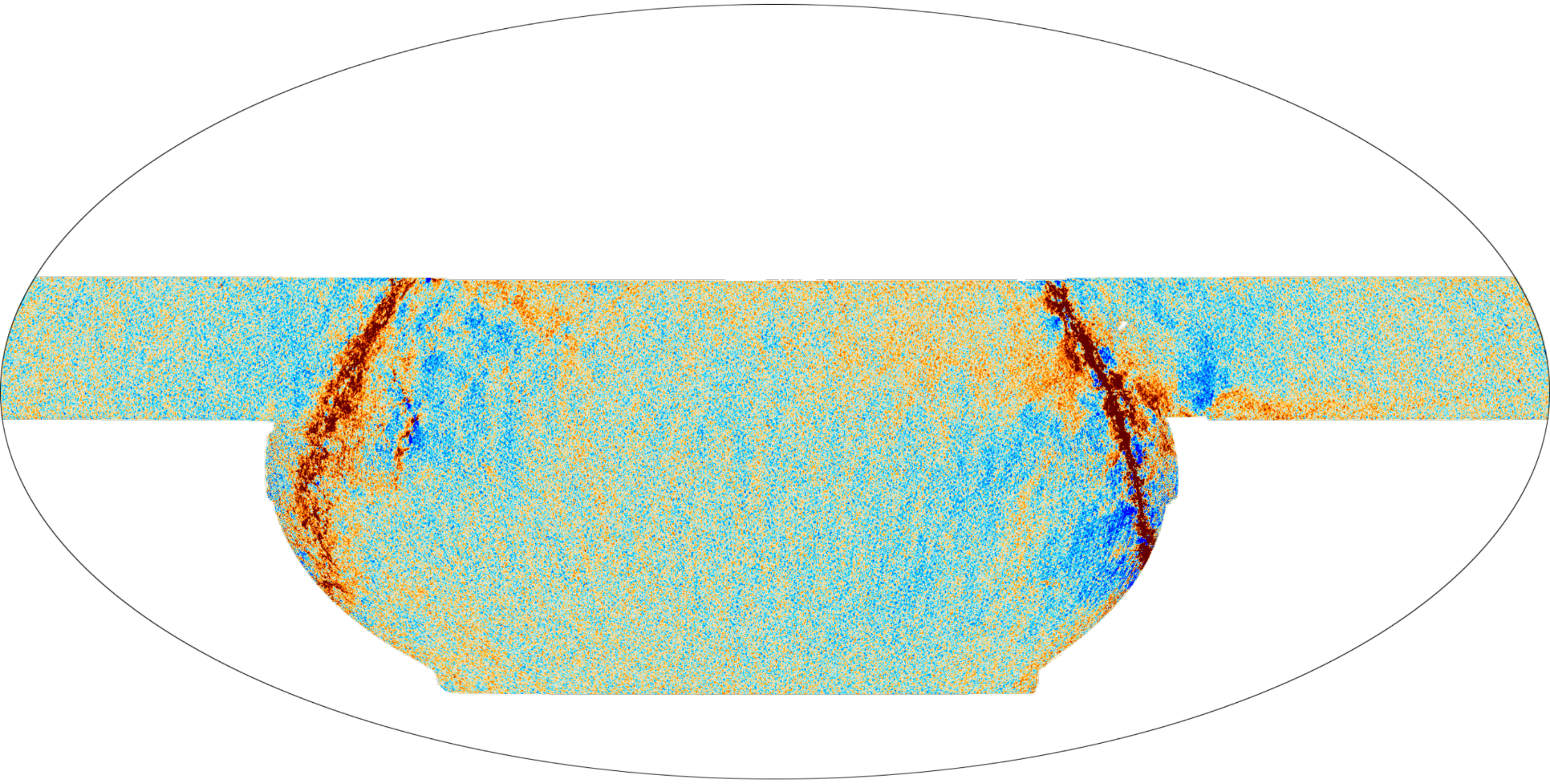

ACT+Planck E

Planck + ACT temperature power spectra

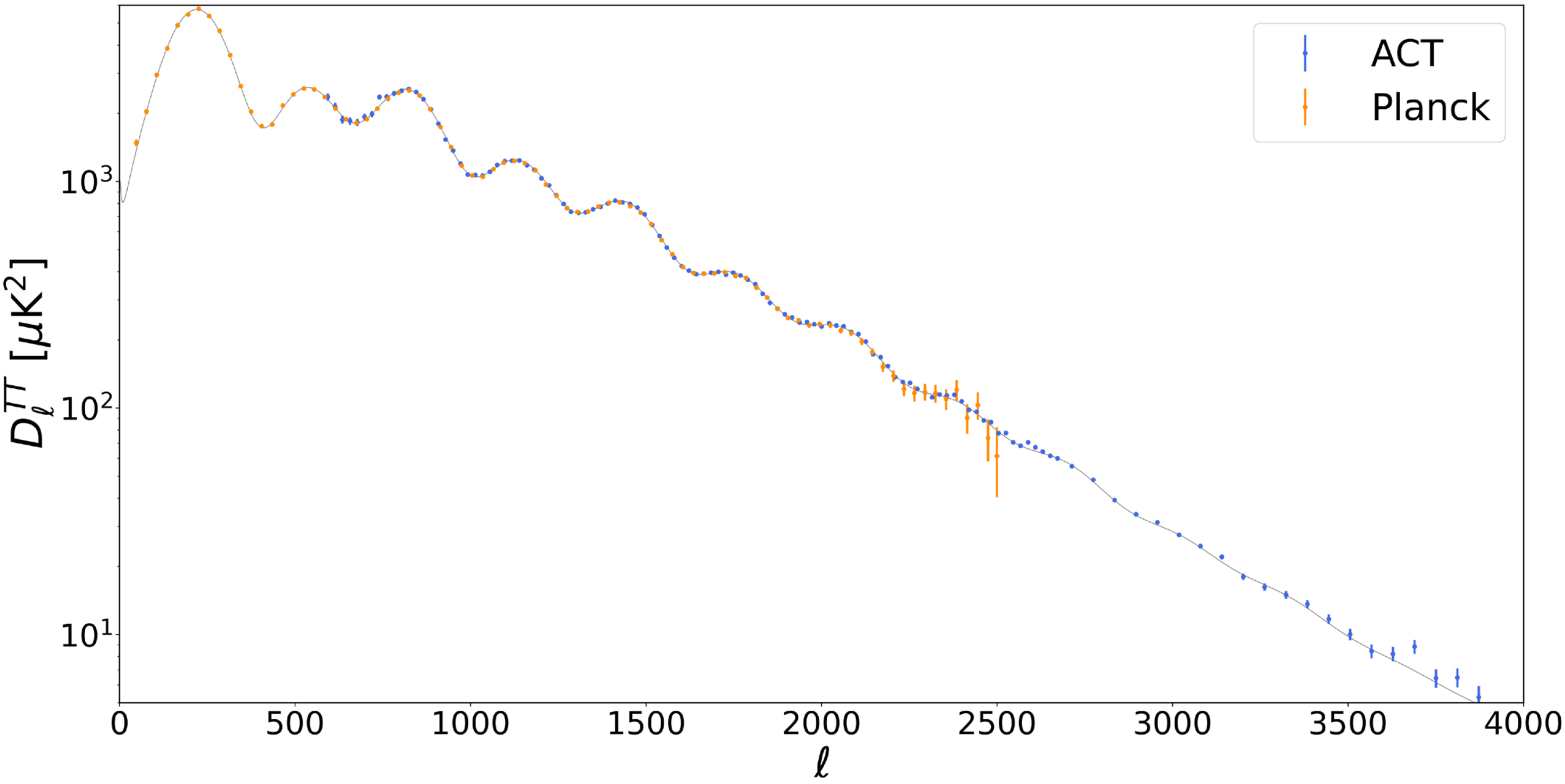

ACT data 1) extend Planck measurement to small angular scales.
2) are very consistent with Planck data on overlapping angular scales.
3) + Planck data are fitted by a common model

Planck + ACT E modes power spectra

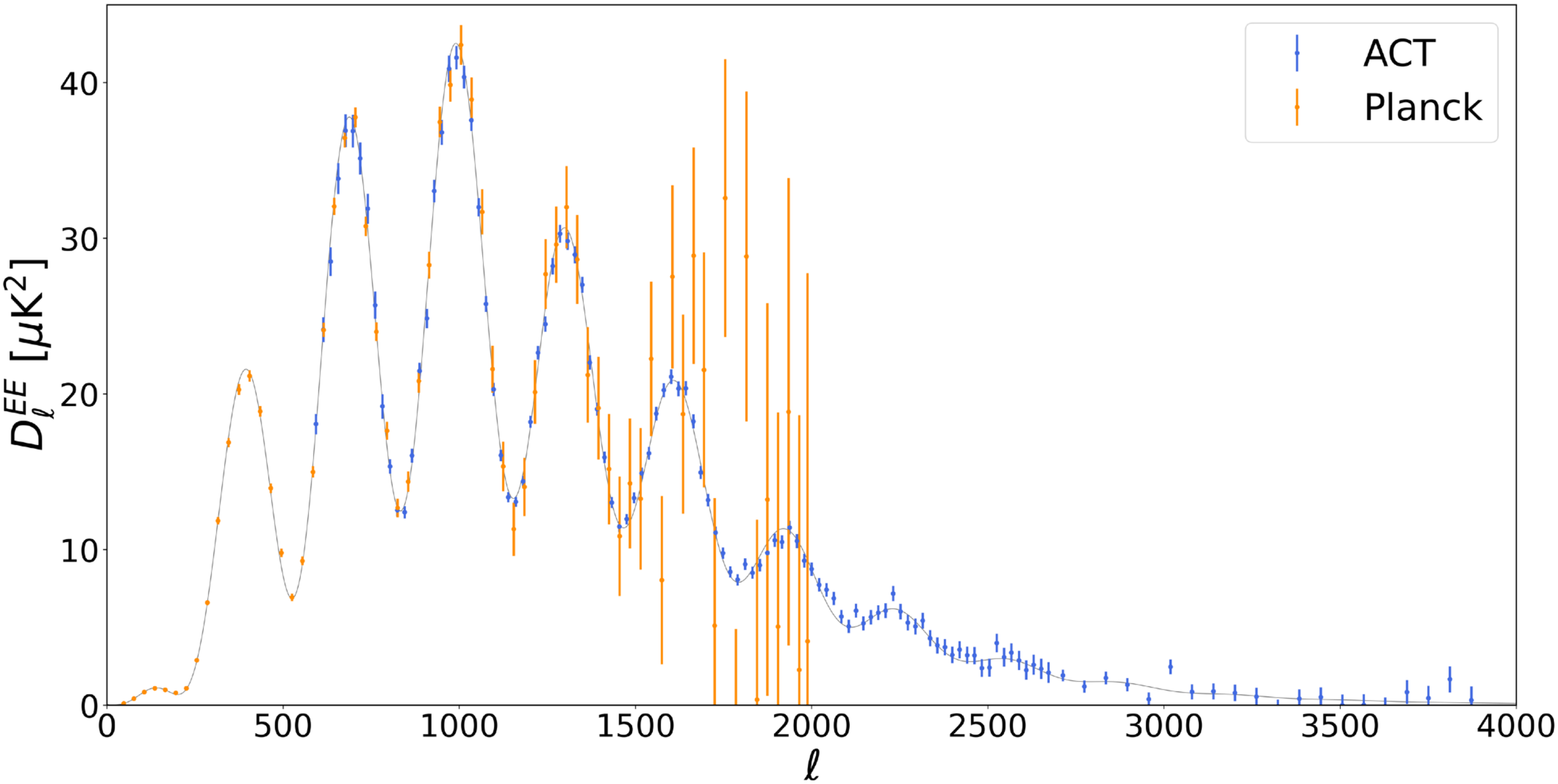

ACT DR6 EE is more sensitive than Planck for multipoles $\ell > 600$

Planck + ACT TE power spectrum

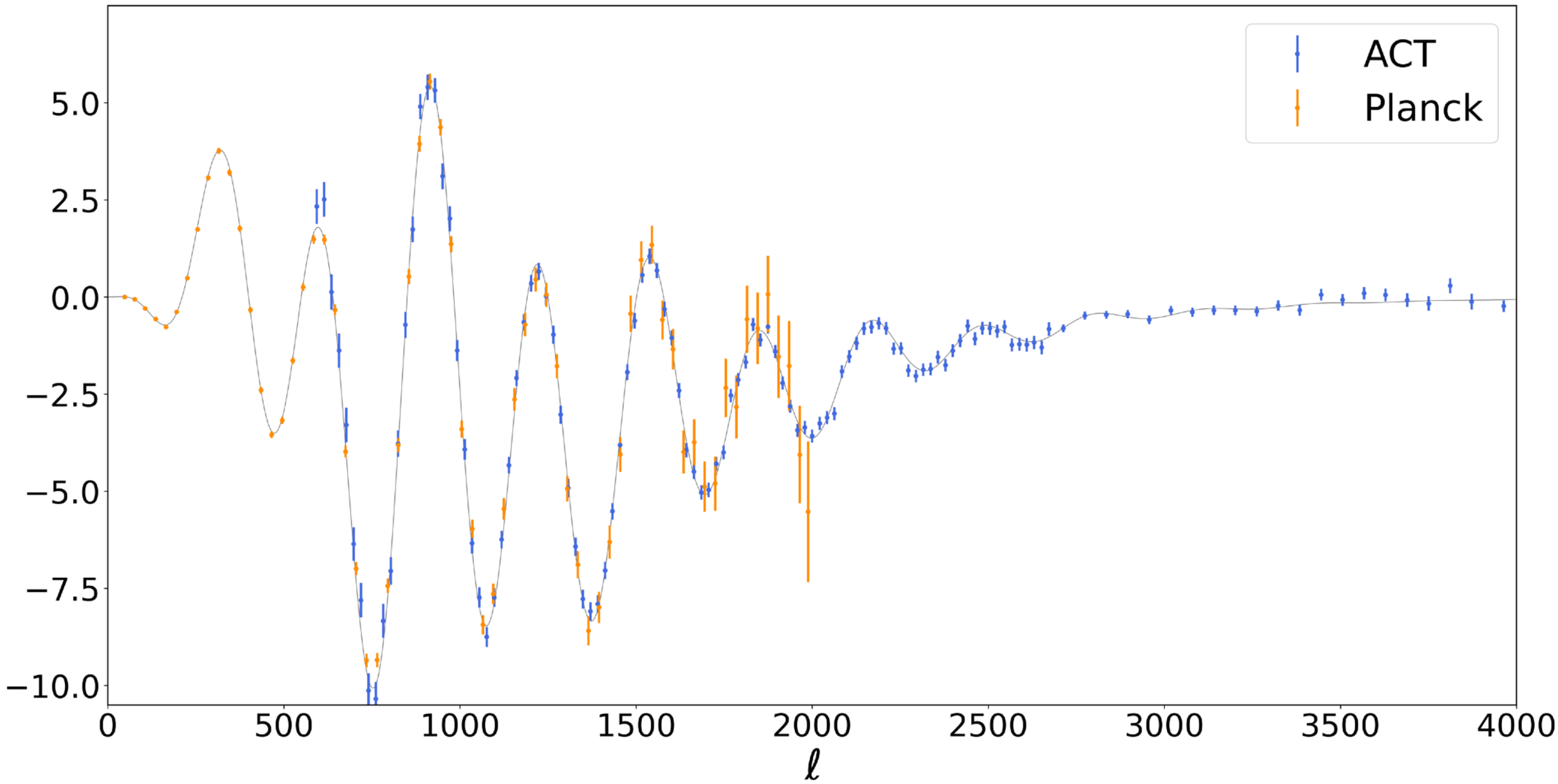

Very clean, foreground free cosmology,
1.1 % constraint on H0 from TE alone

Excellent agreement with Planck (PR3) in LCDM

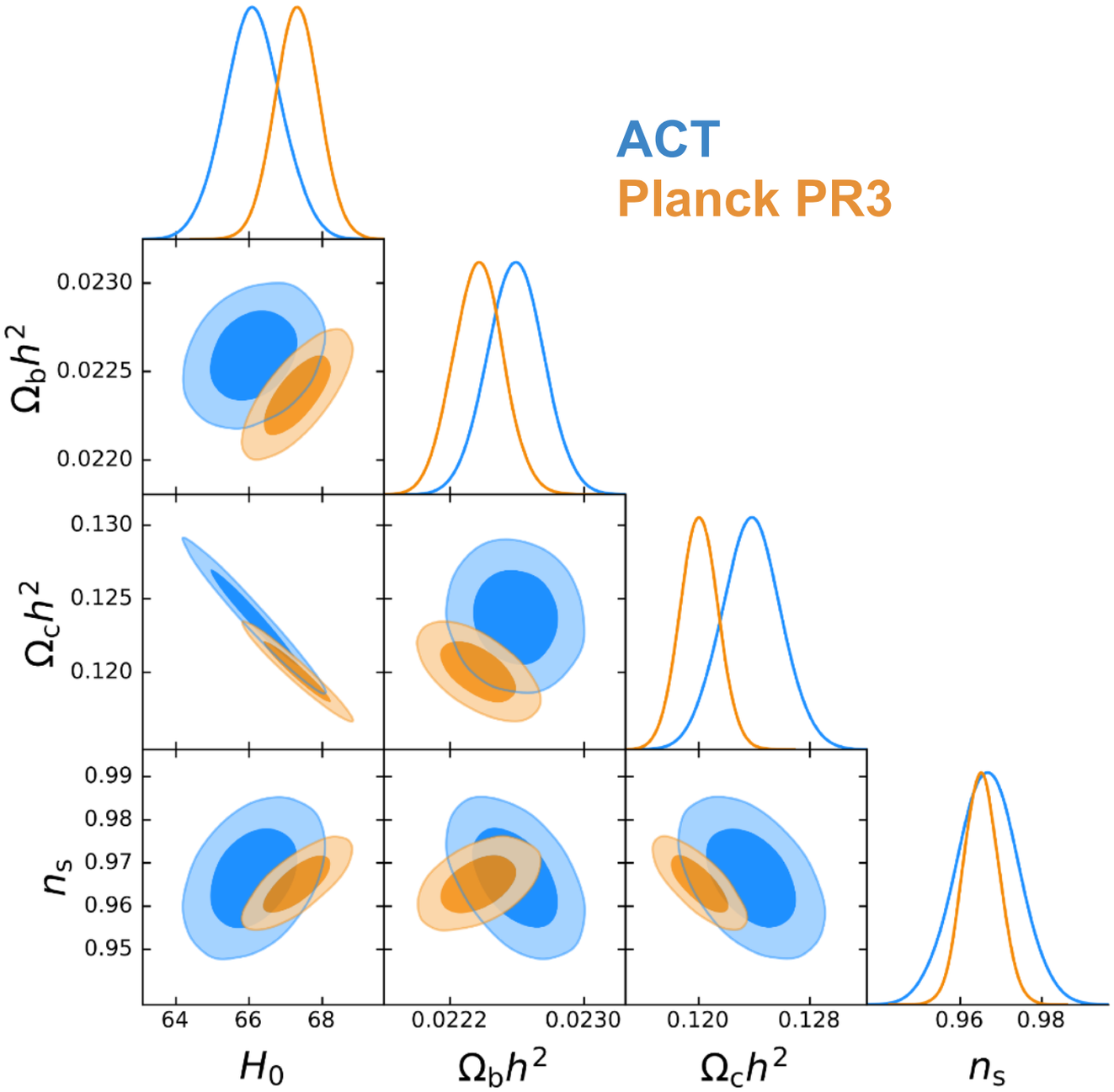

The Atacama Cosmology Telescope: DR6 Power spectra, Likelihood and ΛCDM parameters

Thibaut Louis,[1] Adrien La Posta,[2] Zachary Atkins,[3] Hidde T. Jense,[4] and ACT Collaboration

[1] *Université Paris-Saclay, CNRS/IN2P3, IJCLab, 91405 Orsay, France*
[2] *Department of Physics, University of Oxford, Denys Wilkinson Building, Keble Road, Oxford OX1 3RH, United Kingdom*
[3] *Joseph Henry Laboratories of Physics, Jadwin Hall, Princeton University, Princeton, NJ, USA 08544*
[4] *School of Physics and Astronomy, Cardiff University, The Parade, Cardiff, Wales, UK CF24 3AA*

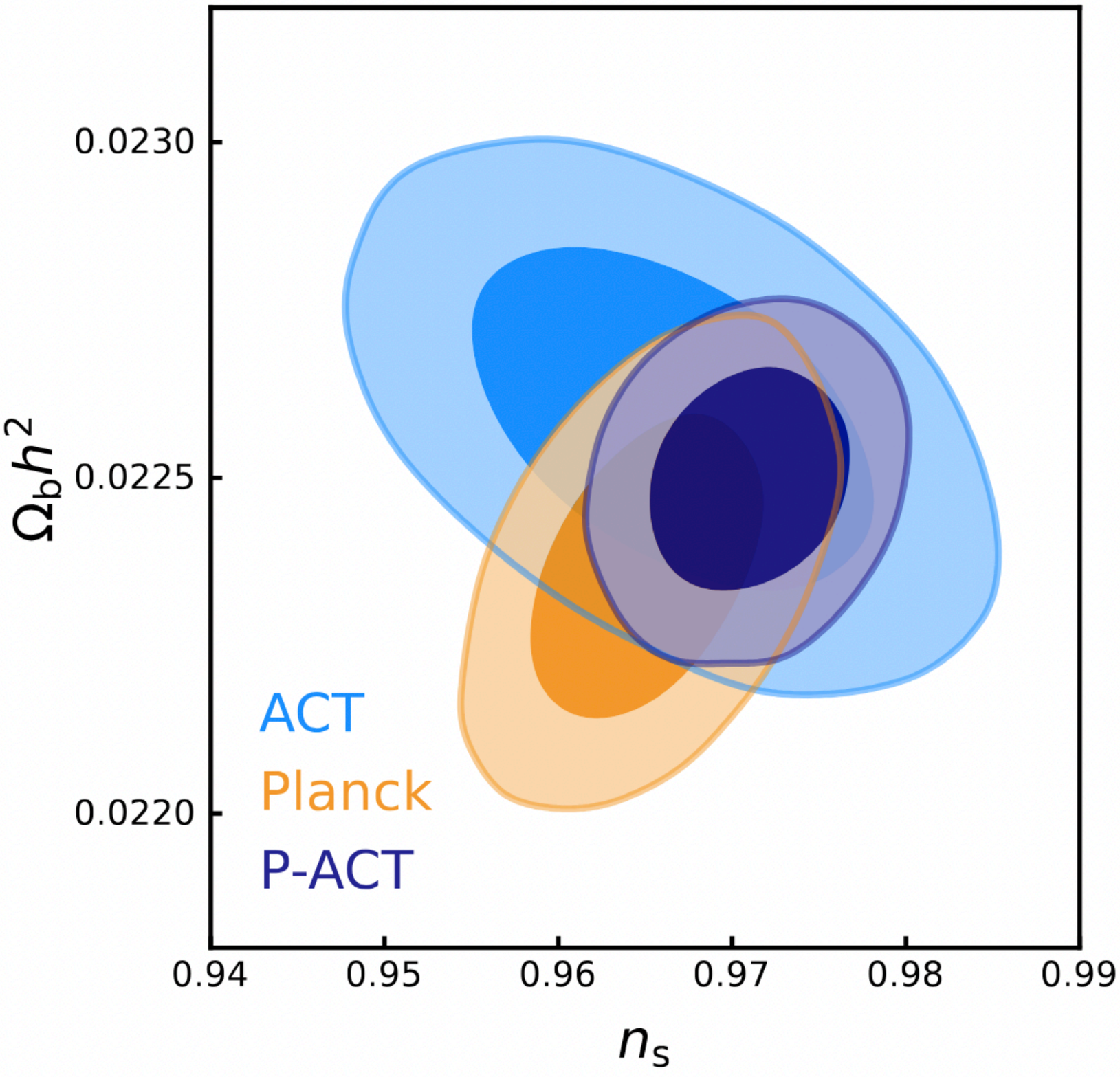
0.0230
0.0225
0.0220
$\Omega_b h^2$
ACT
Planck
P-ACT
0.94
0.95
0.96
0.97
0.98
0.99
n_s

The three possible solutions to the H0 measurement problem

1) SH0ES constraint is affected by un-modelled systematics (leading to artificial high H0)

2) Planck measurement is affected by un-modelled systematics (leading to artificial low H0)

3) Need new physics beyond LCDM ?

An Hubble constant measurement nowhere near the SH0ES value

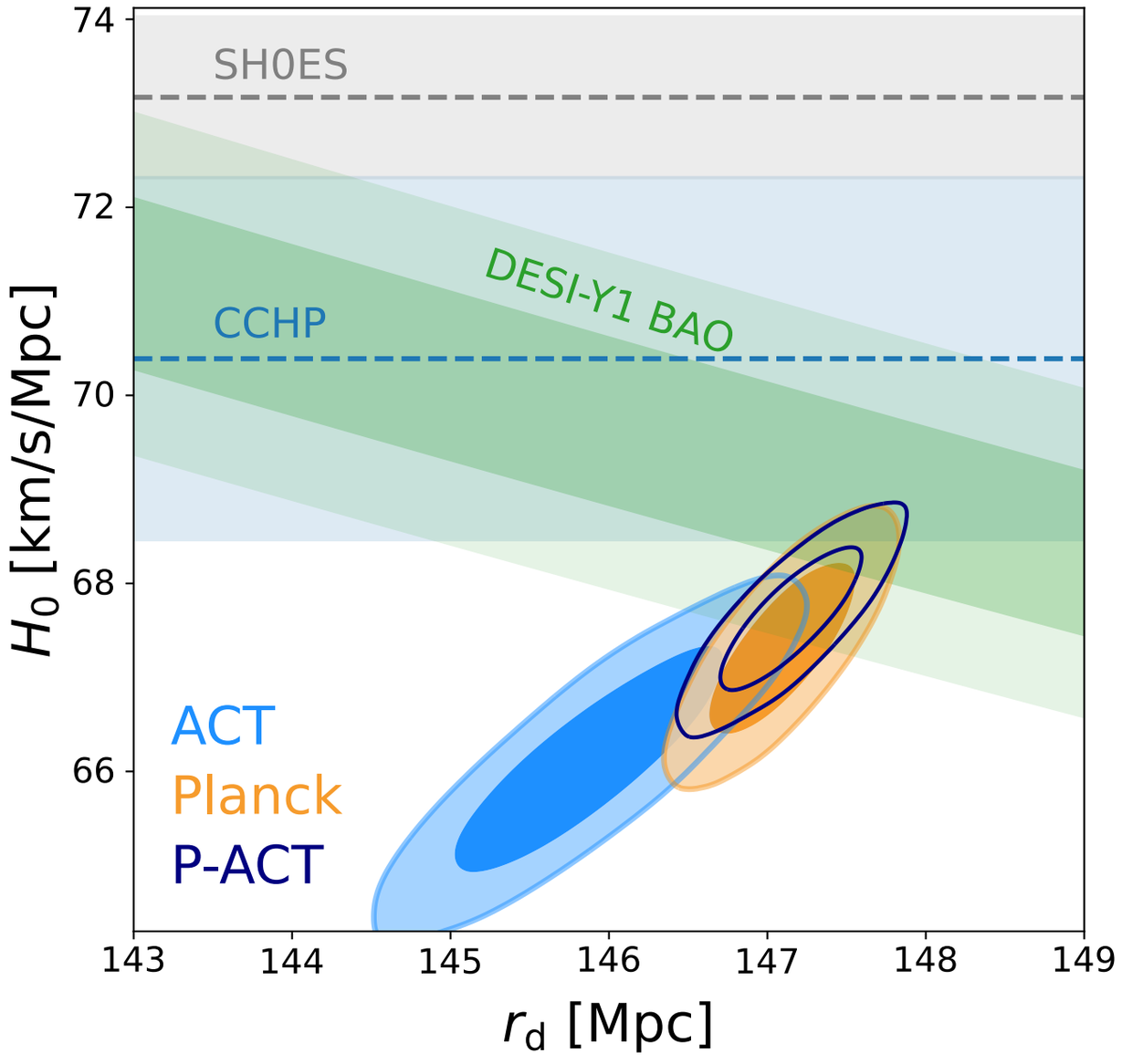

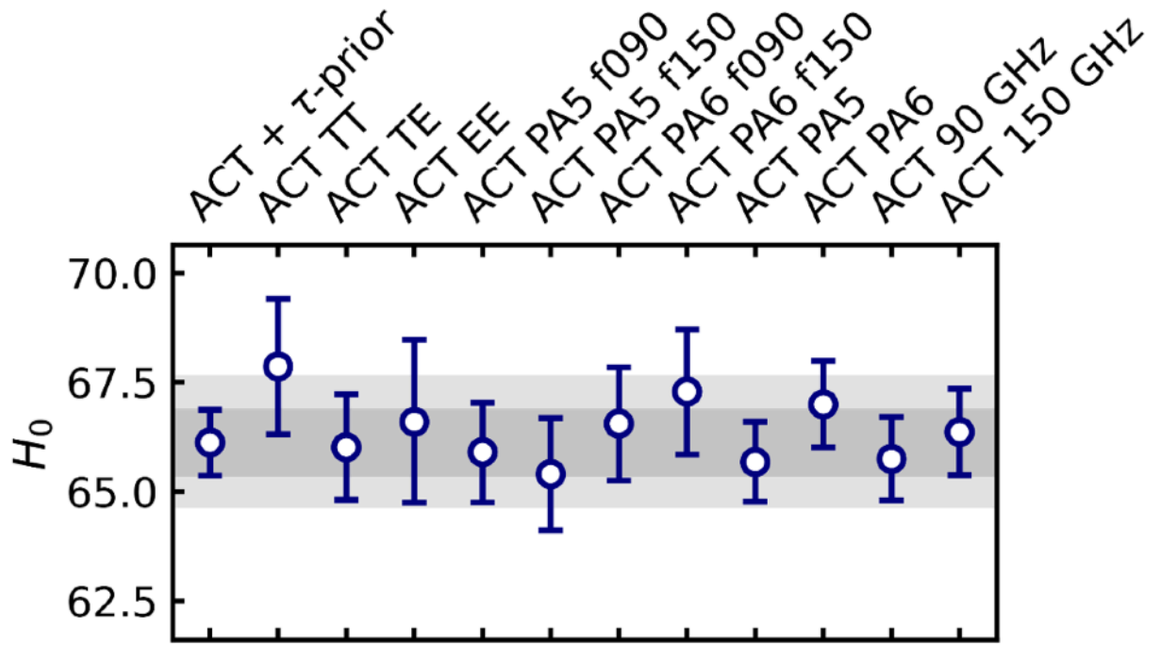

None of ACT probes exceed H0=68 km/s/Mpc

SH0ES: *Breuval et al.* 2024, *Riess et al.* 2022 (Cepheids)
CCHP : Chicago–Carnegie Hubble Program : *Freedman et al.* 2024 (Tip of the Red Giant Branch and J-Region Asymptotic Giant Branch)

The three possible solutions to the H0 problem

1) SH0ES constraint is affected by un-modelled systematics (leading to artificial high H0)

2) ~~Planck measurement is affected by un-modelled systematics (leading to artificial low H0)~~

3) Need new physics beyond LCDM ?

We tested a large class of extensions, Using CMB, CMB lensing and DESI DR1, None of them are preferred over ΛCDM.

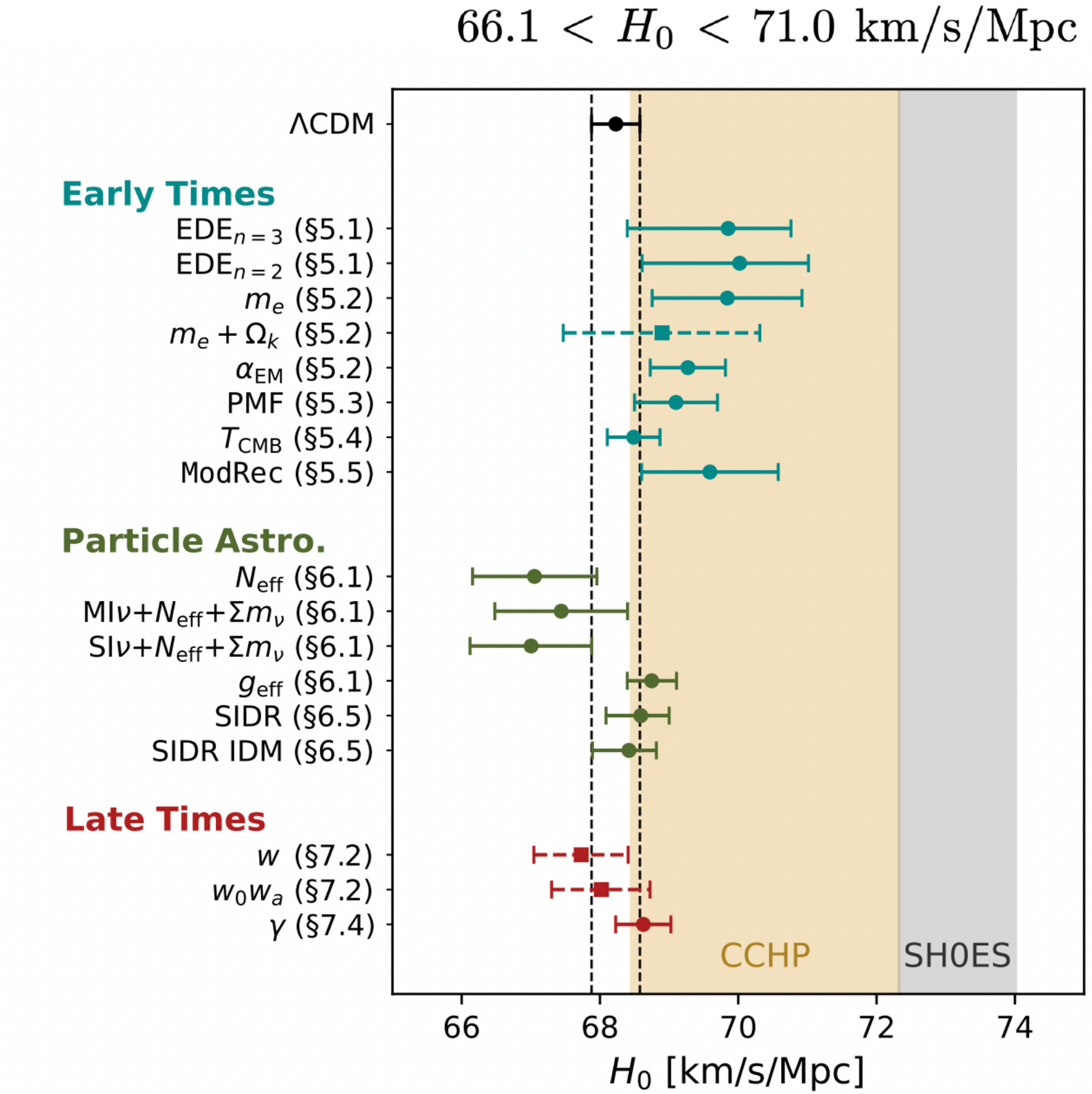

Solid (dashed) bars are constraints at 68% confidence derived from P-ACT-LB (P-ACT-LBS).

The three possible solutions to the H0 problem

1) SH0ES constraint is affected by un-modelled systematics (leading to artificial high H0)

2) ~~Planck measurement is affected by un-modelled systematics (leading to artificial low H0)~~

3) Need new physics beyond LCDM ?

Hard to cross definitely, but P-ACT poses a challenge to the proposed models

What about B modes ?

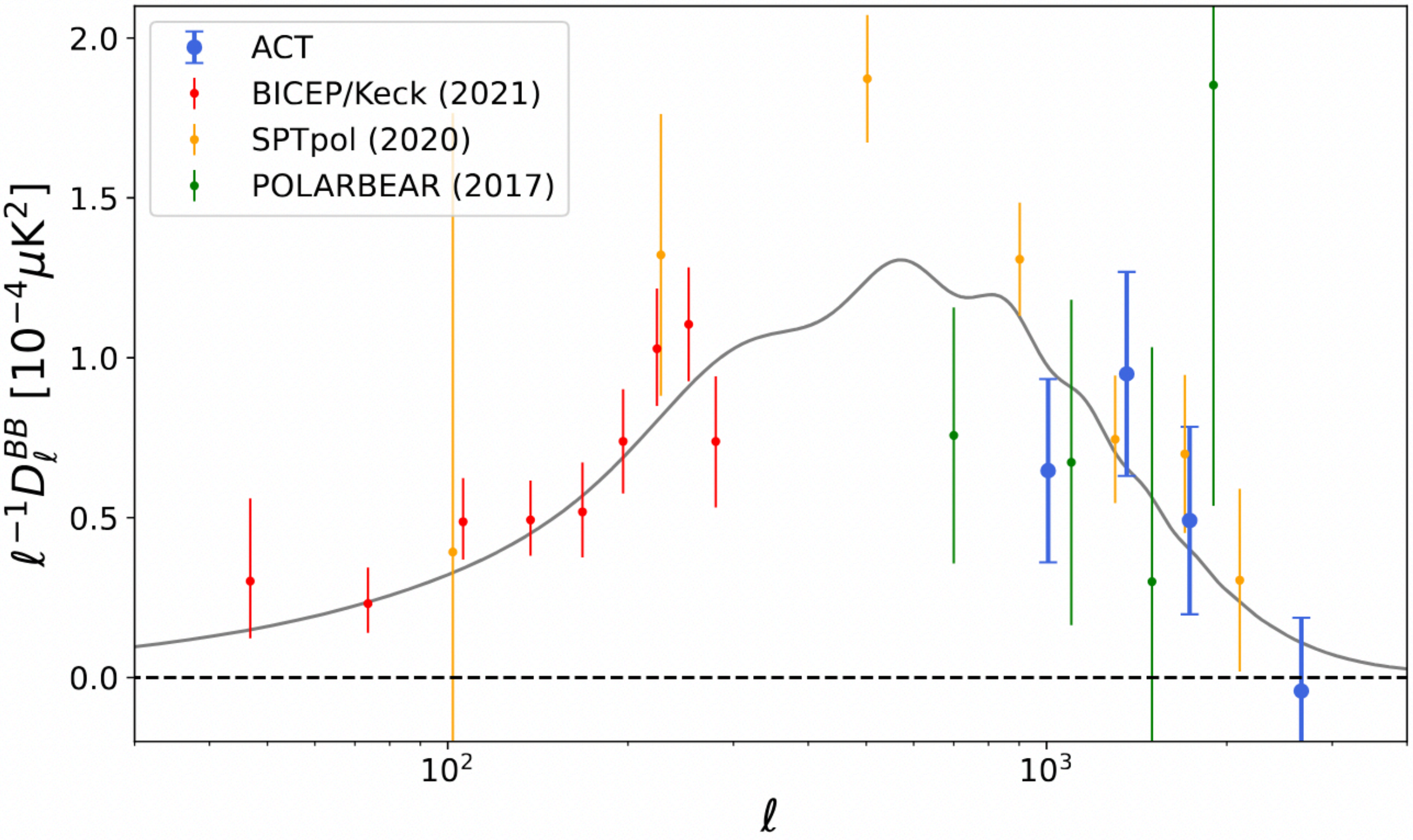

Simons Observatory (2025-2035)

Large Aperture Telescope

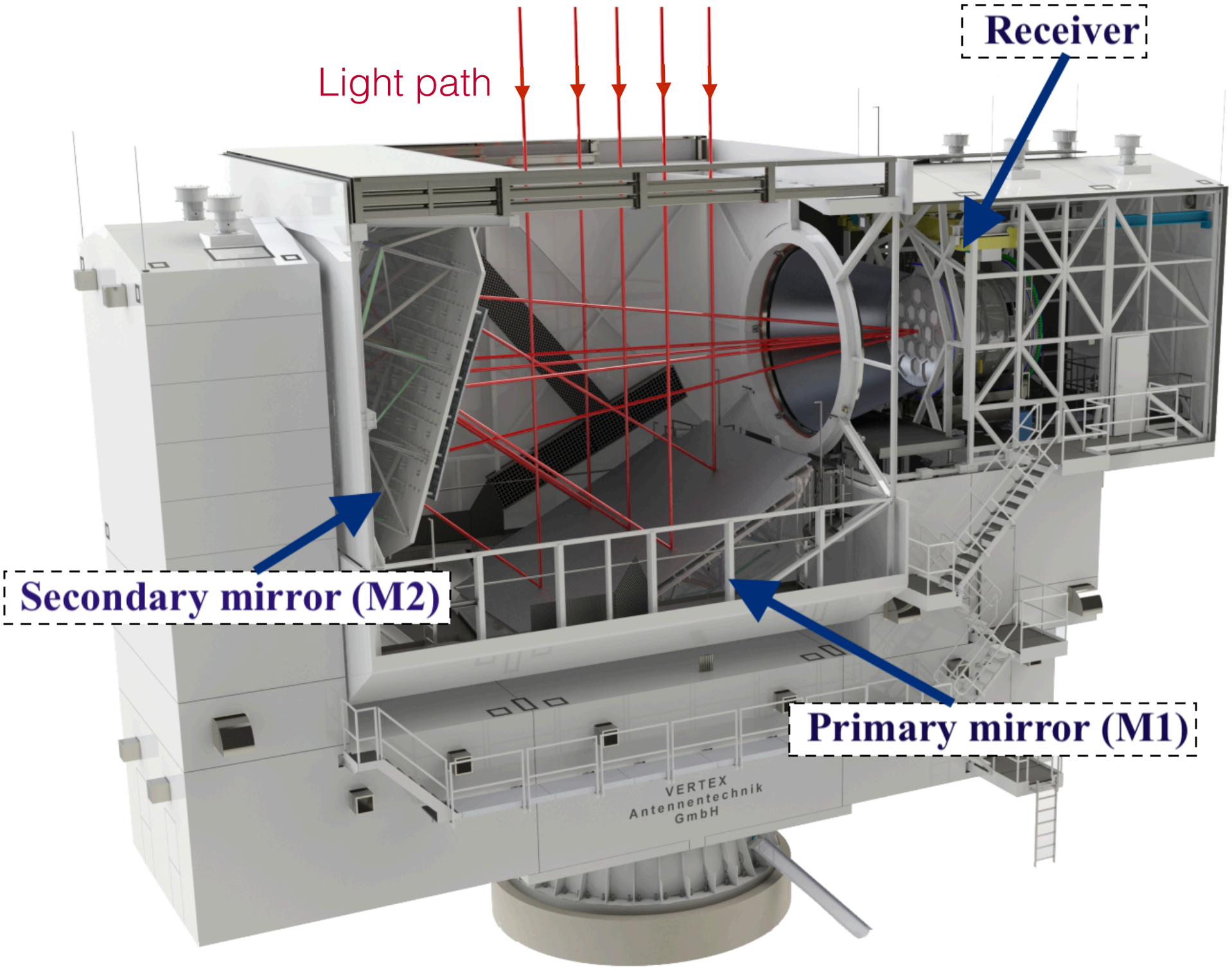

6m primary mirror in cross Dragone configuration

Large Aperture Telescope Receiver

2.4 m in diameter, can host a total of
60 000 detectors in 13 optics tubes

Large Aperture Telescope Receiver

2.4 m in diameter, can host a total of
60 000 detectors in 13 optics tubes

ACT Receiver

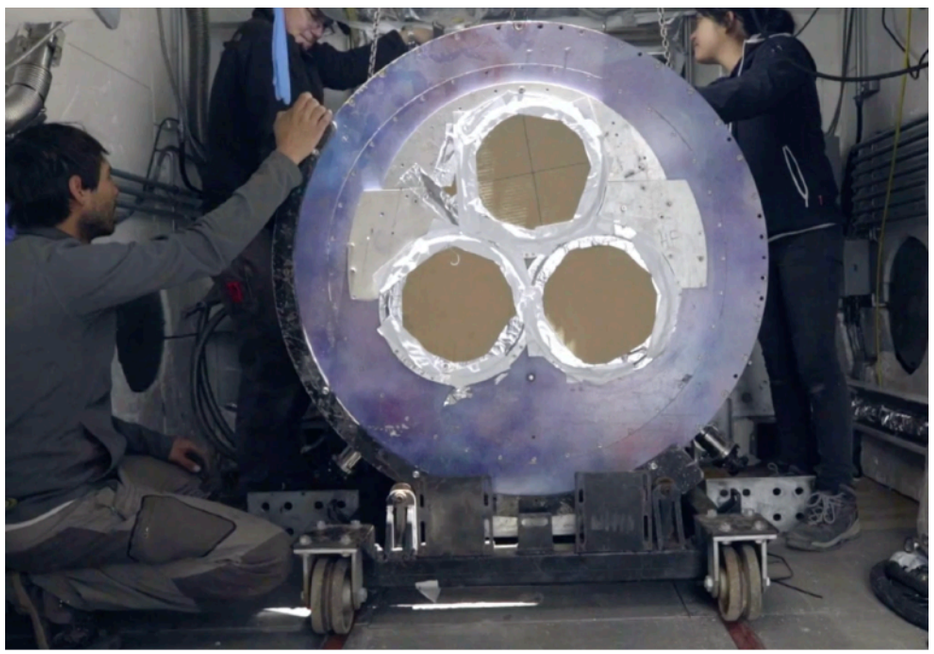

SPT-3G Receiver

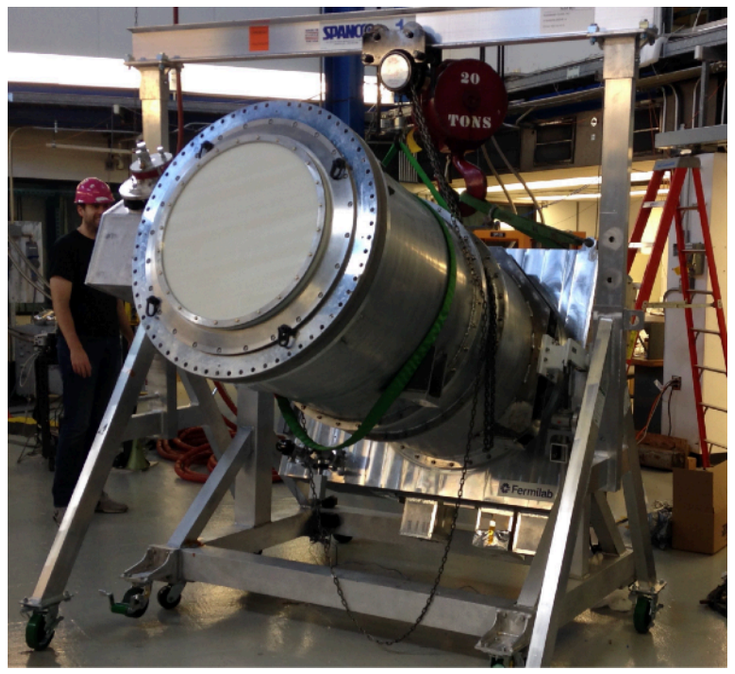

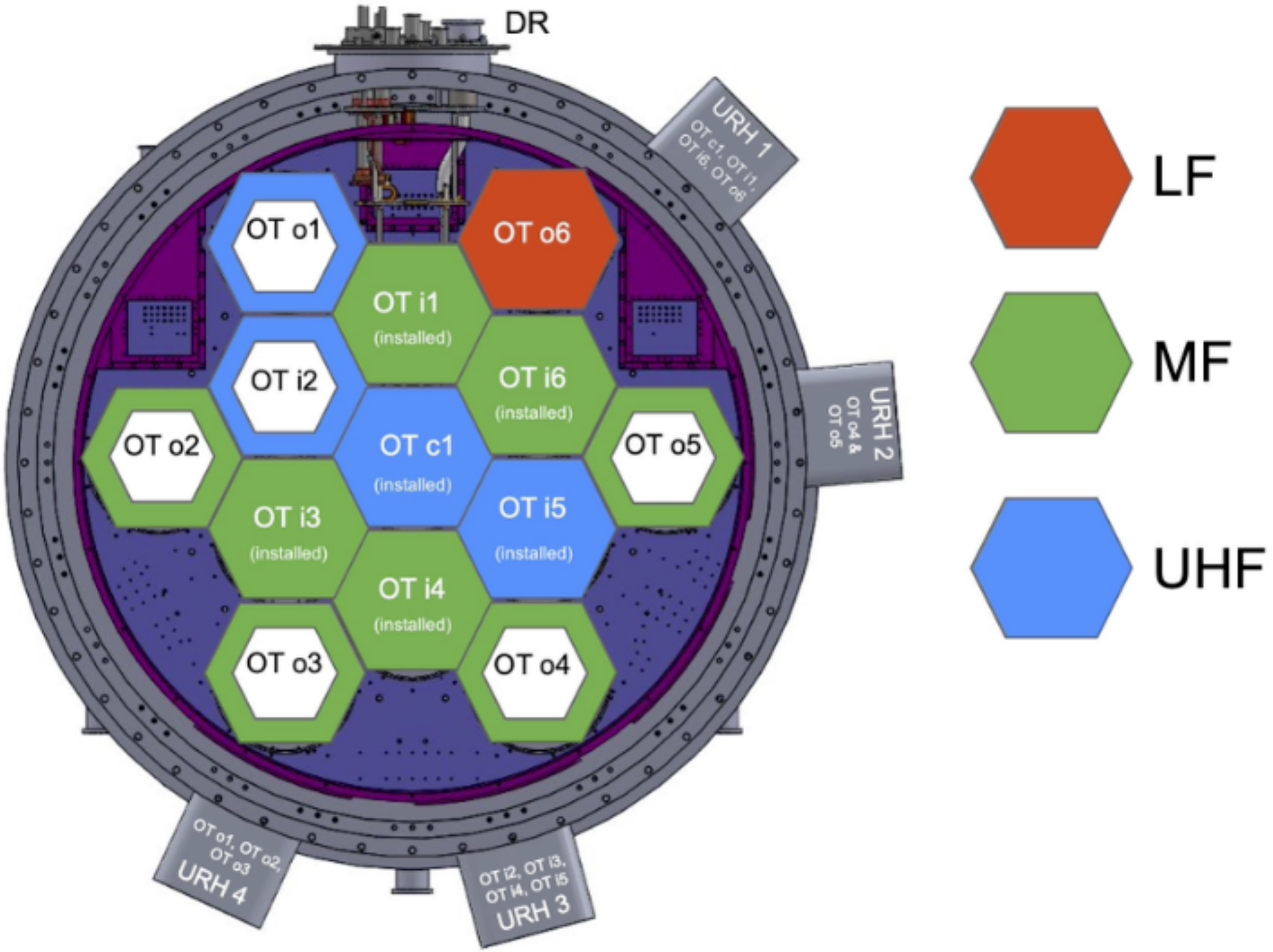

Each tube is expected to have a sensitivity comparable to ACT

Large Aperture Telescope – First Light February 2025!

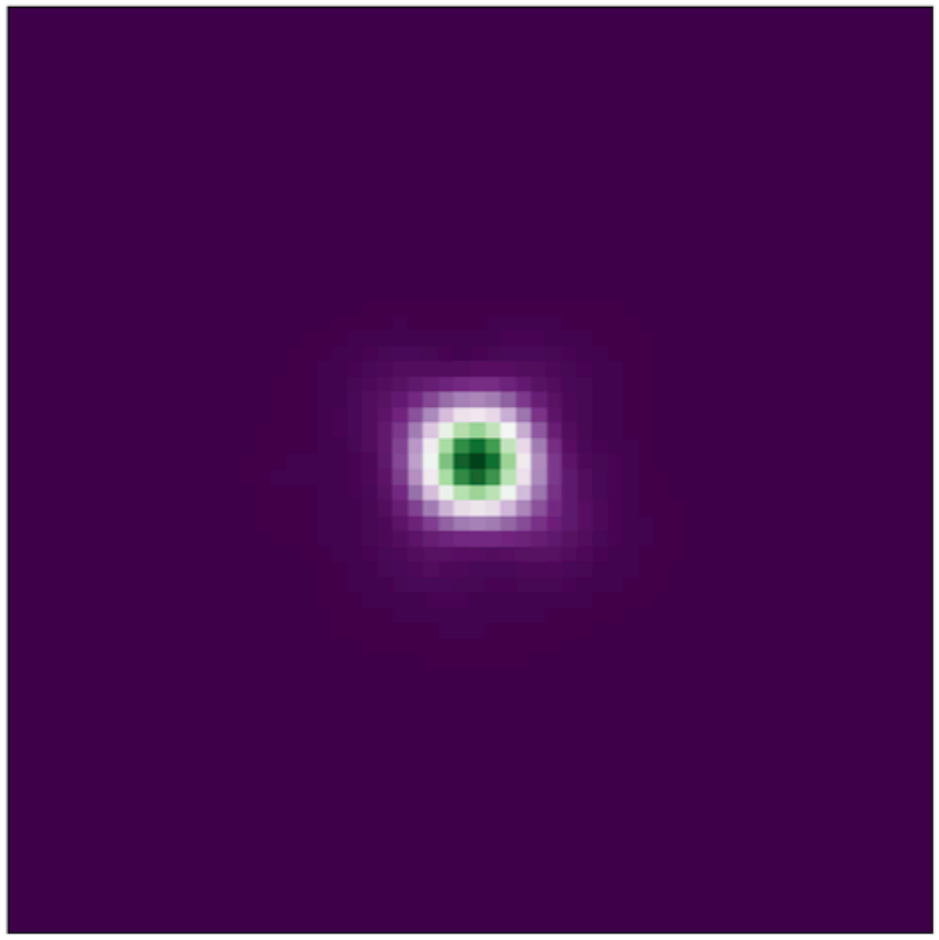

24,000 + Detectors on the Sky.

- Mirrors not yet aligned/focused.
- Signal to Noise of 4000+ per detector.
- 640 detectors used the Mars map.
- CMB maps are already being made.

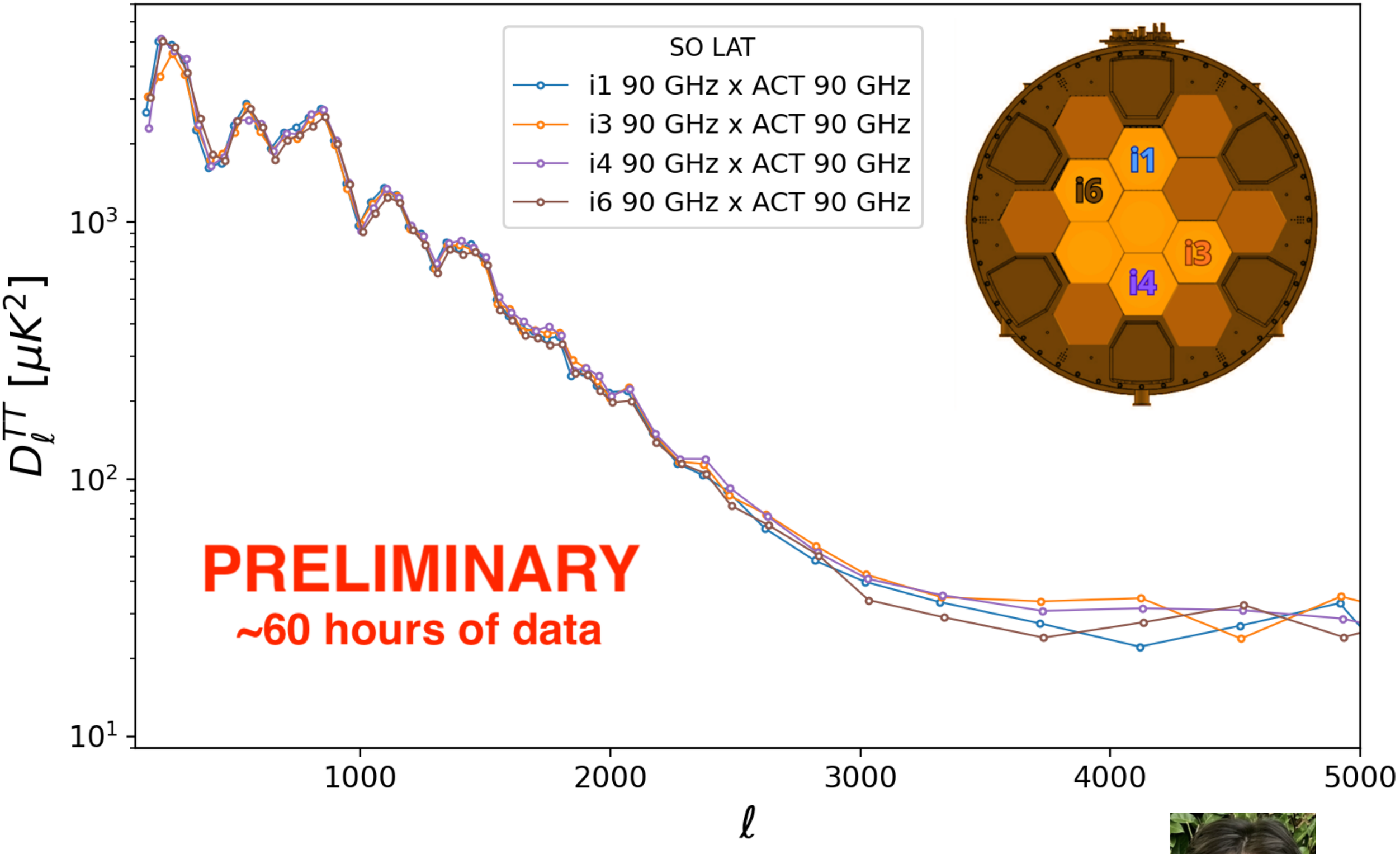

Plot from Merry Duparc for the SO collaboration

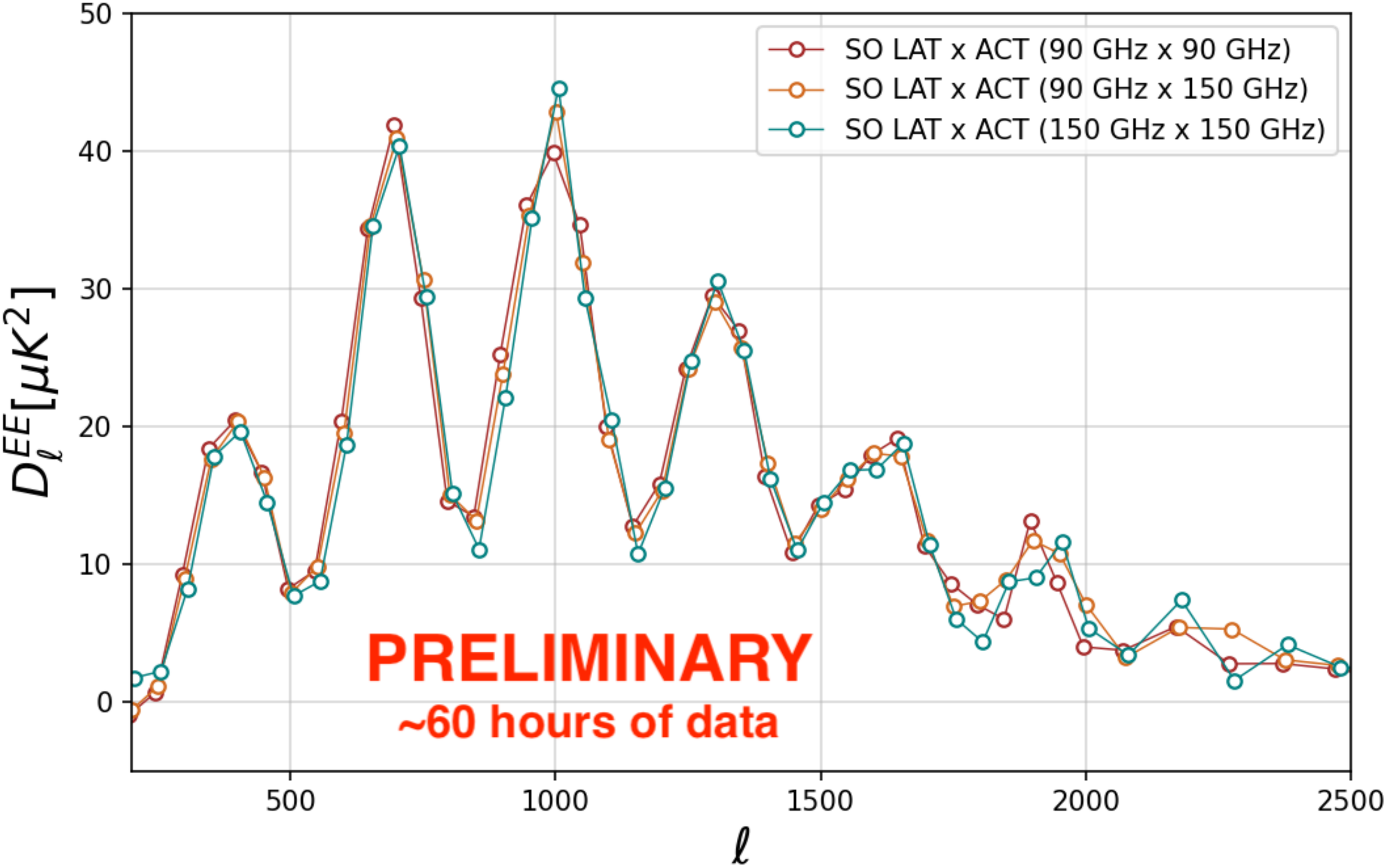

Plot from Merry Duparc for the SO collaboration

Preliminary

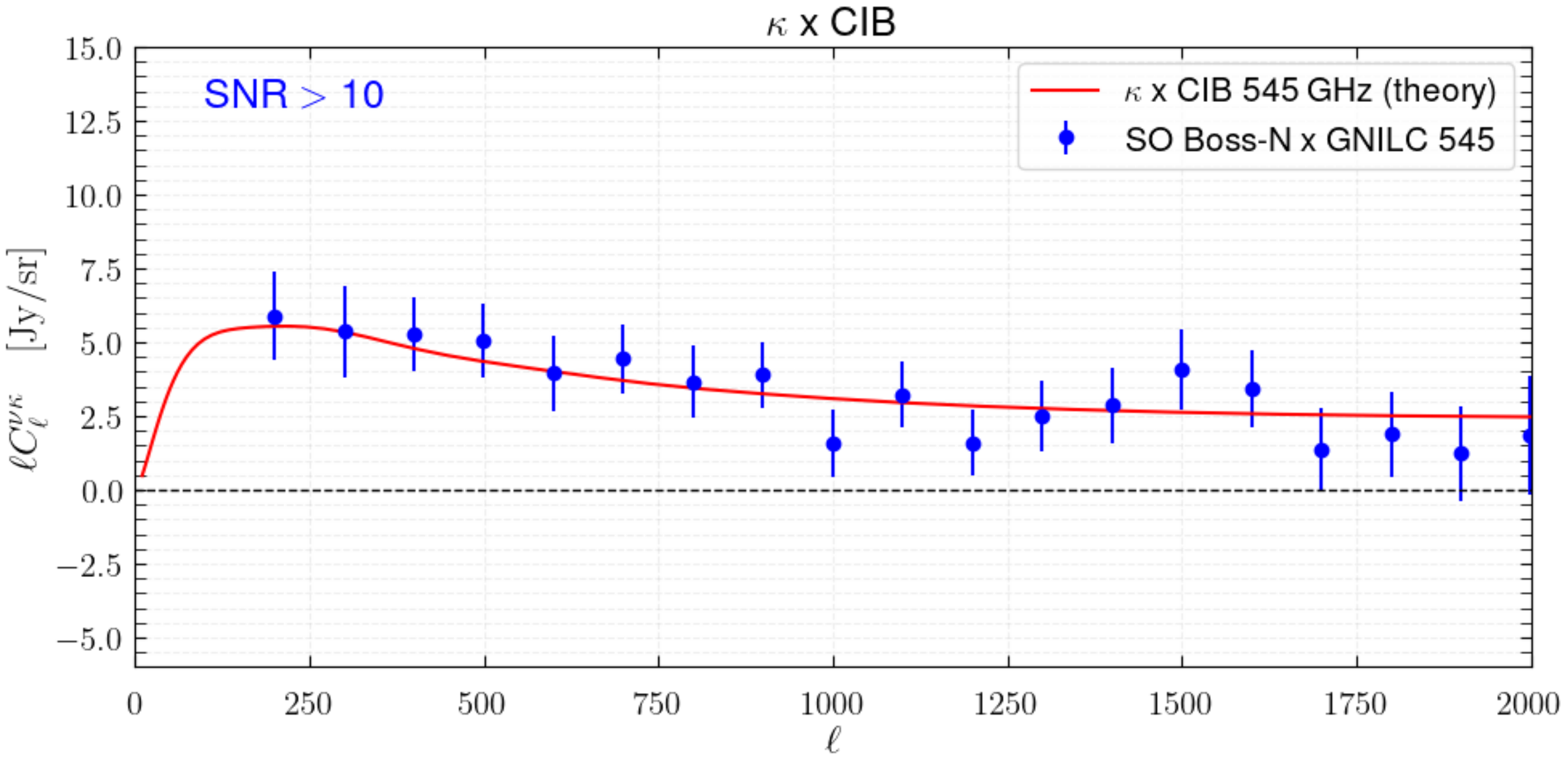

Plot from Ola Kusiak for the SO collaboration

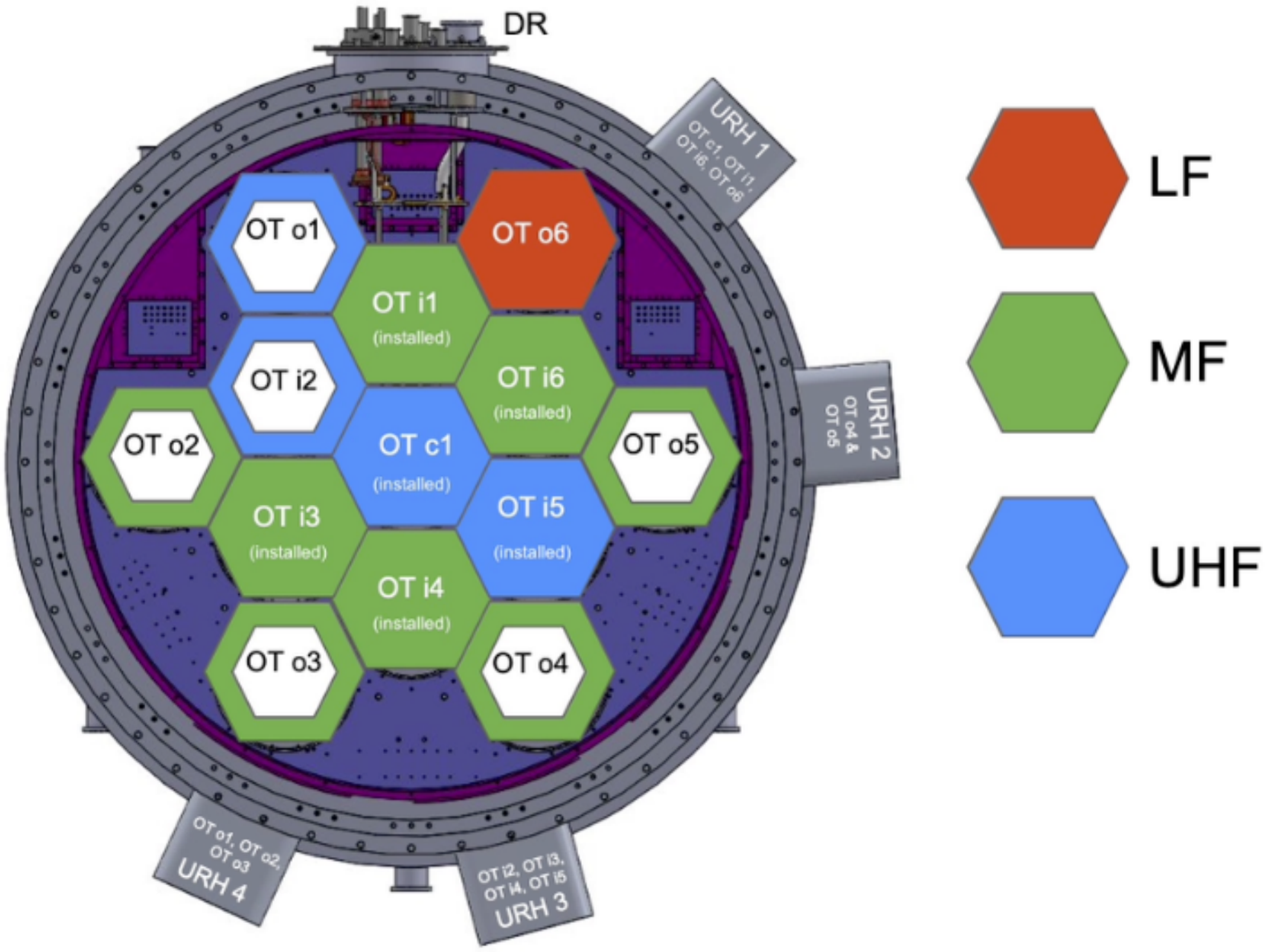

The full focal plane will be populated next year (2026),
13 tubes : 60 000 detectors on the sky expected

3 Small Aperture Telescopes (2 MF + 1 UHF) installed on site (10 k detectors each)

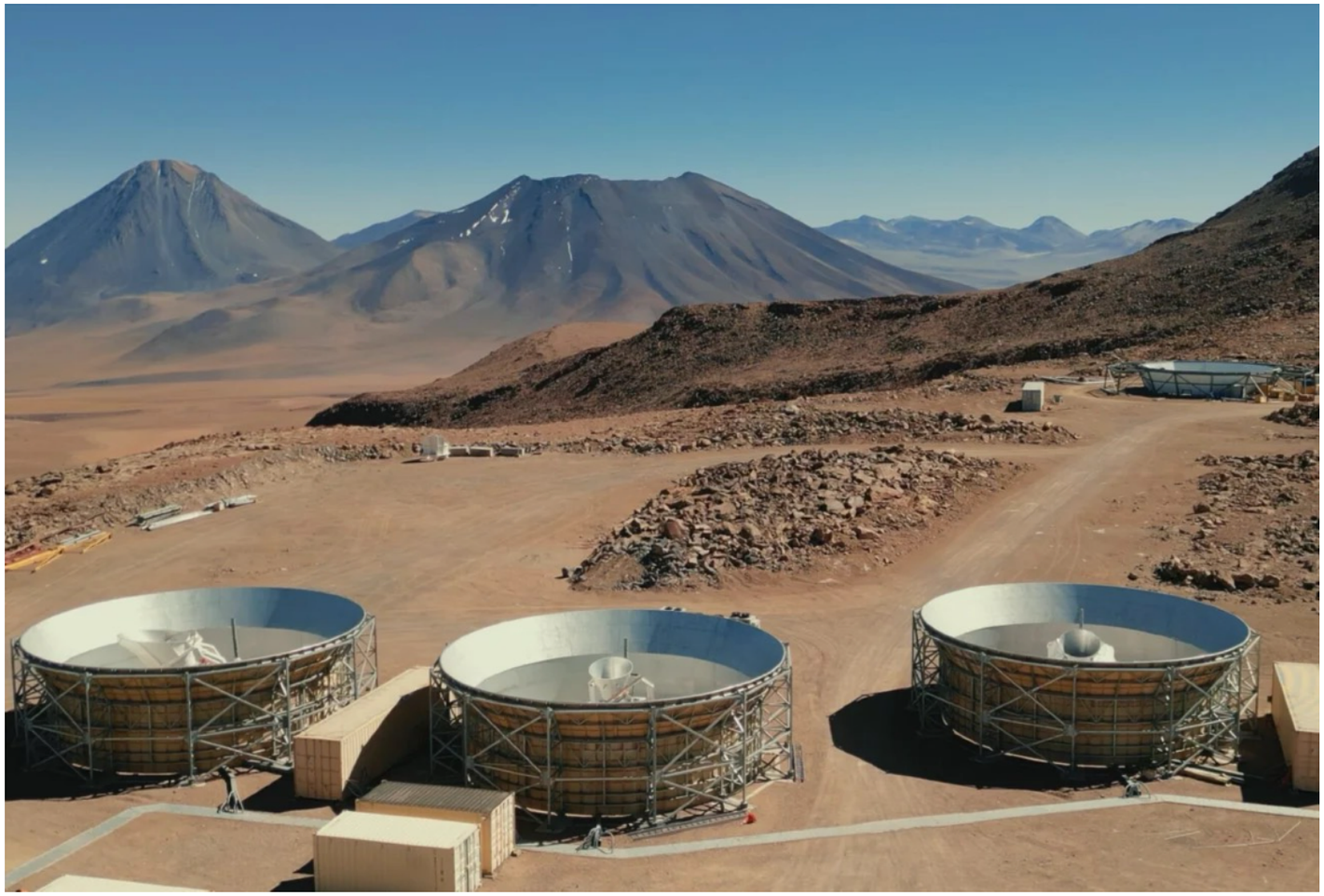

SAT: very « simple » refractive telescopes

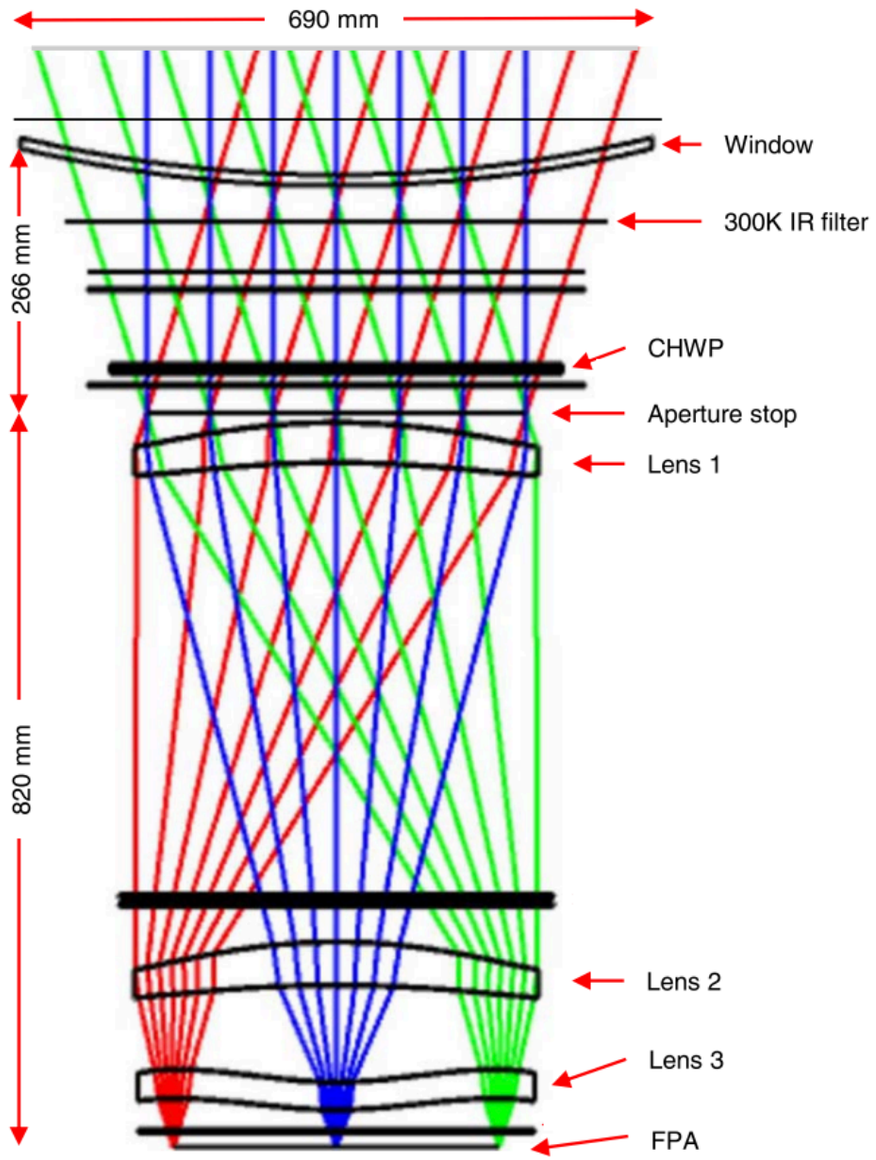

Why LAT + SATs ?

The large aperture telescope is optimized for high resolution measurement of the CMB small scales.
The small aperture telescopes are optimized for recovering the large scales of the CMB with a pristine control of systematic effects (they are very « simple » refractive telescopes, with optics cooled down at cryo temperature)

3 more SATs are being built (2 MF (with KIDs) UK, 1 LF Japan)

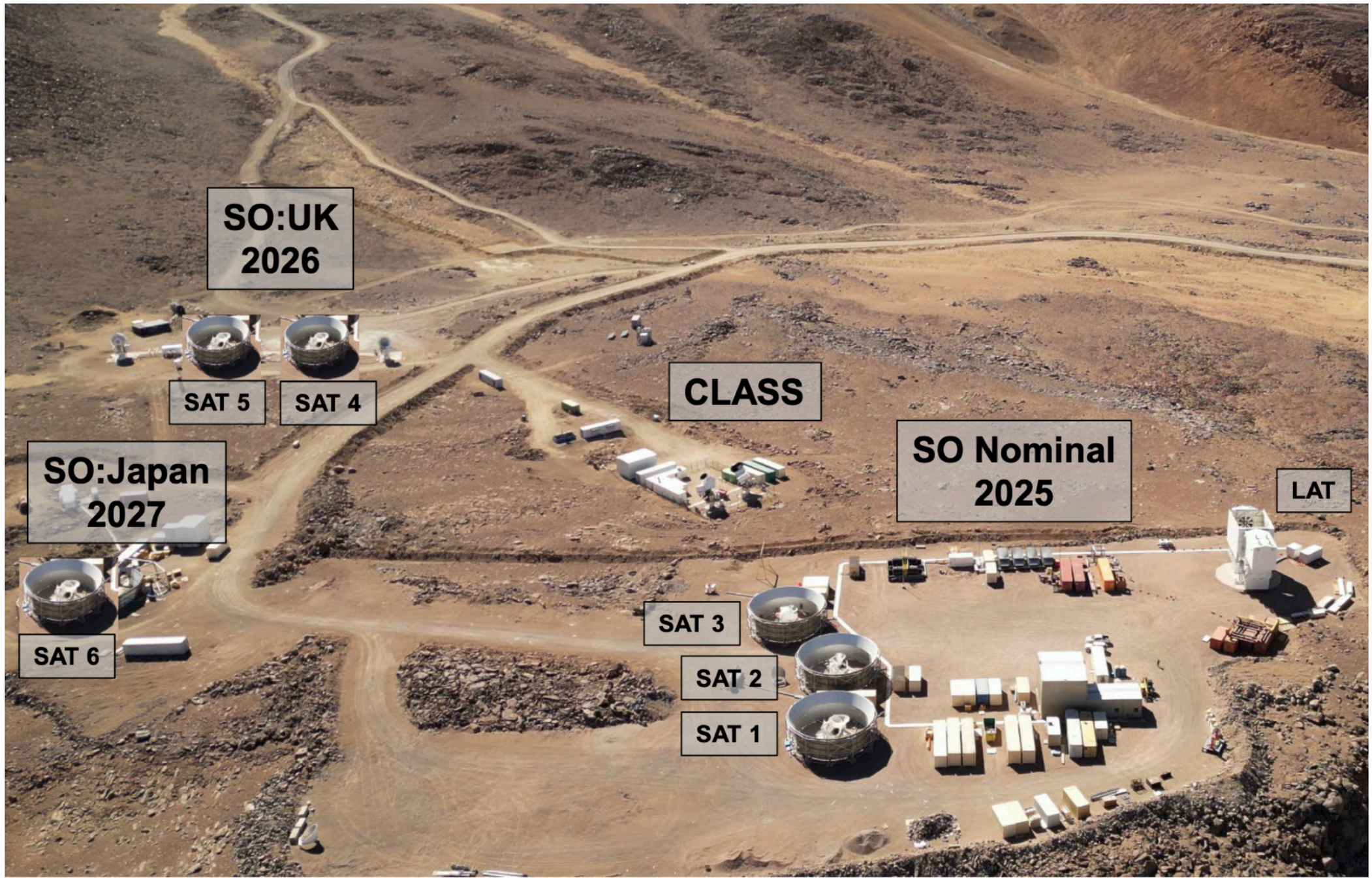

Discussion for a DOE contribution to SO (following the cancellation of S4)
+ a French contribution ?

SAT maps:

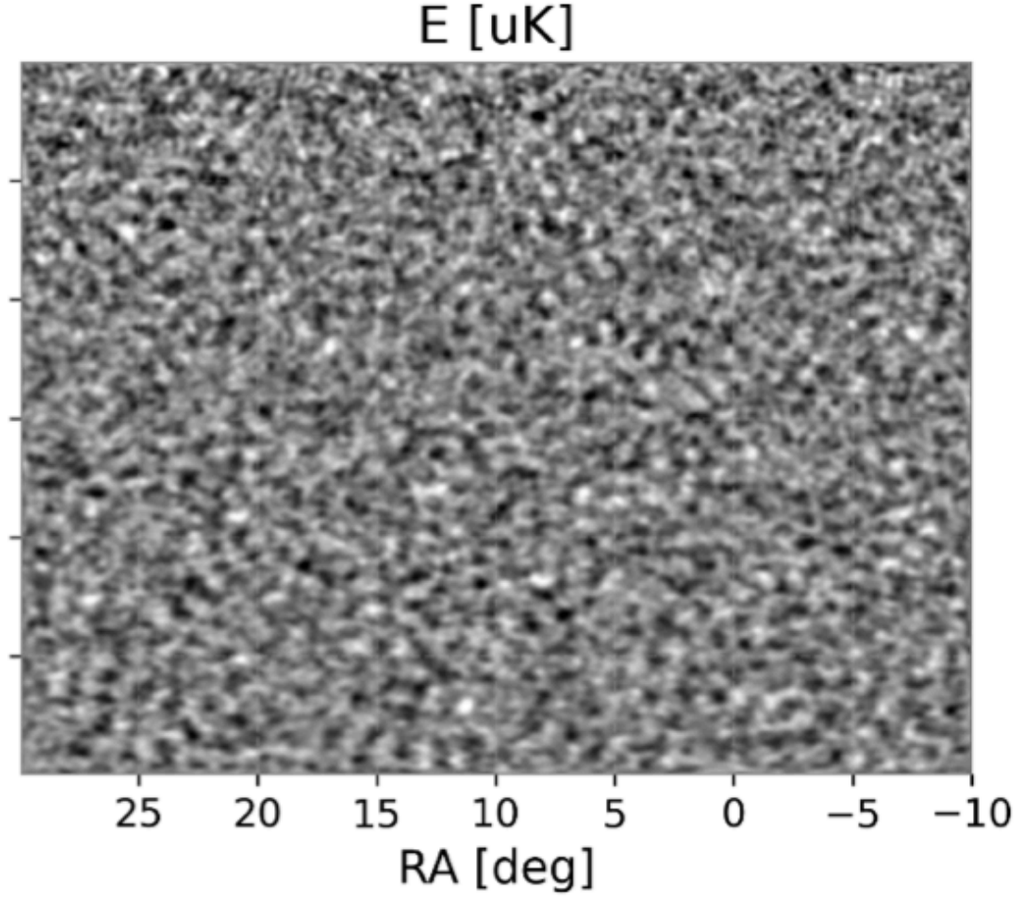

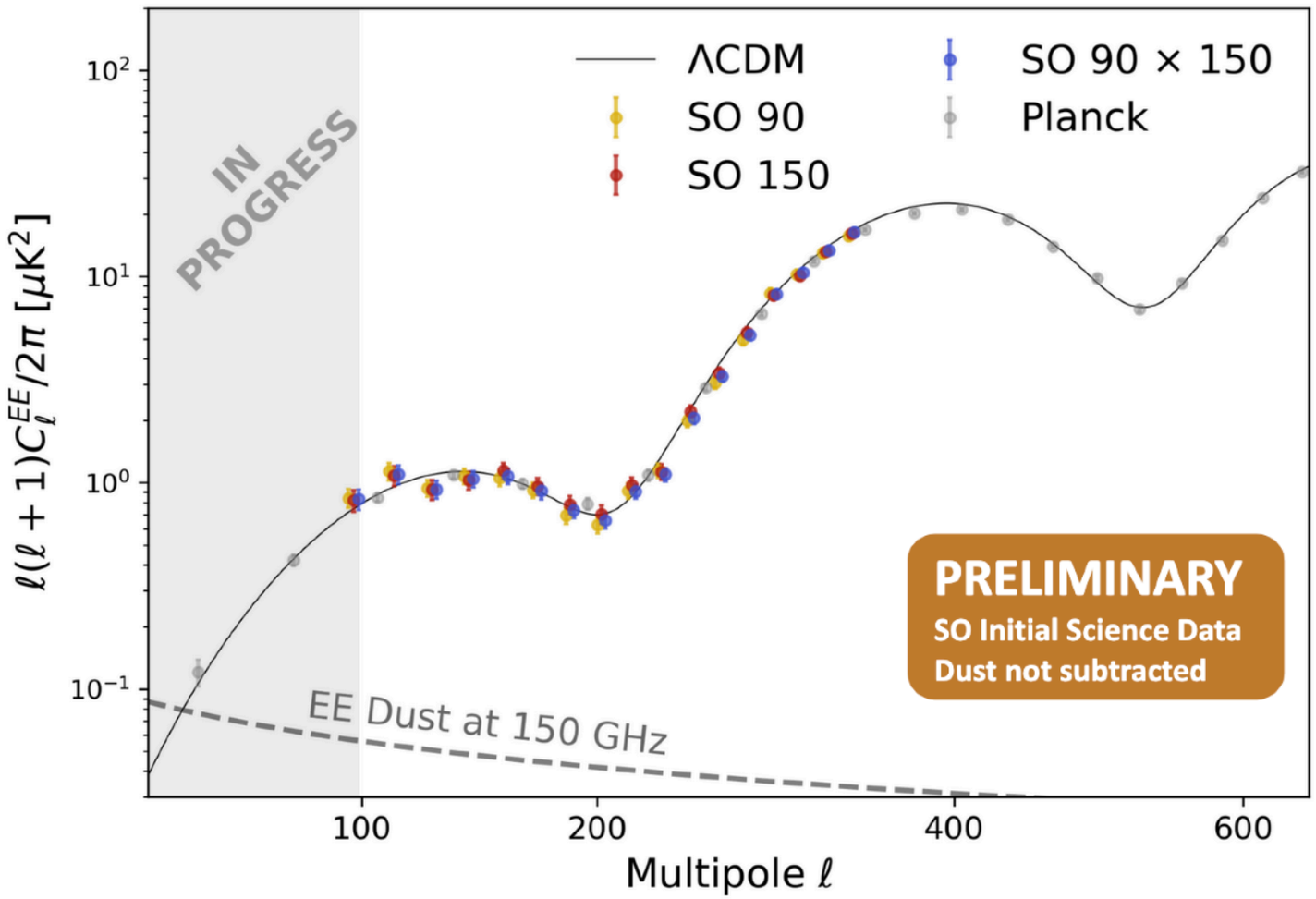

Plots from Susanna Azzoni for the SO collaboration

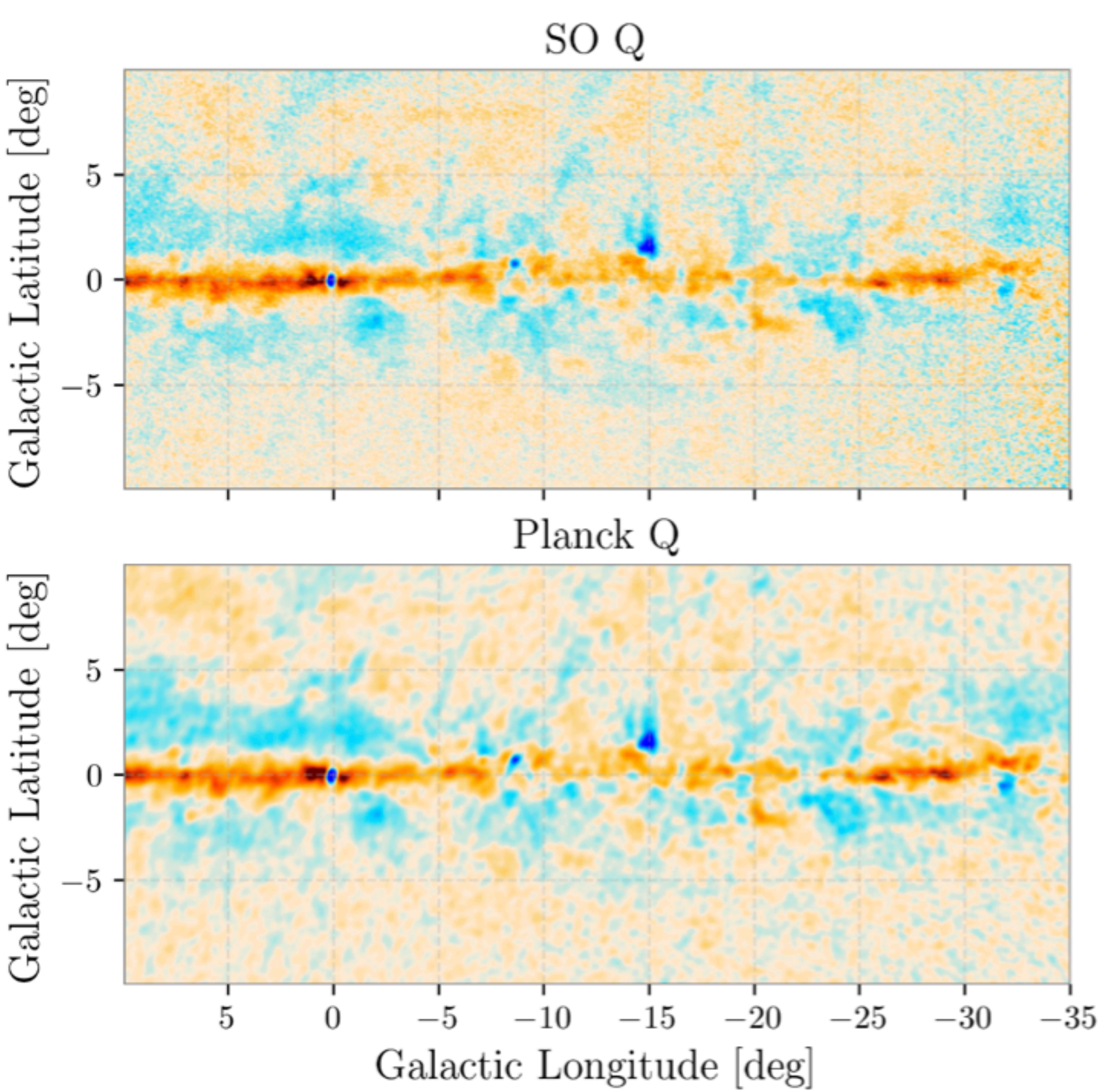
SO Q
Galactic Latitude [deg]
5
0
−5
Planck Q
Galactic Latitude [deg]
5
0
−5
5
0
−5
−10
−15
−20
−25
−30
−35
Galactic Longitude [deg]

What are we trying to do ?

100 sigma detection of the B modes power spectrum

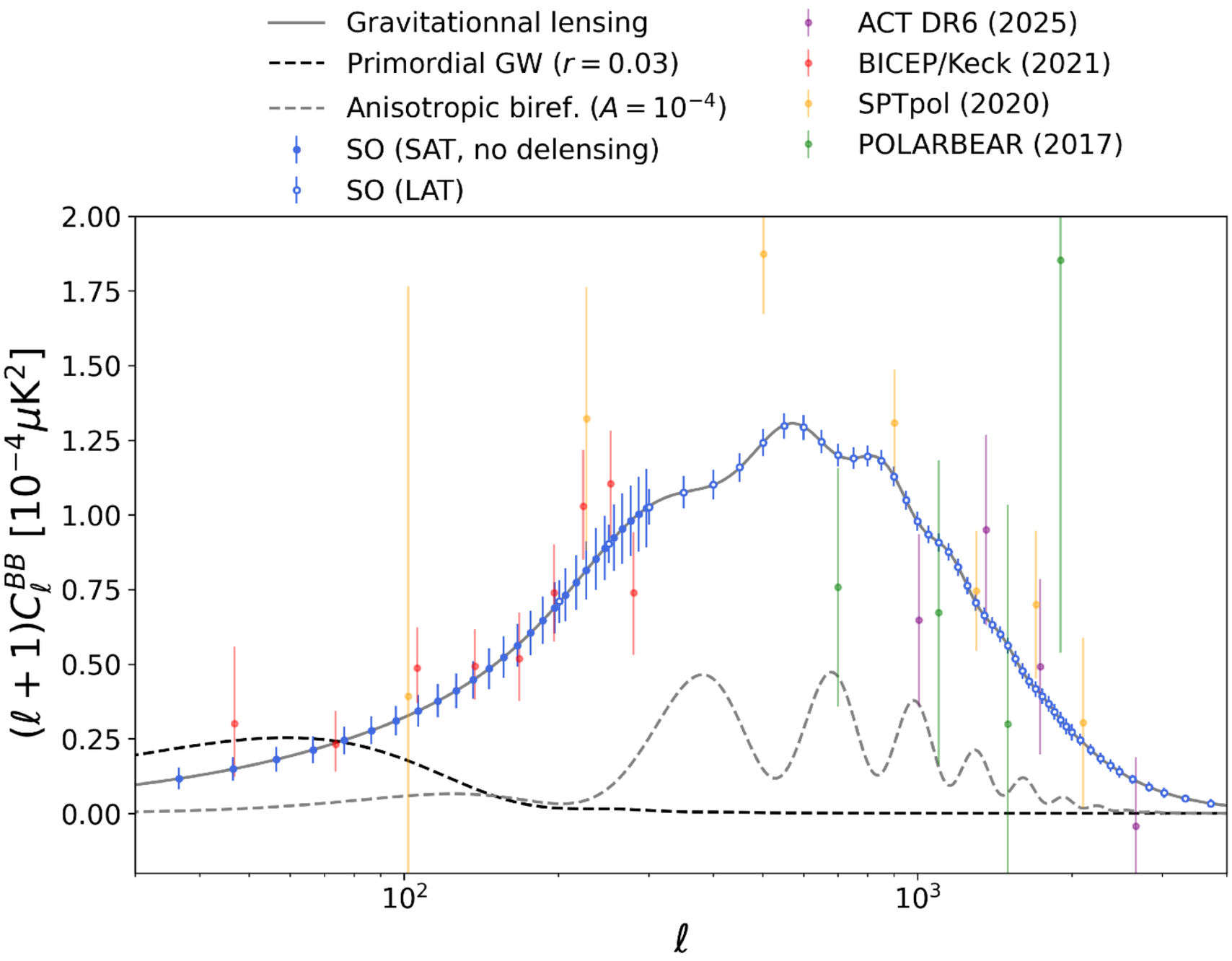

Target $\sigma(r) = 1 - 2 \times 10^{-3}$ after a 10 year survey

A very deep E mode measurement over 40% of the sky

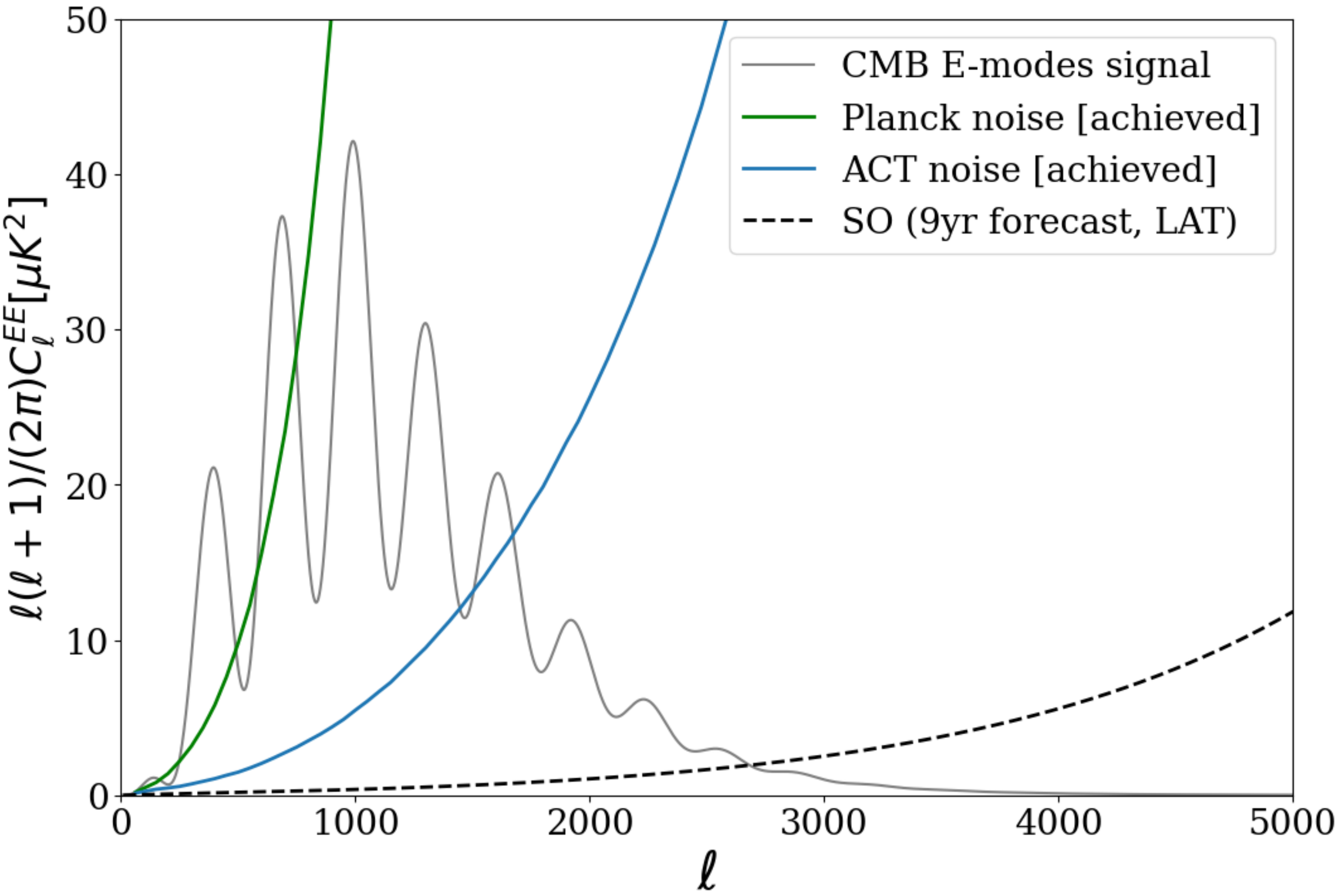

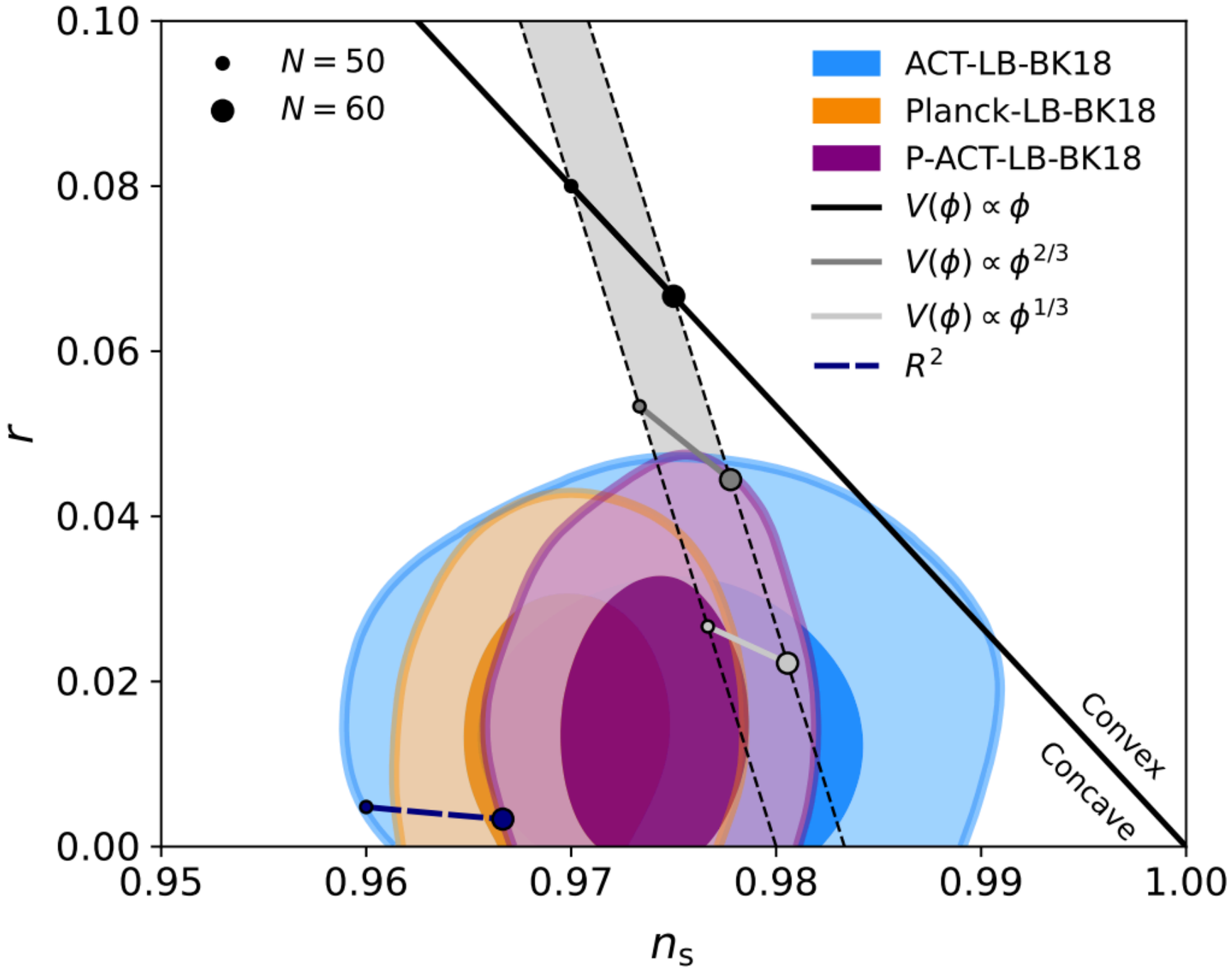

Improvement of a factor 2 in ns and a factor 3 in Neff uncertainties with respect to current CMB data

A wealth of cross correlation with large scale structure survey (Due to the unique location of SO)

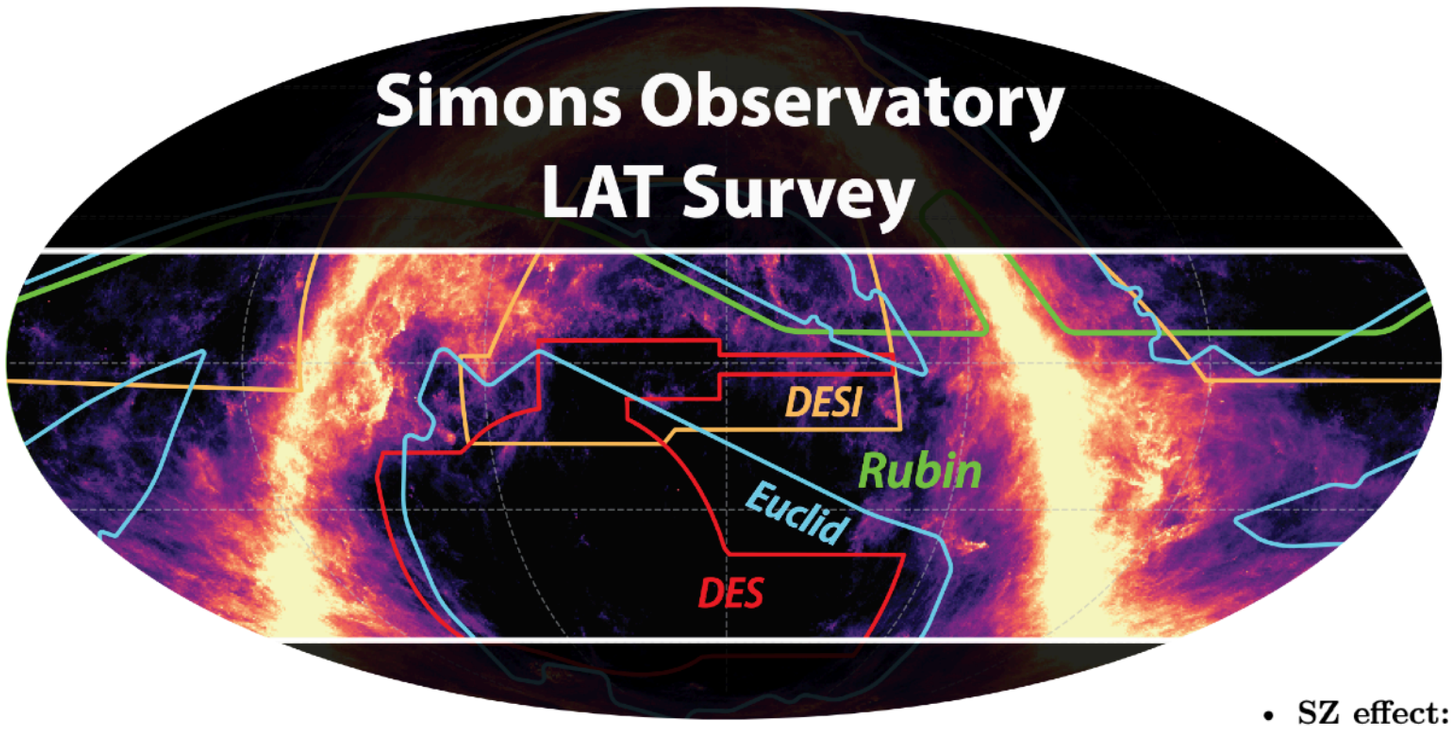

- **Lensing:**
  - High-redshift measurement of structure growth from the cross-correlation of Quaia quasars and CMB lensing from ACT DR6 and Planck PR4 (Villagra et al., 2025)
  - Structure growth measurements from the cross-correlation of DESI Legacy Imaging galaxies and CMB lensing from ACT DR6 and Planck PR4 (Qu et al., 2024)
  - Multi-probe cosmology with unWISE galaxies and ACT DR6 CMB lensing (Farren et al., 2025)
  - Cosmological constraints from the cross-correlation of DESI Luminous Red Galaxies with CMB lensing from Planck PR4 and ACT DR6 (Sailer et al., 2025)
  - Structure formation over cosmic time with a measurement of the cross-correlation of CMB Lensing and DESI Luminous Red Galaxies (Kim et al., 2024)
  - DR6 Gravitational Lensing and SDSS BOSS cross-correlation measurement and constraints on gravity with the EG statistic (Wenzl et al., 2025)
  - Cosmology from cross-correlations of unWISE galaxies and ACT DR6 CMB lensing (Farren et al., 2024)

- **SZ effect:**
  - Large-scale velocity reconstruction with the kinematic Sunyaev–Zel'dovich effect and DESI LRGs (McCarthy et al., 2024)
  - Backlighting extended gas halos around luminous red galaxies: kinematic Sunyaev-Zel'dovich effect from DESI Y1 x ACT (Guachalla et al., 2025)
  - Measurements of the Thermal Sunyaev-Zel'dovich Effect with ACT and DESI Luminous Red Galaxies (Liu et al., 2025)
  - Evidence for large baryonic feedback at low and intermediate redshifts from kinematic Sunyaev-Zel'dovich observations with ACT and DESI photometric galaxies (Hadzhiyska et al., 2025)

Reconstruct the growth of structure as a function of redshift

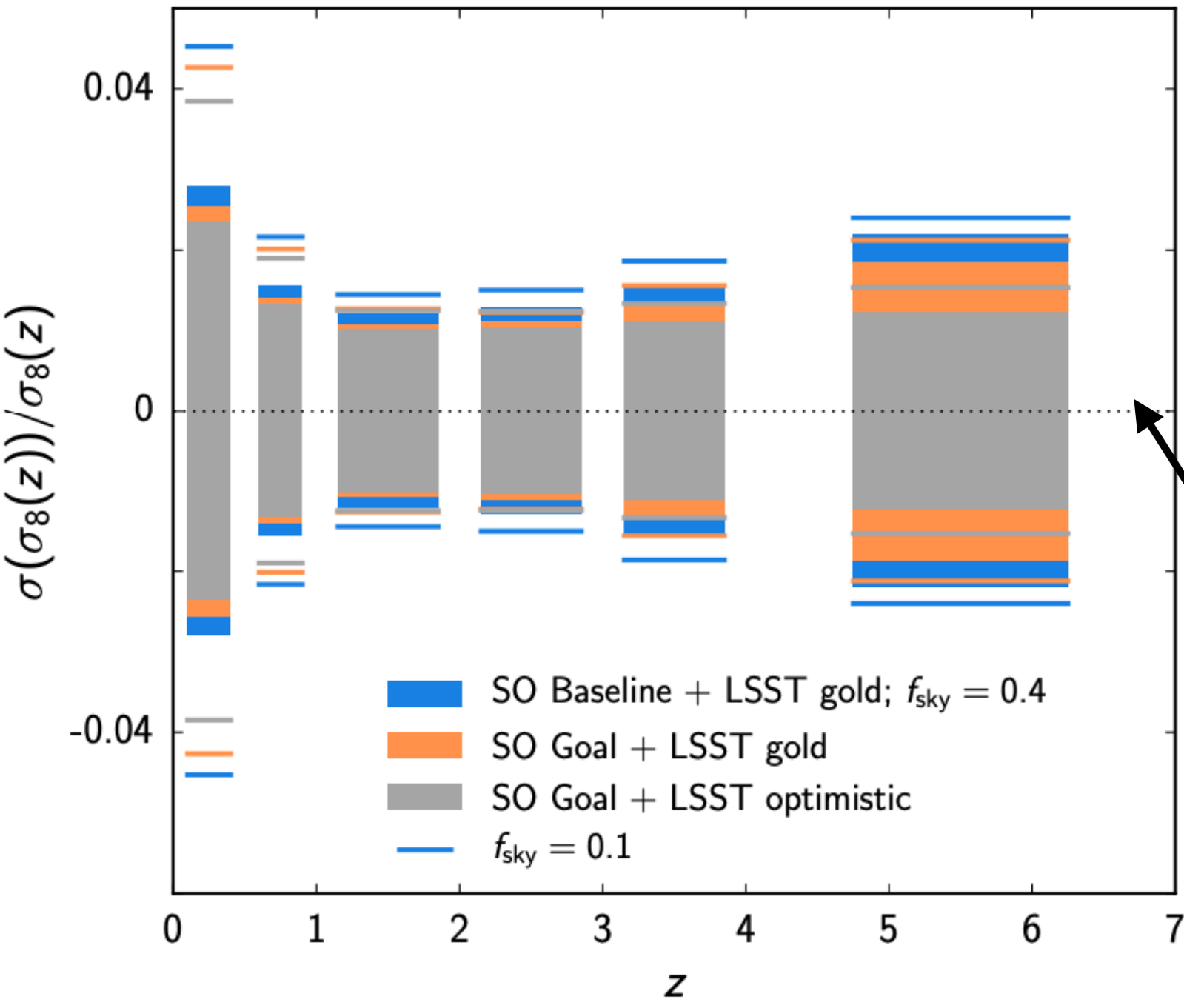

Relative uncertainties on sigma8 as a function of z of order few %

Understand how baryons behaves in galaxies

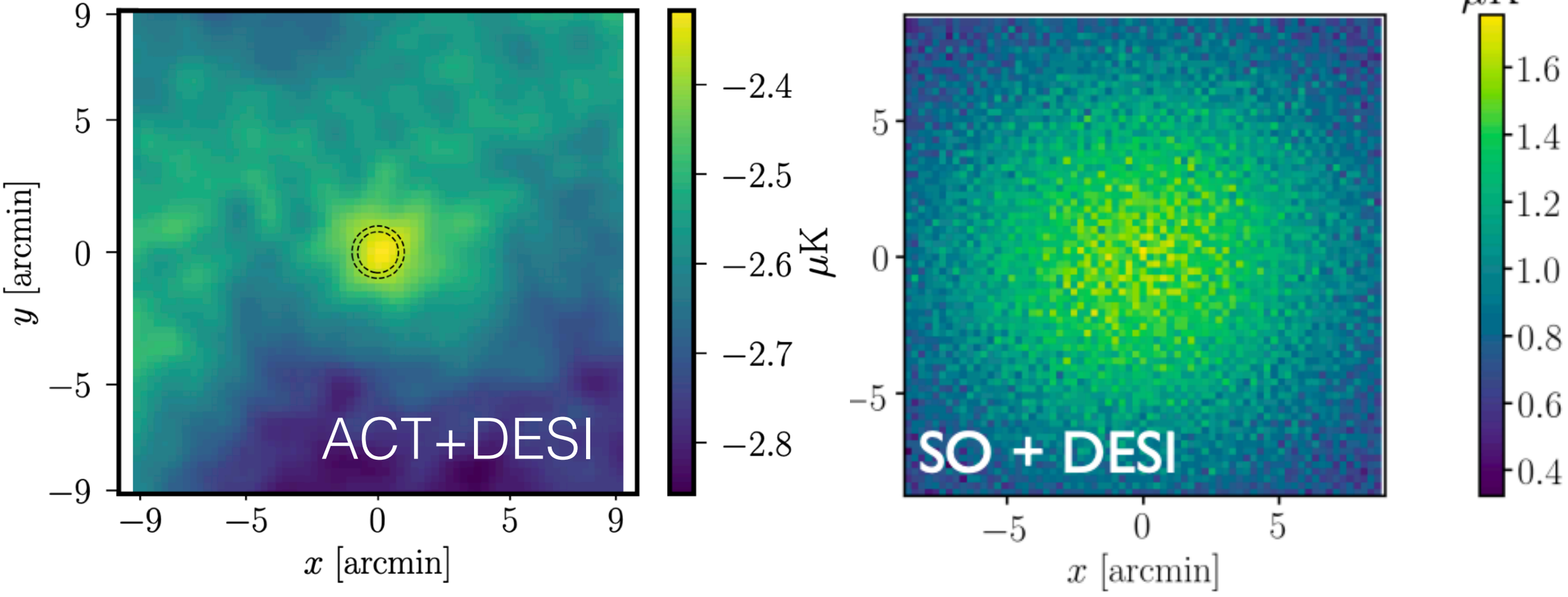

$$T_{\rm kSZ} \propto n_e(\vec{v}.\hat{n})$$

Conclusions

-The Simons Observatory has started collecting data, and the initial results look very promising!

-Major upgrades to the Large Aperture Telescope are planned for next year, and three additional Small Aperture Telescopes are currently under construction. Discussions with the DOE are also underway (+ possible French contribution).

-The CMB remains a unique window into physics at the

highest energy scales, through parameters such as r, ns and Neff, and is crucial to interpreting any hints of new physics emerging at low redshift.

-Strong and growing synergies with large-scale structure surveys

from lensing and SZ effect.

In many cases we combine SO forecasts with DESI and LSST. For LSST we consider an overlap area of $f_{\rm sky} = 0.4$ and two possible galaxy samples. First is the 'gold' sample, which has galaxies with a dust-corrected $i < 24.5$ magnitude cut after three years of LSST observations. This corresponds to 29.4 galaxies arcmin^{-2} and $n(z) \propto z^2 \exp[-(z/0.27)^{0.92}]$ following LSST Science Collaboration (2009) and Chang et al. (2013). Second, we consider a more optimistic LSST galaxy sample with dust-corrected $i < 27$ and a $S/N > 5$ cut with ten years of LSST observation, following Gorecki et al. (2014). In that sample we include a possible sample of Lyman-break galaxies at z=4–7, identified using the dropout technique (see Dunlop 2012 for a review), with a number density estimated by extrapolating recent Hyper Suprime-Cam (HSC) results (Ono et al. 2018, Harikane et al. 2017, following Schmittfull and Seljak 2018).

For DESI we include projected measurements of the baryon acoustic oscillation (BAO) scale, by imposing a prior on r_s/D_V at multiple redshifts, as described in Levi et al. (2013). Here, r_s is the sound horizon at decoupling and D_V is the volume distance. We consider the DESI Luminous Red Galaxy (LRG) catalog as providing the target galaxies for the SZ studies described in Sec. 7. In these forecasts we assume an overlap area of 9000 square degrees between SO and DESI ($f_{\rm sky} = 0.23$).

Throughout the paper we will retain two significant figures in many of our forecast errors to enable comparison of different experimental configurations. In the summary table we restrict errors to one significant figure.

Data Combinations

We make use of several external datasets and combinations.

Planck	$Planck^{\mathrm{TT/TE/EE}}$ + Sroll2
ACT	$\mathrm{ACT}^{\mathrm{TT/TE/EE}}$ + Sroll2
P-ACT	$\mathrm{ACT}^{\mathrm{TT/TE/EE}}$ + $Planck_{\mathrm{cut}}^{\mathrm{TT/TE/EE}}$ + Sroll2
W-ACT	$\mathrm{ACT}^{\mathrm{TT/TE/EE}}$ + $\mathrm{WMAP}^{\mathrm{TT/TE/EE}}$ + Sroll2
followed by	
-LB	when adding CMB lensing and BAO
-LS	when adding CMB lensing and SNIa
-LBS	when adding CMB lensing, BAO, and SNIa

- Sroll2 uses low-E data from Planck
- P-ACT uses Planck cut at 1000/600/600, with full ACT and Sroll2
- CMB Lensing is from ACT DR6 and Planck PR4
- BAO measurements from DESI Y1 as baseline, BOSS/eBOSS BAO data are used as cross-check in some cases
- Type Ia Supernovae from Pantheon+

BEYOND LCDM models

Exploration of extended cosmological models

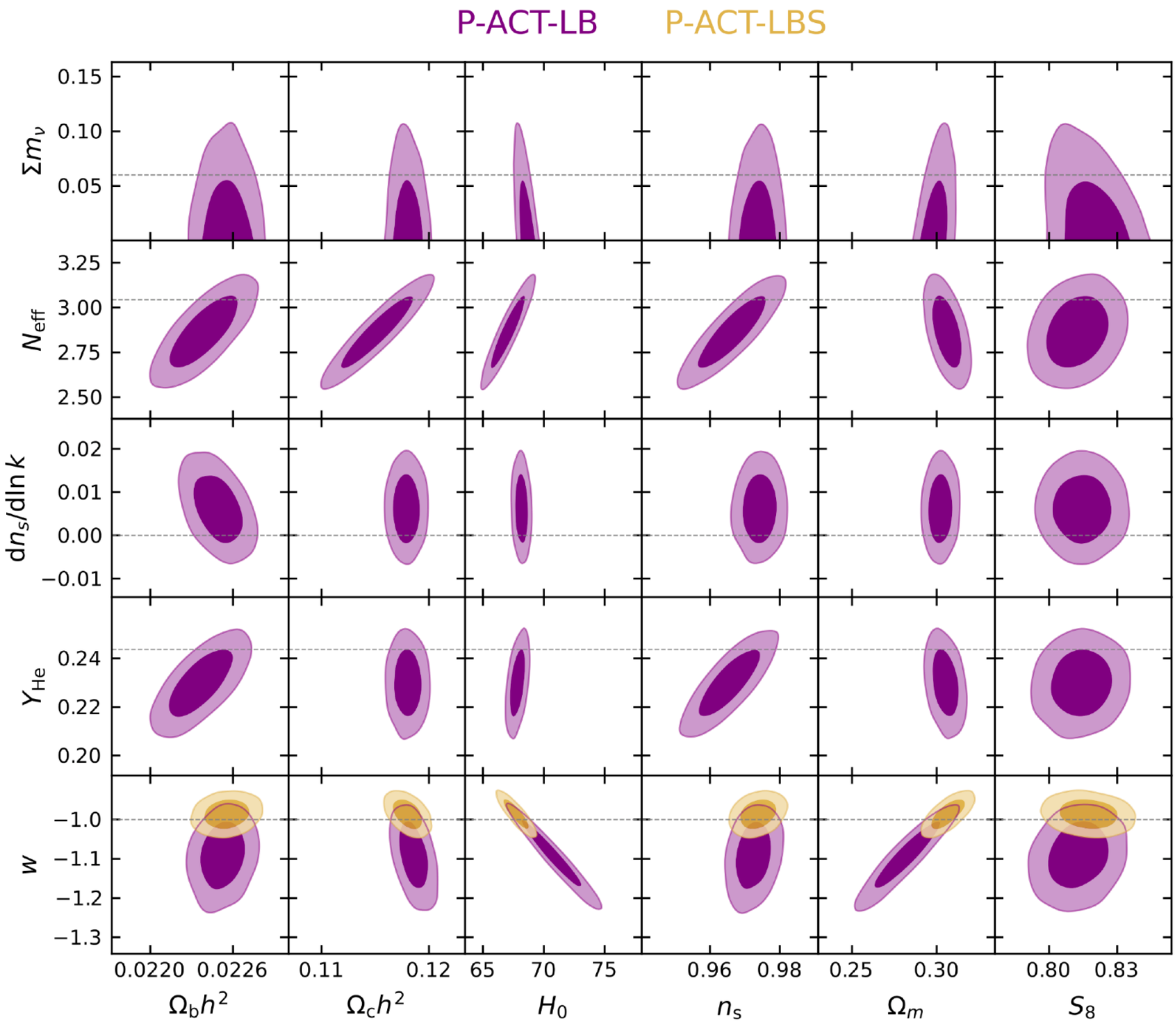

Exploration of extended cosmological models

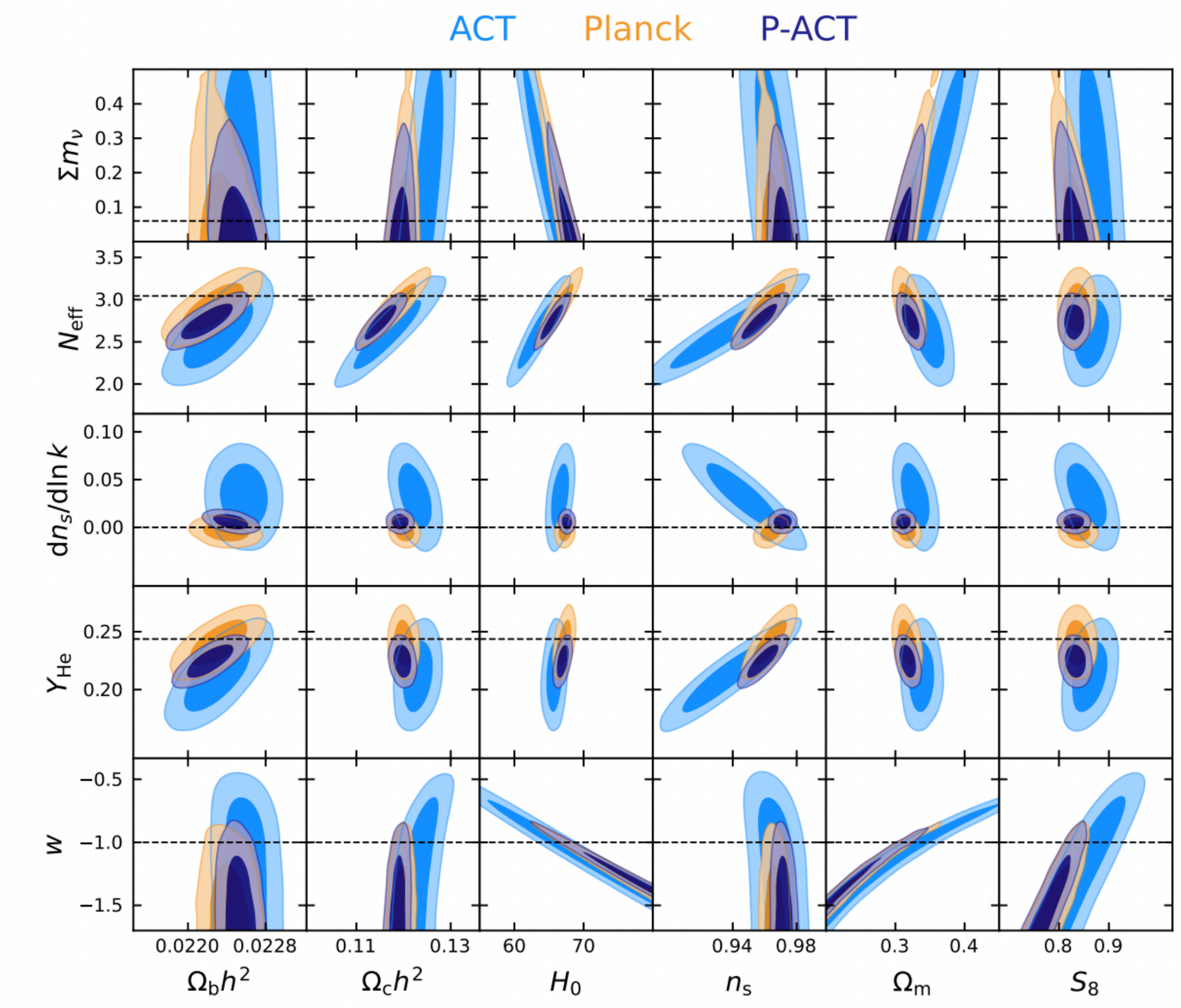

Primordial perturbations and inflation

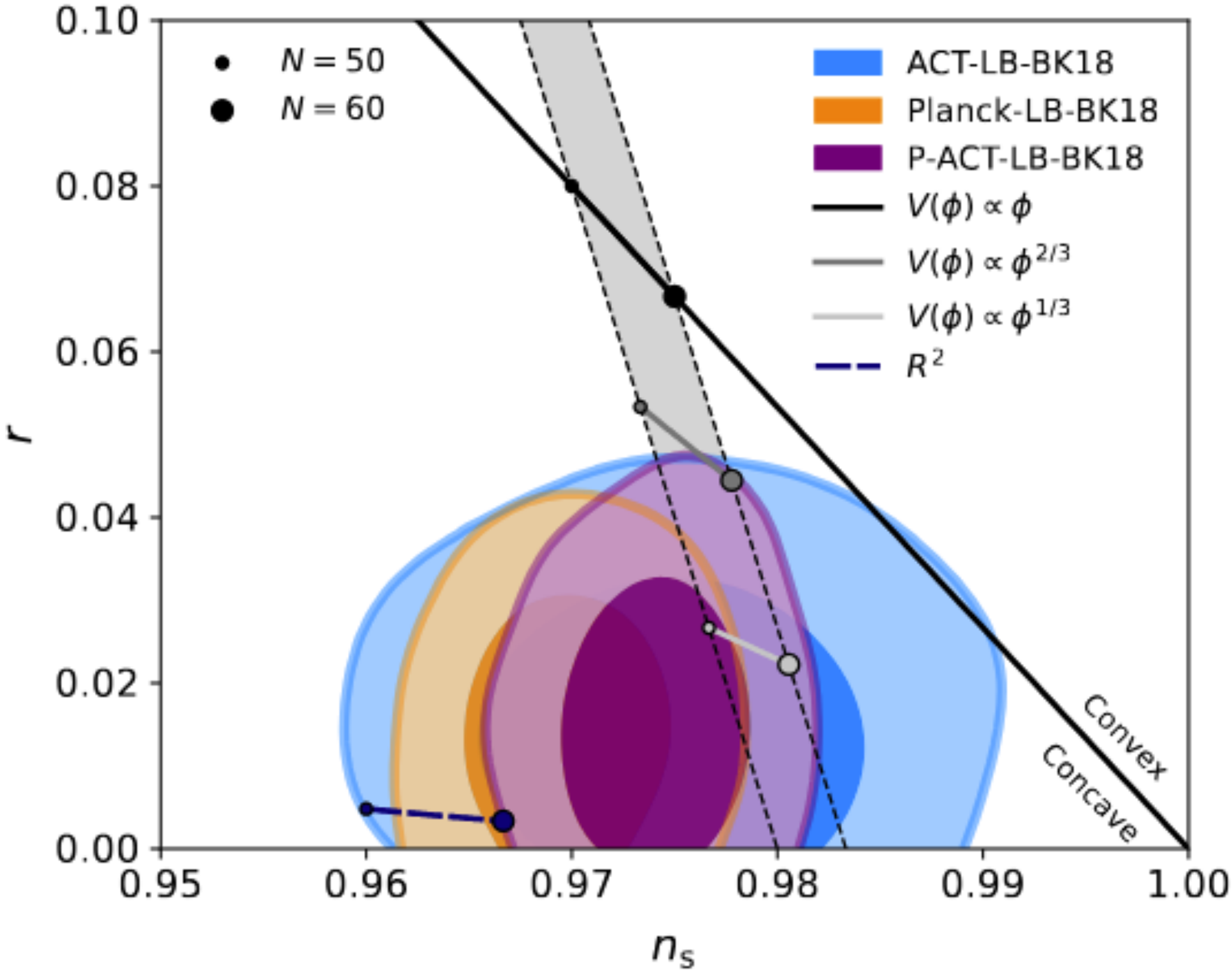

Information on inflation models from scalar spectral index

A_lens

model prediction. The PR3 analysis found $A_{\rm lens} > 1$ at the almost 3σ level (Planck Collaboration 2020d), with $A_{\rm lens} = 1.180 \pm 0.065$. Analyses of the NPIPE data, using larger fractions of sky, found lower departures of only 1.7σ for the CamSpec likelihood, with $A_{\rm lens} = 1.095 \pm 0.056$ (Rosenberg et al. 2022), or 0.75σ using the Hillipop likelihood, with $A_{\rm lens} = 1.039 \pm 0.052$. (Tristram et al. 2024). No excess lensing was observed in the ACT DR4 data, with $A_{\rm lens} = 1.01 \pm 0.11$ (Aiola et al. 2020).

the ACT power spectrum data:

$$
\begin{aligned}
A_{\rm lens} &= 1.007 \pm 0.057 \quad \text{(ACT)} \\
&= 1.08^{+0.10}_{-0.12} \quad \text{(ACT-TT)} \\
&= 1.24^{+0.18}_{-0.22} \quad \text{(ACT-TE)} \\
&= 0.89^{+0.10}_{-0.23} \quad \text{(ACT-EE)} \\
A_{\rm lens} &= 1.043 \pm 0.049 \quad \text{(W-ACT)},
\end{aligned}
$$

of $A_{\rm lens}$ with the matter density. In the *Planck* PR3 data an oscillatory residual for TT in the range $1000 < \ell < 2000$ was identified as driving the preference for the enhanced lensing; we do not see evidence for this in the ACT data. For P-ACT we find $A_{\rm lens} = 1.081 \pm 0.043$ which is consistent with e.g., Rosenberg et al. (2022).

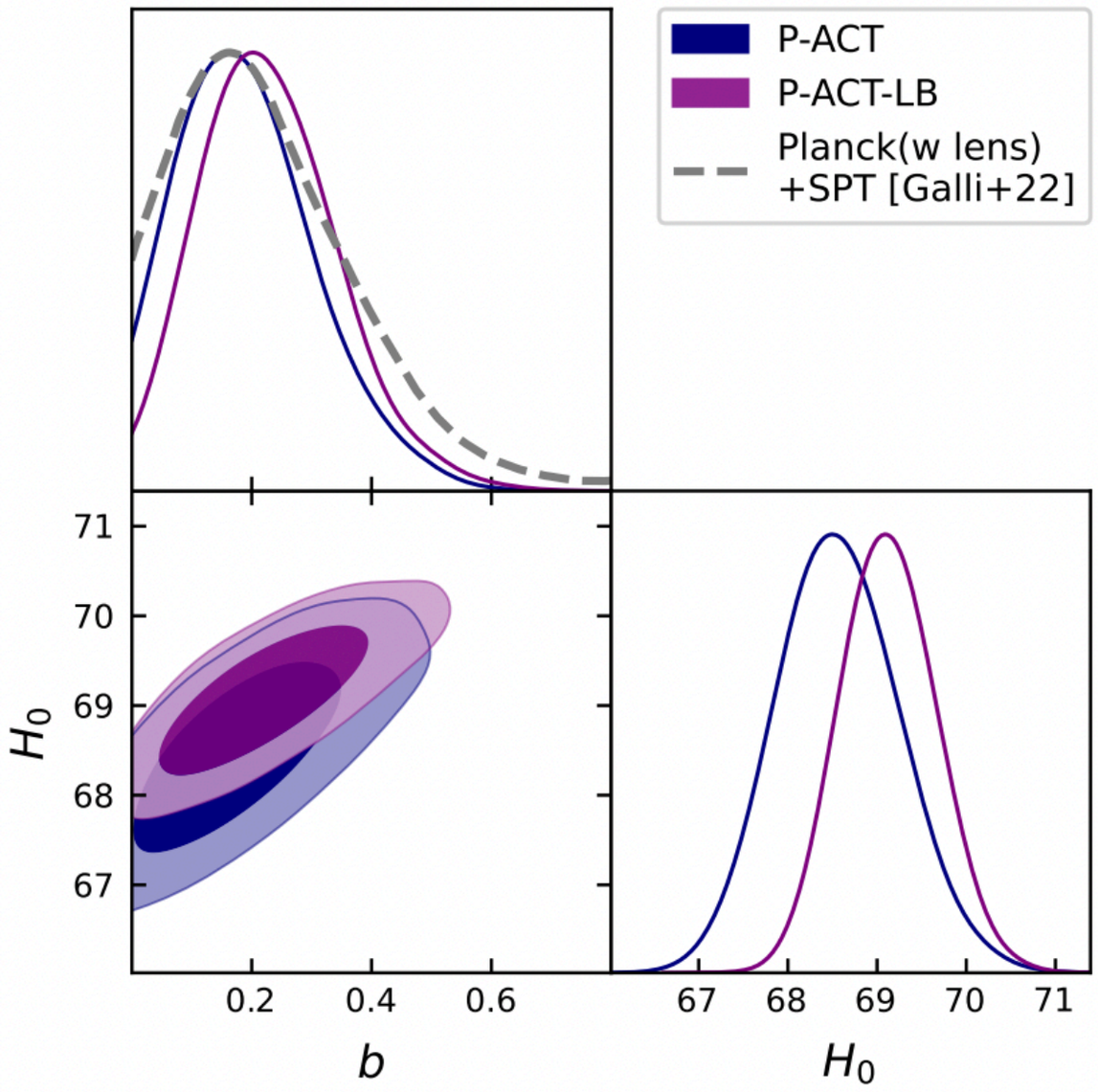

Figure 15. Constraints on the variance b of the small-scale baryon density distribution at recombination from P-ACT (navy) and P-ACT-LB (purple), compared with the latest results from *Planck* (including CMB lensing) combined with SPT small-scale polarization (gray dashed line). Primordial magnetic fields would induce baryon clumping on small scales, and hence $b > 0$. No evidence of clumping is seen in our analysis.

Varying m_e + curvature

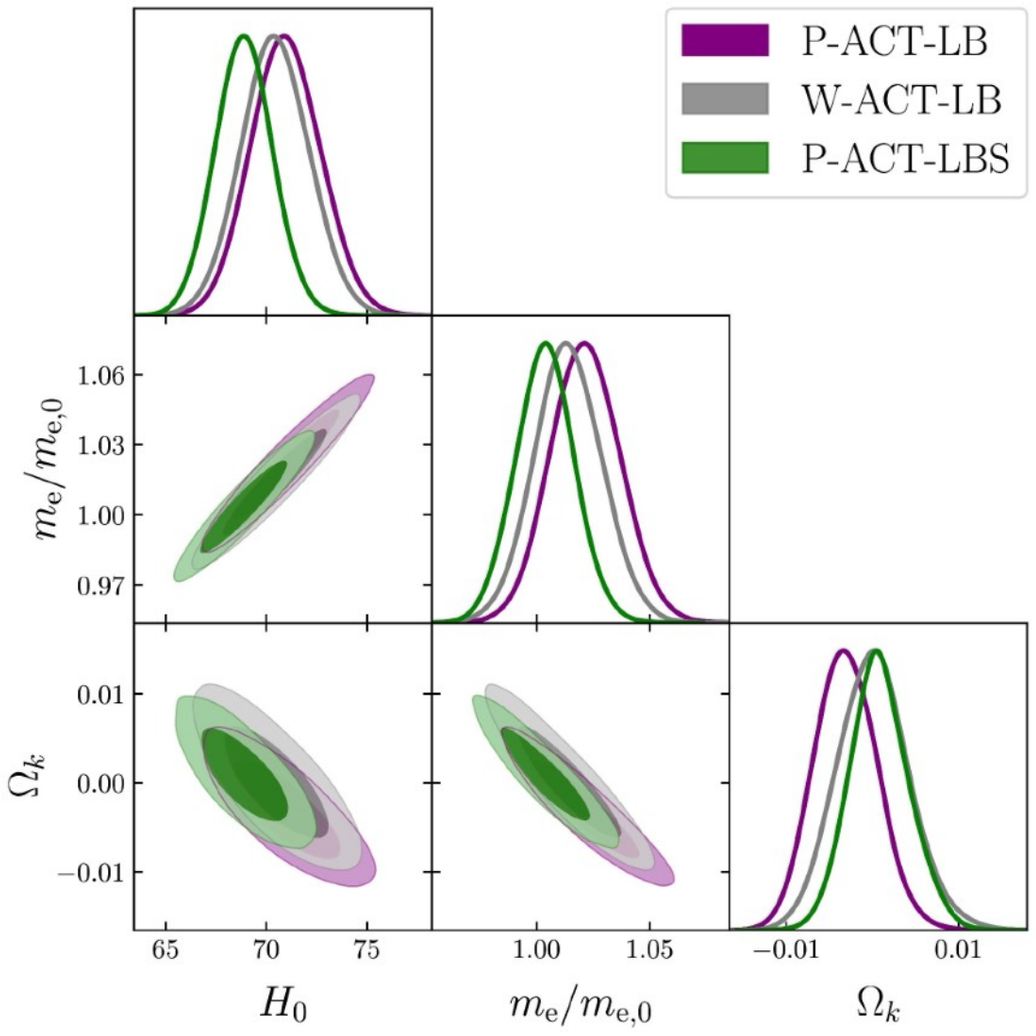

Particle cosmology

No evidence for new light, relativistic species

Free-streaming:

N_{eff} = 2.86 ± 0.13 (68%, P-ACT-LB)
N_{eff} = 2.89 ± 0.11 (68%, P-ACT-LB-BBN)

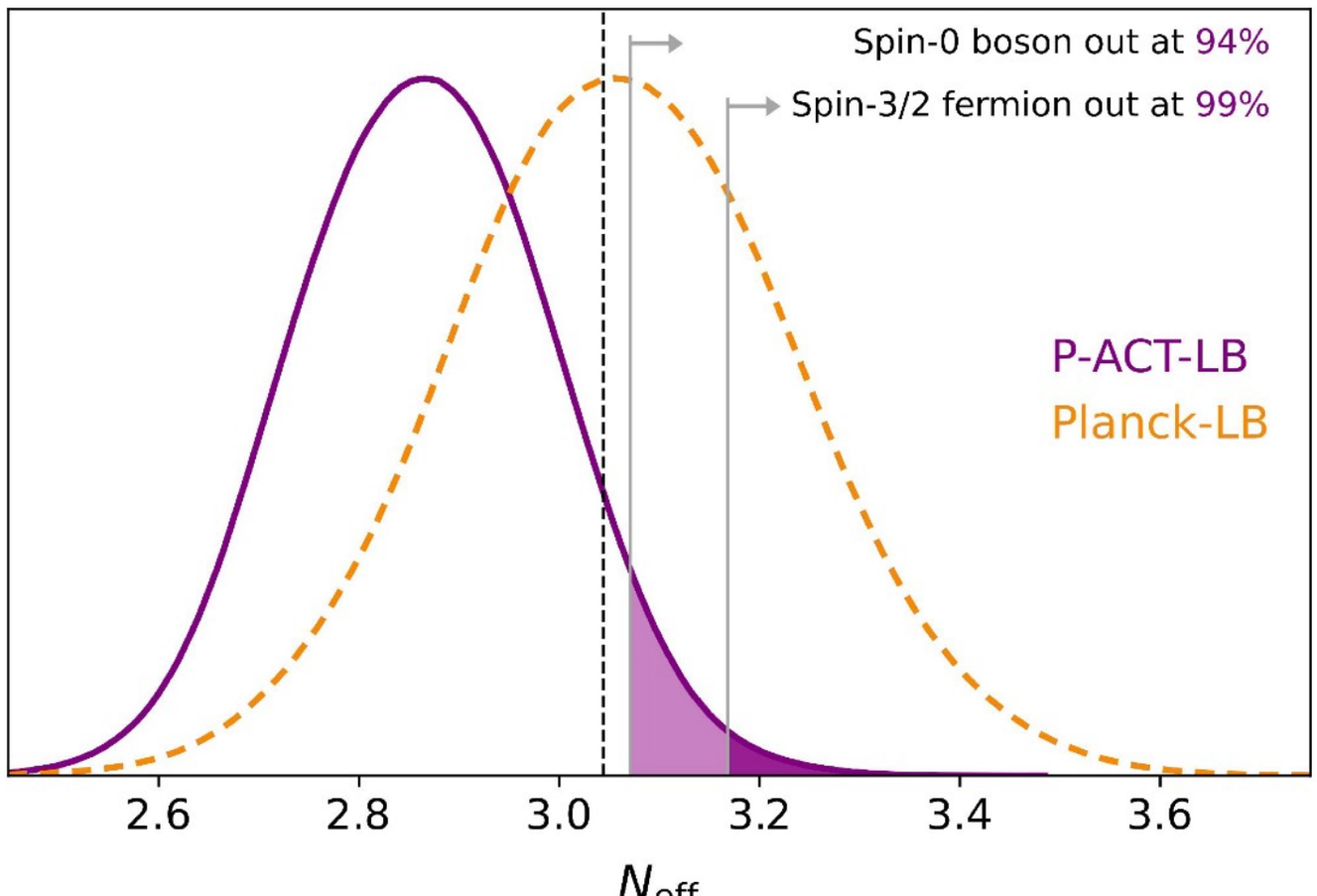

in the acoustic peaks (Bashinsky & Seljak 2004). Combining the *Planck* legacy CMB with *Planck* CMB lensing and BOSS BAO, the neutrino number is measured to be $N_{\rm eff} = 2.99 \pm 0.17$ at 68% CL (Planck Collaboration 2020c), or $N_{\rm eff} = 3.06 \pm 0.17$ at 68% CL when we evaluate this estimate using Planck-LB.

With the new ACT DR6 spectra we find $N_{\rm eff} = 2.60^{+0.21}_{-0.29}$ at 68% CL, combining into

$$\begin{aligned} N_{\rm eff} &= 2.73 \pm 0.14 \quad (68\%, \text{P-ACT}), \\ &= 2.86 \pm 0.13 \quad (68\%, \text{P-ACT-LB}), \end{aligned} \tag{30}$$

Particle cosmology

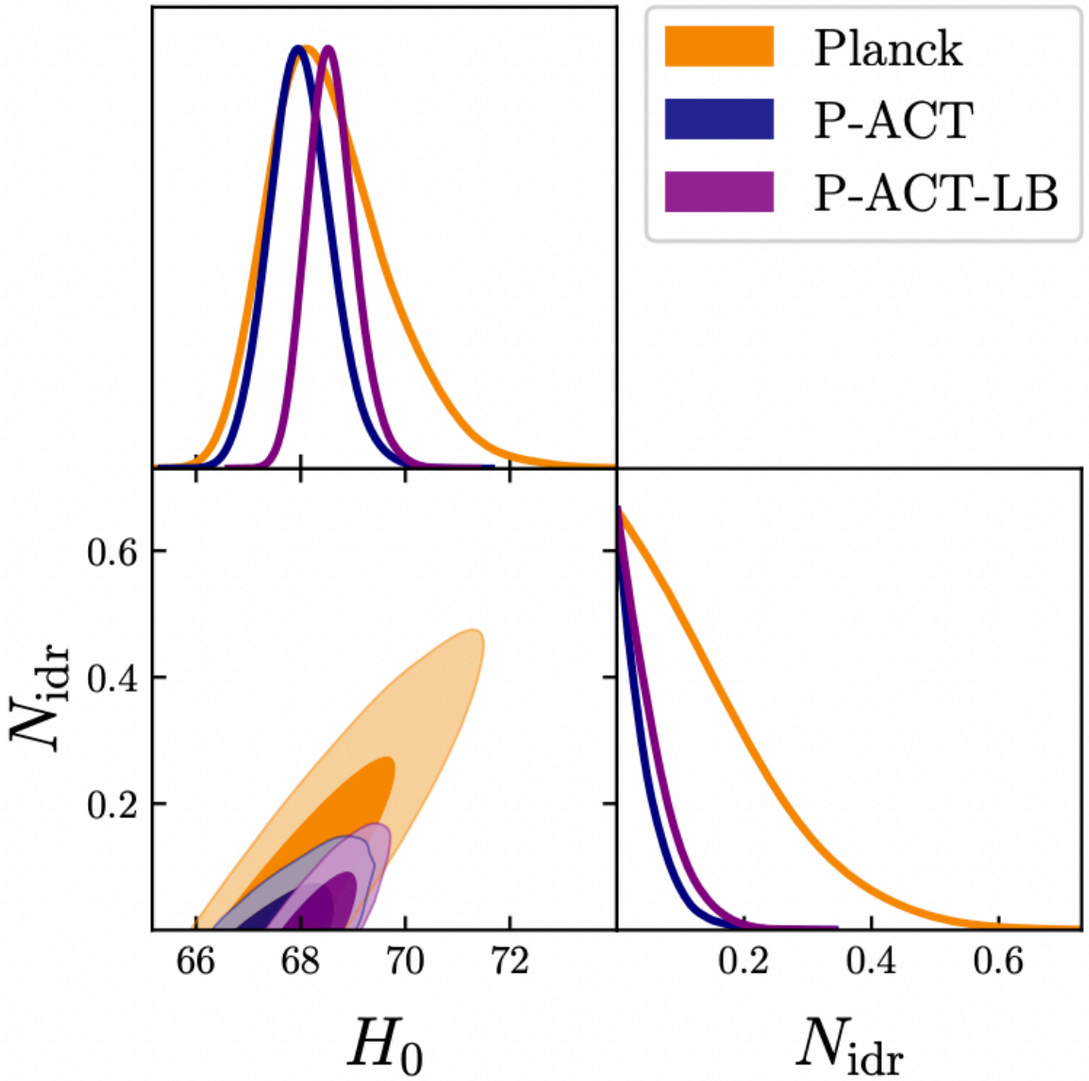

Figure 34. Constraints on the number of strongly self-interacting dark relativistic species, $N_{\rm idr}$. The addition of ACT DR6 spectra improves the constraint from *Planck* by more than a factor of three (navy versus orange) and notably disfavors values of H_0 above 70 km/s/Mpc that are allowed by *Planck* alone. Inclusion of CMB lensing and DESI BAO data (purple) slightly weakens the SIDR upper limit due to small shifts in the best-fit model parameters, but nevertheless further tightens the H_0 posterior. These are the tightest bounds on SIDR obtained to date.

Pre- and modified recombination physics

No evidence for an early dark energy (EDE) component:

A mild hint (2-3σ) of EDE was seen in ACT DR4 (Hill+2022); the new ACT DR6 spectra show that this was a statistical fluctuation.

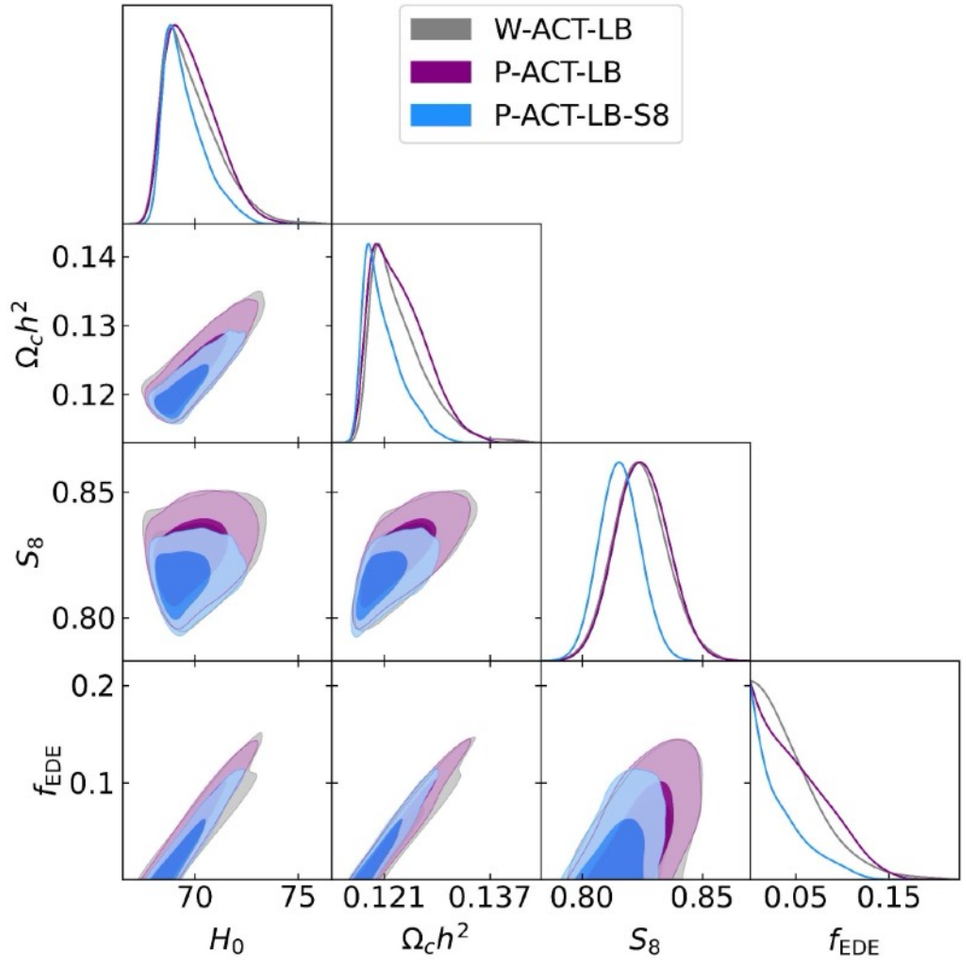

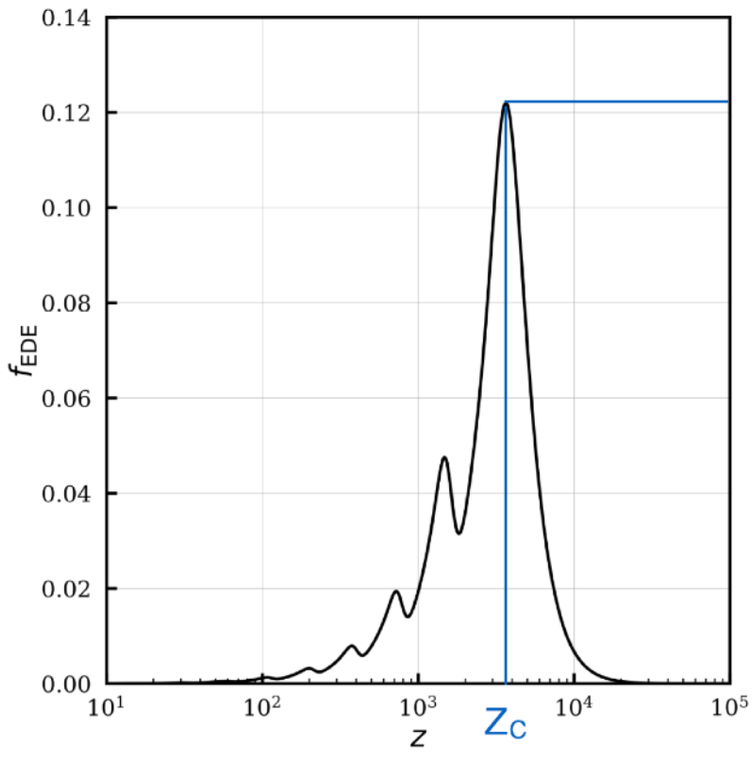

Maximal contribution:

$$f_{\rm EDE}(z_c) \equiv (\rho_{\rm EDE}/3M_{pl}^2H^2)|_{z_c}$$

which occurs at redshift z_c

Final parameter: $\theta_i = \phi_i/f$ (initial field displacement)

→ $\{f_{\rm EDE}, z_c, \theta_i\}$

	$\Delta\chi^2$	Pref. in σ	$H_0^{\rm (EDE)}$	$f_{\rm EDE}$	$\log_{10} z_c$
ACT	≈ 0.0	0.0	66.5	0.012	3.00
W-ACT	1.9	0.5	69.9	0.089	3.55
P-ACT	4.3	1.2	70.4	0.091	3.56
W-ACT-LB	2.9	0.8	70.2	0.070	3.52
P-ACT-LB	6.6	1.7	71.2	0.093	3.56

Table 2. The $\Delta\chi^2 = \chi^2_{\Lambda\rm CDM} - \chi^2_{\rm EDE}$ from the `MFLike` likelihood MAP points for the $n = 3$ EDE model compared to ΛCDM for each dataset combination, and preference (in units of σ) for EDE over ΛCDM using the likelihood-ratio test statistic. The values for H_0, $f_{\rm EDE}$, and $\log_{10} z_c$ in the MAP EDE model are also reported. The data show no significant preference for non-zero EDE. For ACT alone, the MAP χ^2 for EDE is indistinguishable from that for ΛCDM within our numerical precision, indicating that adding EDE parameters does not improve the fit at all in this case.

Neutrinos

We find no evidence for non-zero neutrino masses:

$\Sigma m_\nu < 0.082$ eV (95%, P-ACT-LB)

$\Sigma m_\nu < 0.083$ eV (95%, W-ACT-LB)

with significant contribution from DESI BAO

$\Sigma m_\nu < 0.13$ eV (95%, P-ACT-LB$_{BOSS}$)

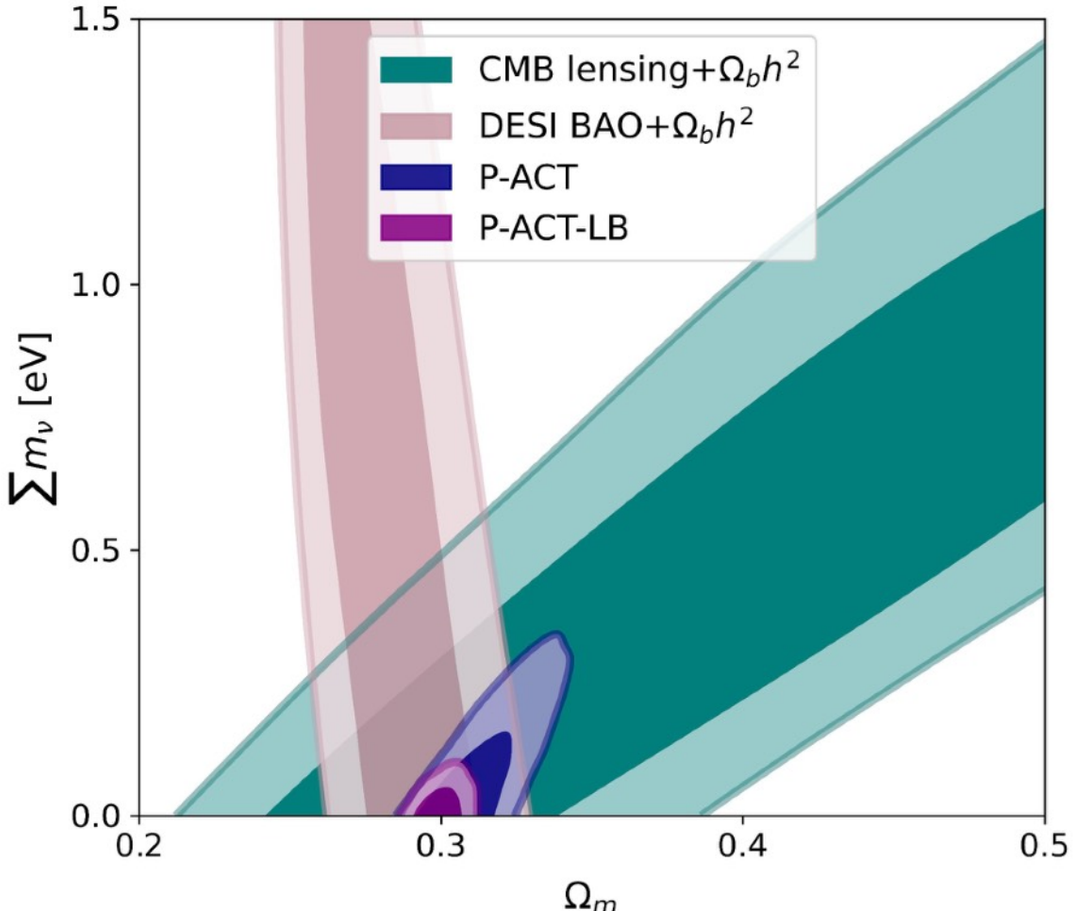

Particle astrophysics

We also find the abundances of primordial elements to be consistent with standard BBN.

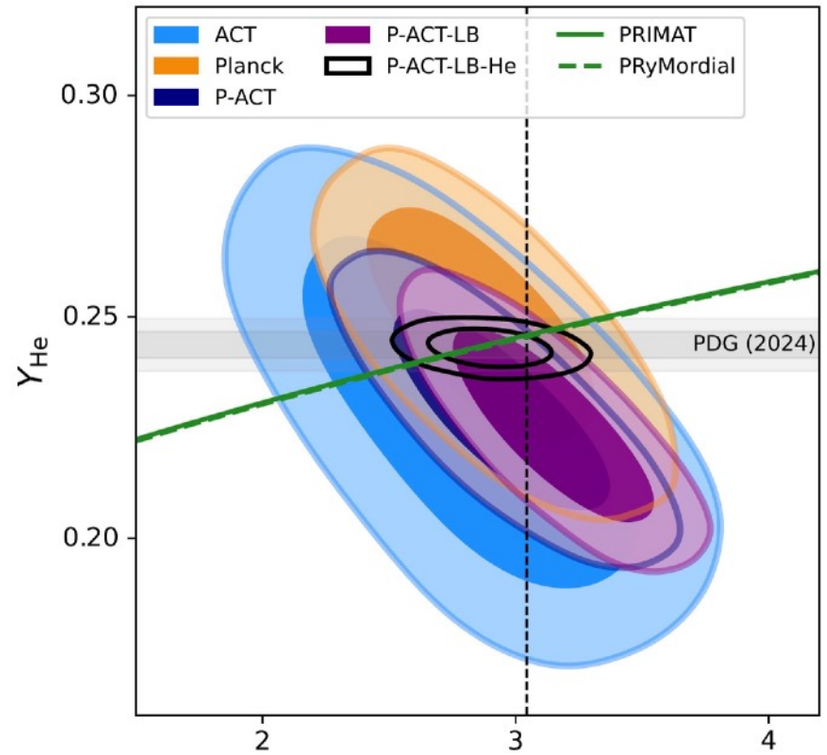

We find dark matter to follow the standard CDM paradigm, with no evidence for scattering with baryons, self-annihilation, contribution from axion-like particles, or scattering off a dark radiation component.

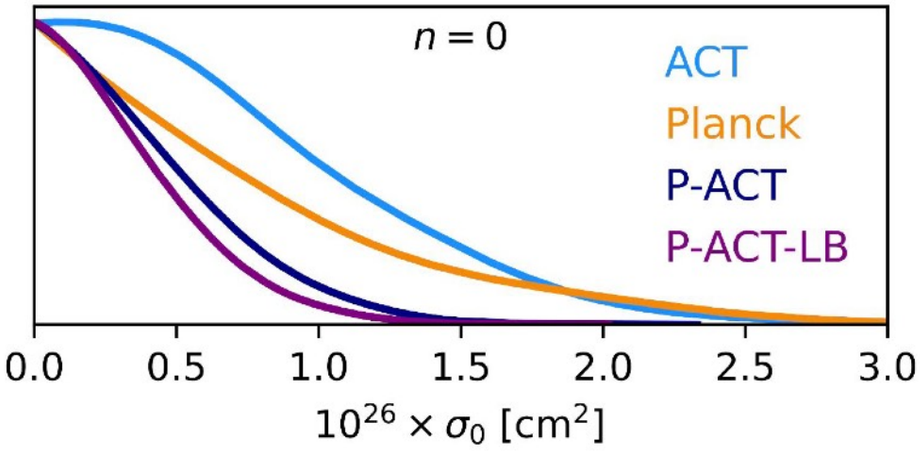

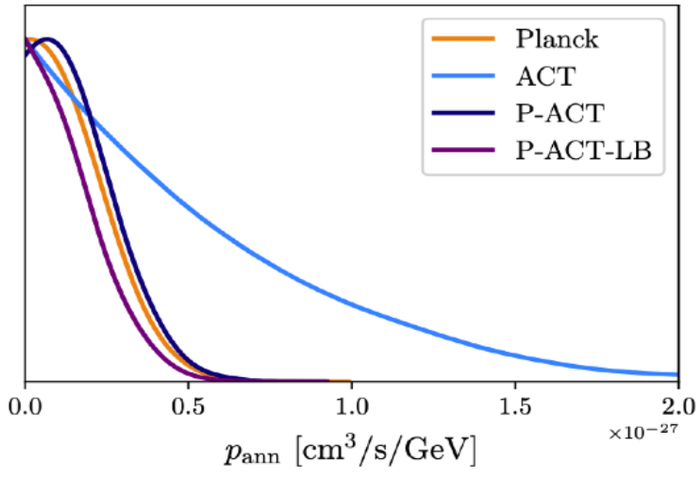

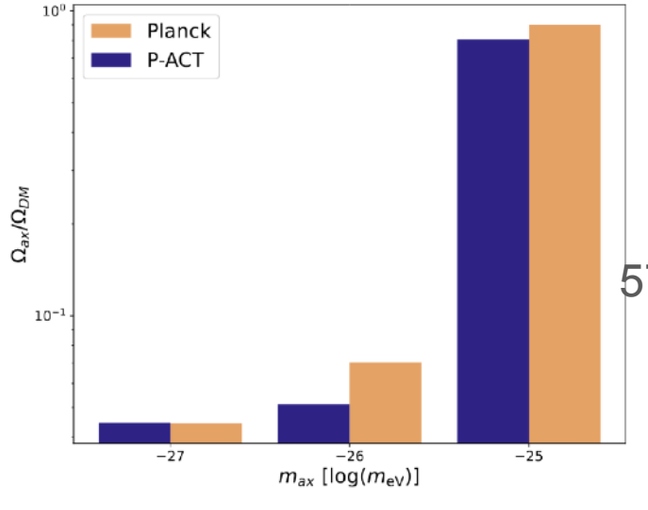

Late-time physics: dark energy

From primary CMB data, we find no evidence for non-standard dark energy; hints of non-standard evolution are driven by low-redshift data and consistent with previous analyses of DESI and SNIa data.

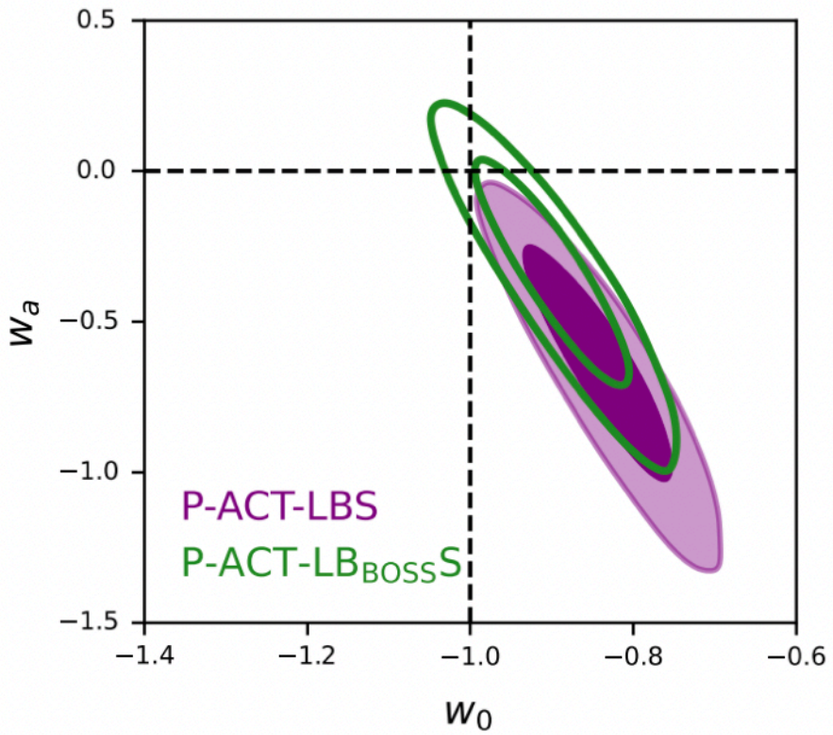

Figure 37. Constraints on the dark energy equation of state parameters, varying both today's value, w_0, and its time variation, w_a. Similar to other studies, we find that DESI drives a preference for time-varying dark energy (compared to the dashed ΛCDM line), which is relaxed when considering BOSS BAO instead (green contours). The CMB contribution to this measurement is sub-dominant, apart from breaking parameter degeneracies, with Planck, W-ACT, and P-ACT giving similar results.

P-ACT-LBS consistent with Λ at 2.2σ [P-LBS (in)consistent with Λ at 2.5σ (DESI+2024)]

$$\left.\begin{aligned} w_0 &= -0.837 \pm 0.061 \\ w_a &= -0.66^{+0.27}_{-0.24} \end{aligned}\right\} \quad (68\%,\ \text{P-ACT-LBS})$$

Late-time physics: modified growth

We also see no evidence of modified growth, e.g., due to beyond-GR gravity (modulo two slightly outlying fσ$_8$ measurements at very low redshifts).

$$f(a) = \Omega_m^{\gamma}(a)$$

$$\left.\begin{aligned} \gamma &= 0.663 \pm 0.052 \\ S_8 &= 0.799 \pm 0.012 \end{aligned}\right\} \ (68\%,\ \text{P-ACT-LB})$$

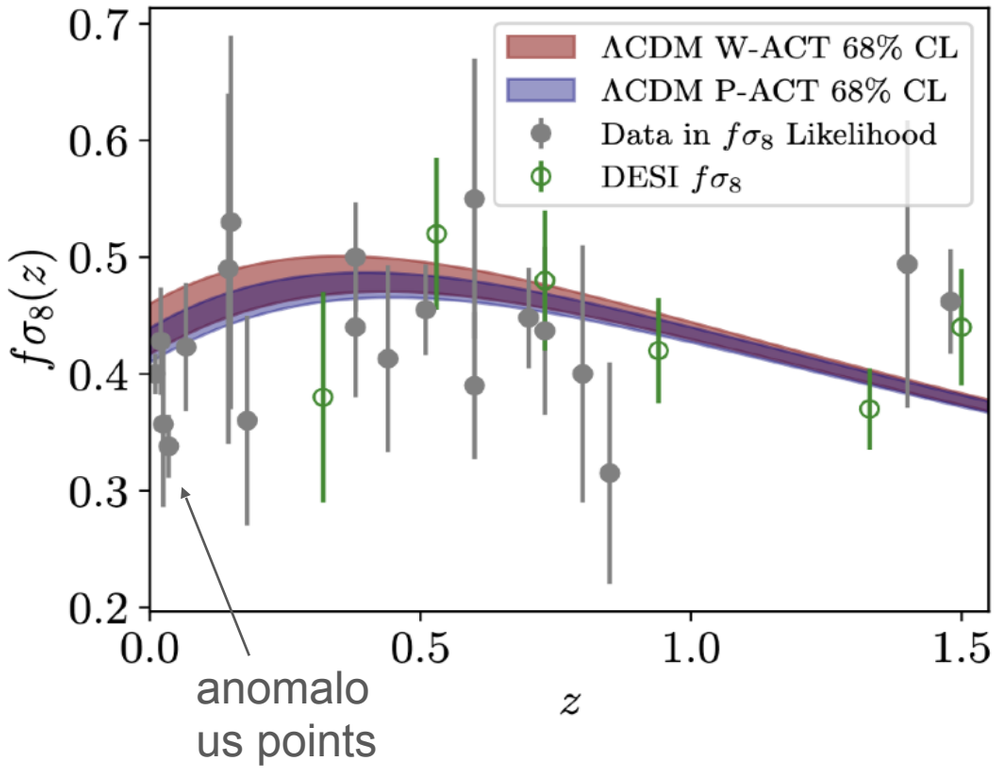

fσ$_8$

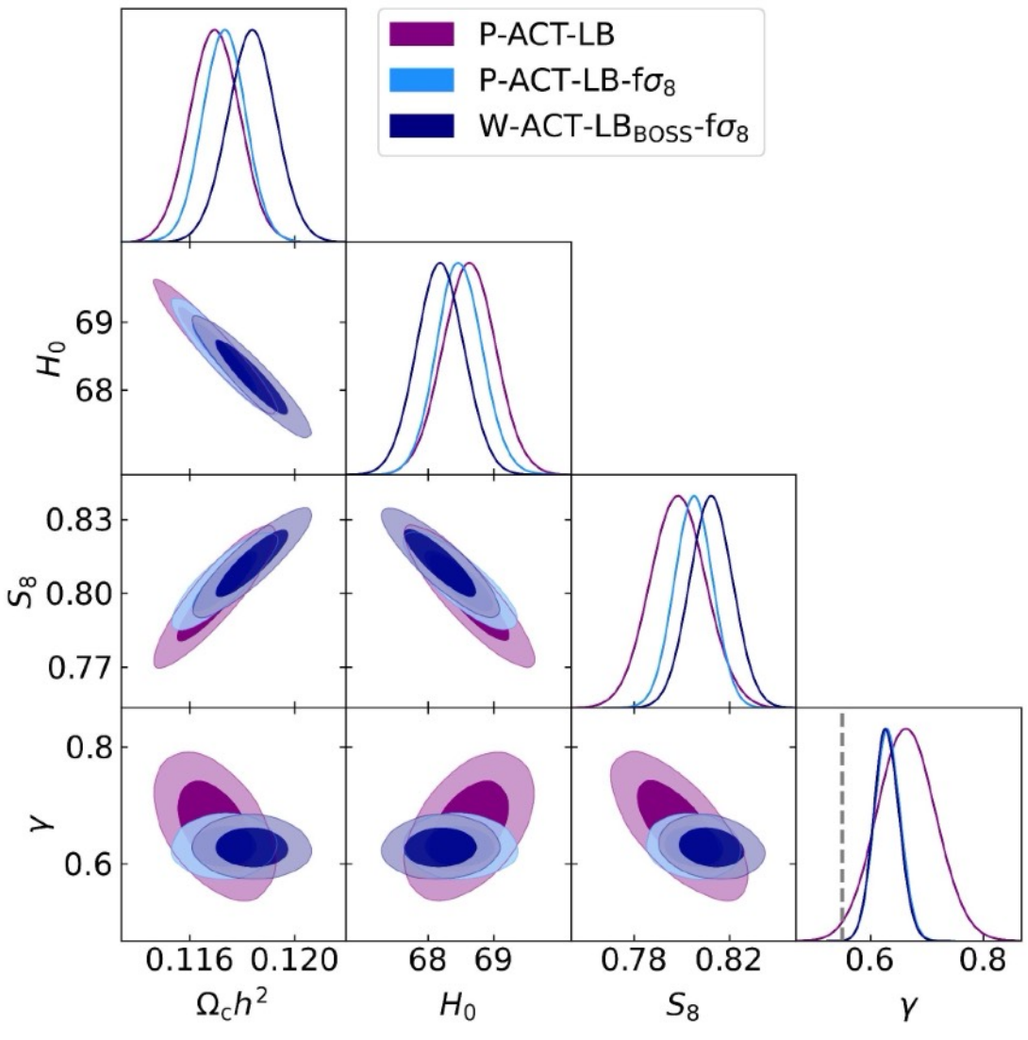

Modified recombination control point

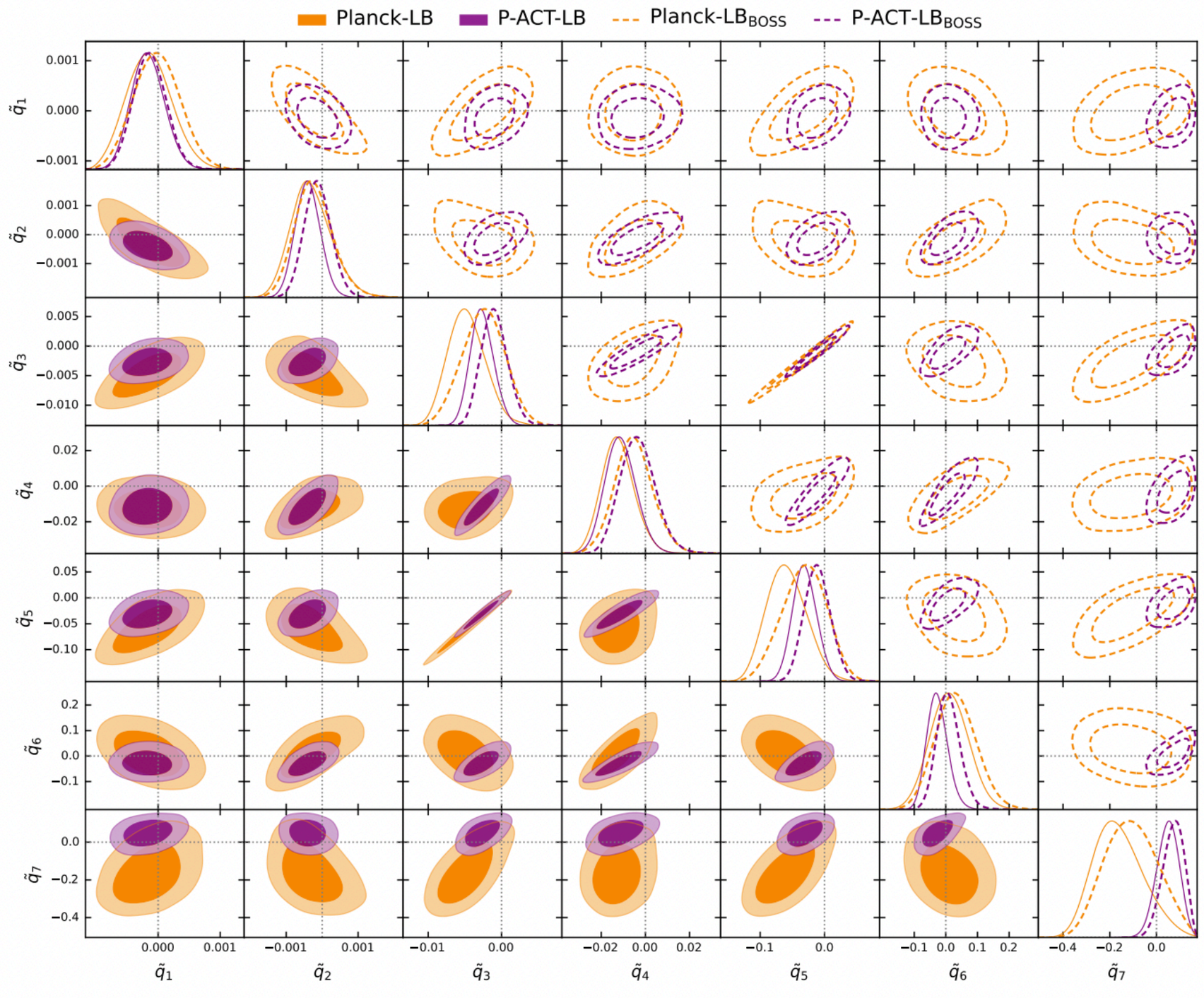

Figure 55. Marginalized parameter posteriors for the control points varied in the `ModRec` scenario analyzed in §5.5. The bottom (top) panels use DESI (BOSS) BAO. The dotted gray lines indicate the standard recombination scenario ($\tilde{q}_i = 0$).

DR6 data set test

We have done around 2000 null tests on the data, we checked that the results do not depends on

- array bands
- weather conditions
- scan elevation
- sky location
- time of observation
- detectors positions

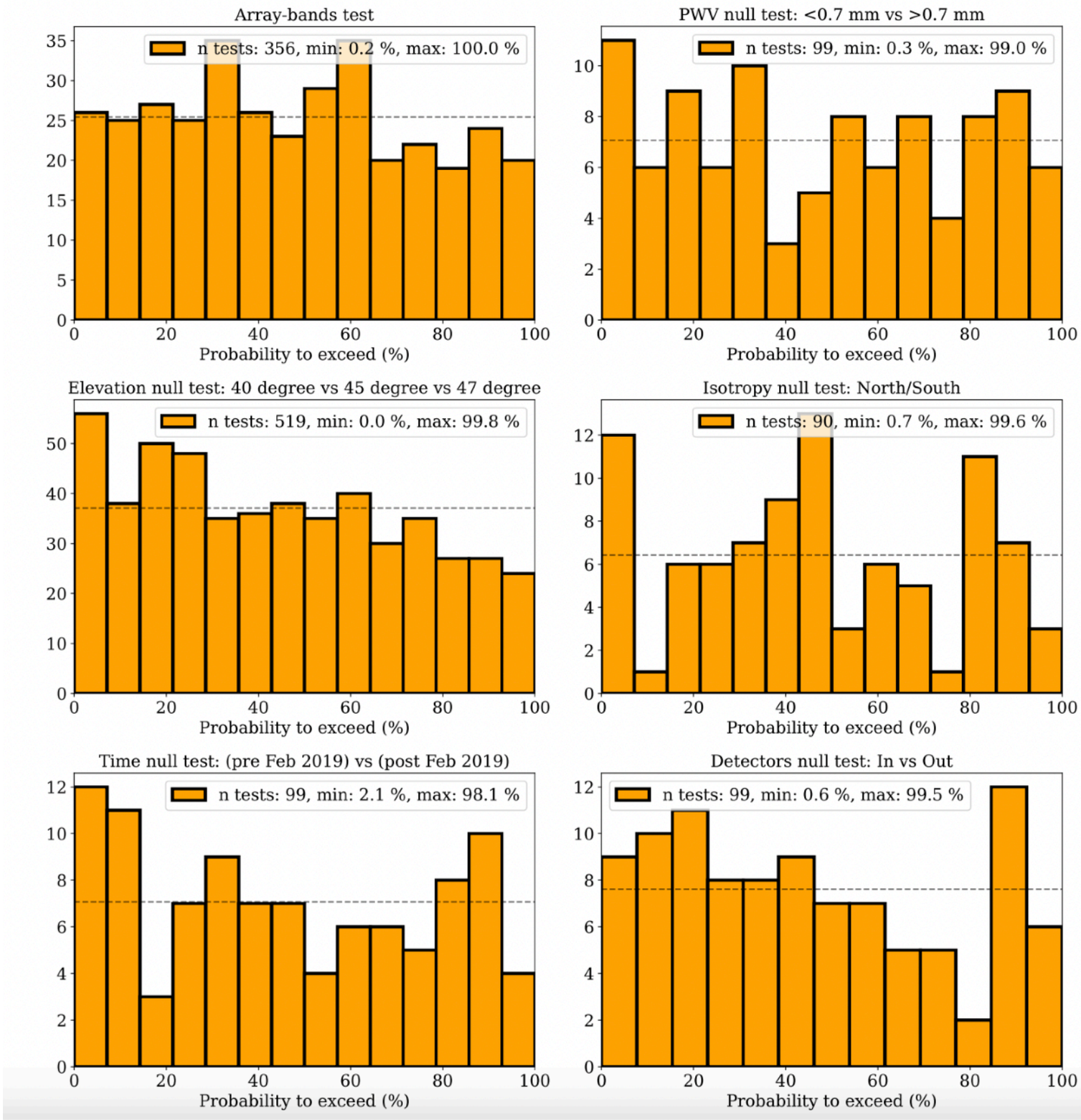

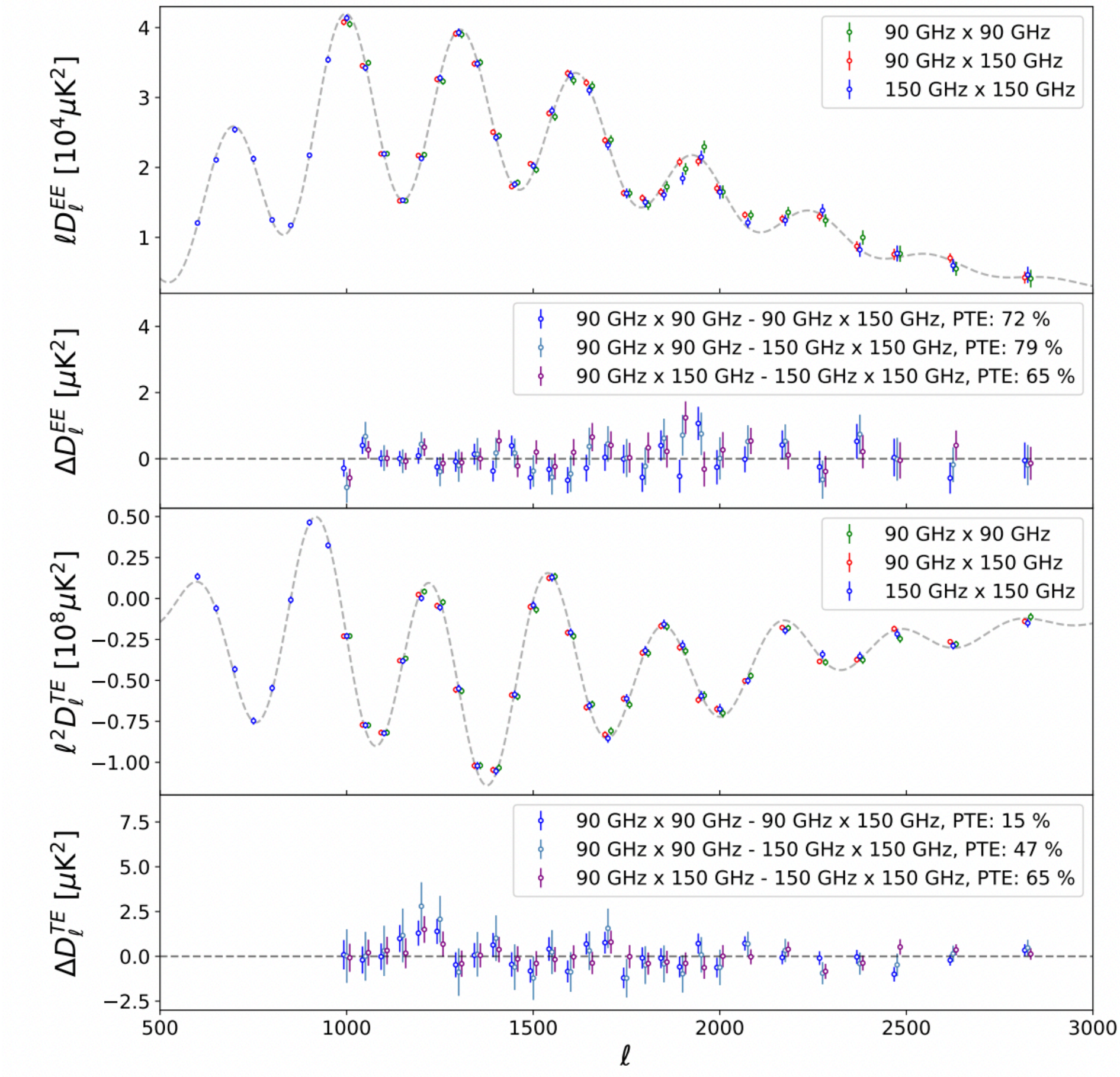
90 GHz x 90 GHz
90 GHz x 150 GHz
150 GHz x 150 GHz
ℓD_ℓ^{EE} [$10^4 \mu K^2$]
90 GHz x 90 GHz - 90 GHz x 150 GHz, PTE: 72 %
90 GHz x 90 GHz - 150 GHz x 150 GHz, PTE: 79 %
90 GHz x 150 GHz - 150 GHz x 150 GHz, PTE: 65 %
ΔD_ℓ^{EE} [μK^2]
$\ell^2 D_\ell^{TE}$ [$10^8 \mu K^2$]
ΔD_ℓ^{TE} [μK^2]
ℓ

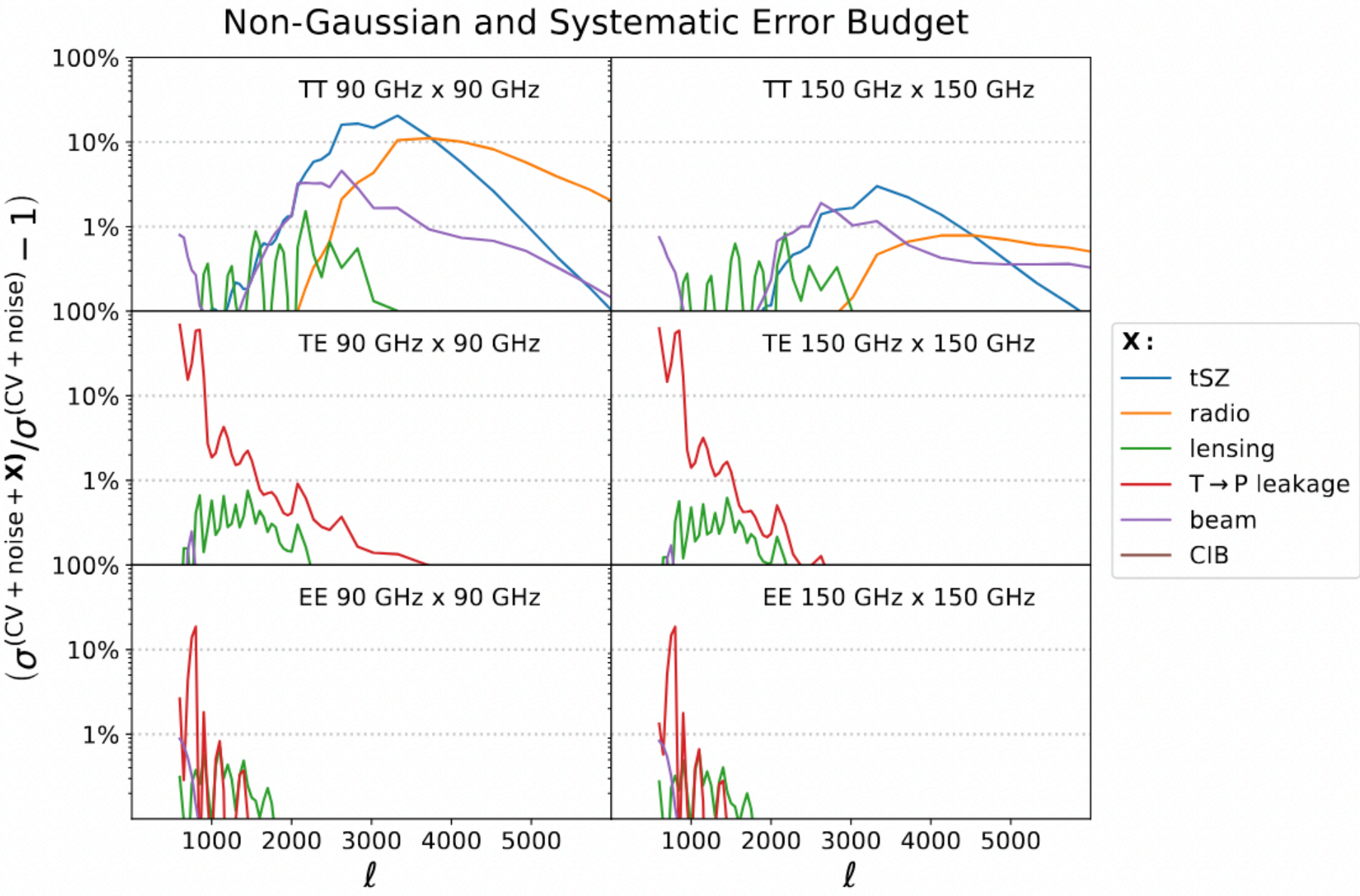

Figure 4. Relative contributions of additional error terms compared to cosmic variance and noise. The contributions to σ_{TT} are shown in the top panel for 90 GHz (left) and 150 GHz (right). For f090, uncertainties from non-Gaussian tSZ and non-Gaussian radio sources are important on small scales. The contribution from unclustered CIB non-Gaussianity is smaller than 0.1% and not visible in the figure. The middle panel shows the contributions to σ_{TE}, where uncertainties in the measurement of the leakage beam are a significant source of uncertainty on large scales. The bottom panel highlights that these uncertainties only mildly affect σ_{EE}, reaching up to 15% at $\ell = 800$. In addition to increasing errors, the additional covariance contributions also result in nonzero off-diagonal correlations.

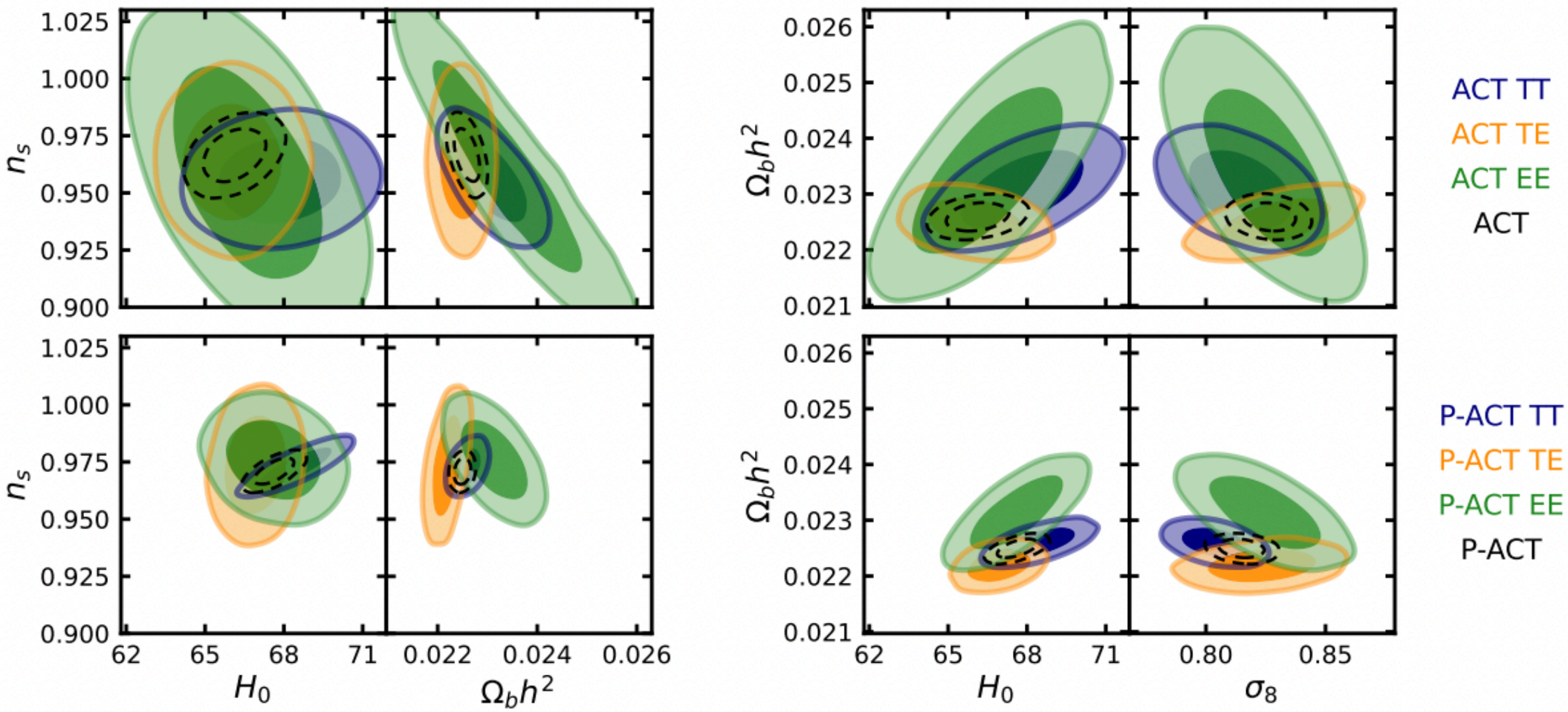

Figure 14. Cosmological parameter distributions estimated from TT, TE or EE from ACT (top) and P-ACT (bottom), including the optical depth prior. Black dashed contours correspond to the distributions estimated from TT, TE, and EE simultaneously, again for ACT (top) and P-ACT (bottom). A prior on the ACT polarization efficiencies, derived from the joint T+E fit, is imposed for the ACT (top) results. For ACT, the TE data provide the tightest constraints on the baryon density, cold dark matter density and the Hubble constant, while the TT data best measure the spectral index. The EE-only constraints are now competitive with those from TT and TE. There is less foreground contamination in the TE and EE spectra than TT; the consistent results add confidence in the model.

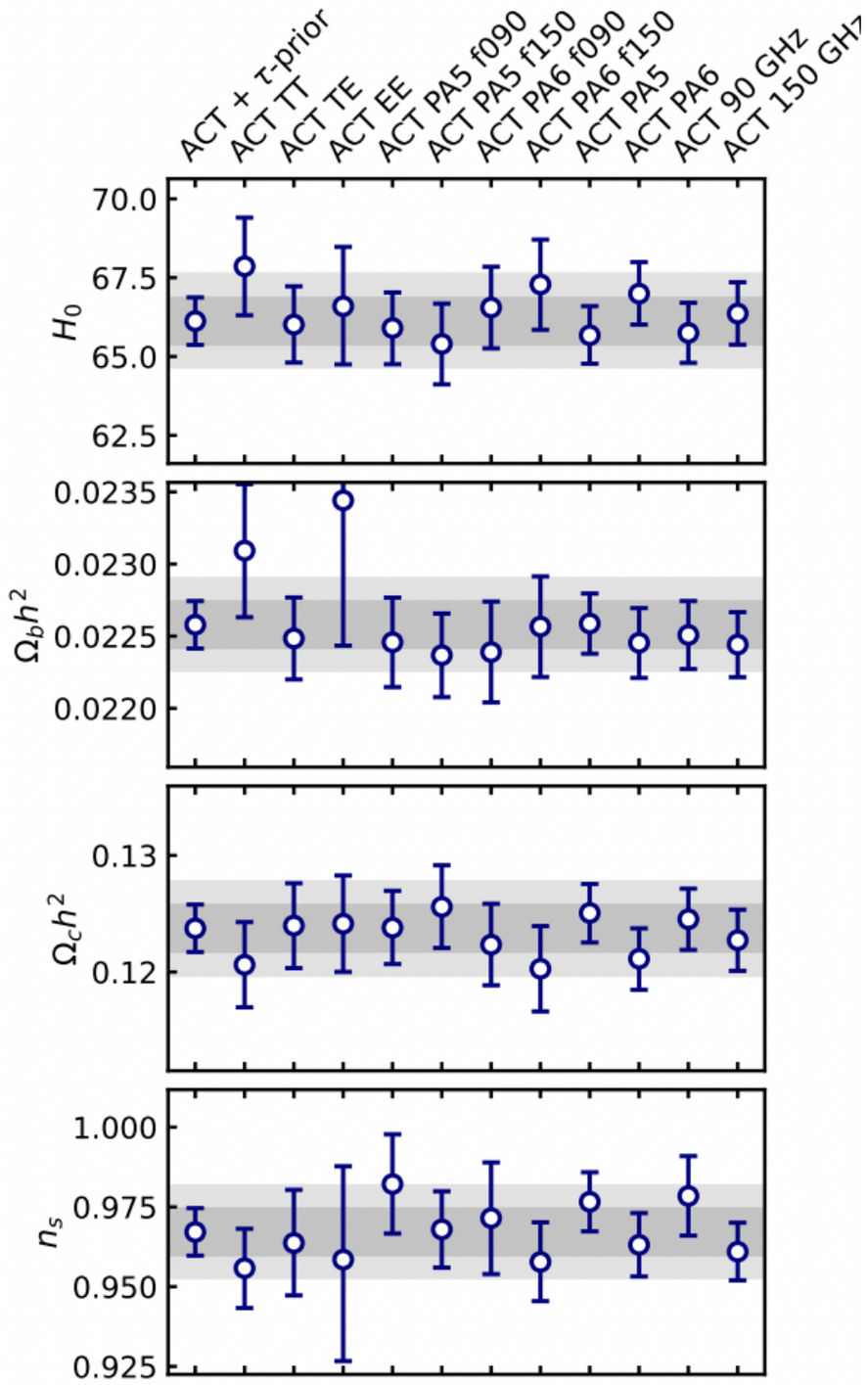

Figure 13. 1D marginalized 68% confidence levels (CL) on cosmological parameters estimated from subsets of the ACT DR6 dataset. The baryon and CDM densities are best measured by the TE spectrum, and the spectral index by the TT spectrum. The different arrays and frequencies give consistent results. All the results shown here use the same optical depth prior. The shaded band shows the 68% and 95% CL on the baseline ACT results.

Breakdown of goodness-of-fit for P-ACT

TT:

- ACT: 566.05/601
- Planck: 89.05/114

TE:

- ACT: 651.77/644
- Planck: 67.82/69

EE:

- ACT: 392.19/406
- Planck: 68.93/69

Parameter	ACT	Planck	W-ACT	P-ACT	P-ACT-LB
Sampled					
$10^4\theta_{\rm MC}$	104.056 ± 0.031	104.088 ± 0.031	104.066 ± 0.029	104.073 ± 0.025	104.086 ± 0.025
$10^2\Omega_{\rm b}h^2$	2.259 ± 0.017	2.237 ± 0.015	2.263 ± 0.012	2.250 ± 0.011	2.256 ± 0.011
$10^2\Omega_{\rm c}h^2$	12.38 ± 0.21	12.00 ± 0.14	12.20 ± 0.18	11.93 ± 0.12	11.79 ± 0.09
$\log(10^{10}A_{\rm s})$	3.053 ± 0.013	$3.054^{+0.012}_{-0.013}$	$3.057^{+0.010}_{-0.012}$	3.056 ± 0.013	$3.060^{+0.011}_{-0.012}$
$n_{\rm s}$	0.9666 ± 0.0077	0.9651 ± 0.0044	0.9660 ± 0.0046	0.9709 ± 0.0038	0.9743 ± 0.0034
τ [%]	$5.62^{+0.53}_{-0.63}$	$5.90^{+0.55}_{-0.65}$	$5.71^{+0.54}_{-0.64}$	$6.03^{+0.55}_{-0.65}$	$6.32^{+0.55}_{-0.66}$
Derived					
H_0 [km/s/Mpc]	66.11 ± 0.79	67.31 ± 0.61	66.78 ± 0.68	67.62 ± 0.50	68.22 ± 0.36
$\Omega_{\rm m}$ [%]	33.7 ± 1.3	31.58 ± 0.85	32.6 ± 1.1	31.16 ± 0.71	30.32 ± 0.48
Ω_b [%]	5.17 ± 0.12	4.937 ± 0.070	5.075 ± 0.098	4.920 ± 0.063	4.847 ± 0.044
Ω_c [%]	28.3 ± 1.2	26.50 ± 0.78	27.37 ± 0.96	26.10 ± 0.65	25.34 ± 0.44
Ω_Λ [%]	66.3 ± 1.3	68.41 ± 0.85	67.4 ± 1.1	68.83 ± 0.71	69.67 ± 0.48
$10^2\Omega_m h^2$	14.70 ± 0.21	14.31 ± 0.13	14.53 ± 0.18	14.25 ± 0.12	14.11 ± 0.08
$n_{\rm s} - 1$ [%]	-3.34 ± 0.77	-3.49 ± 0.44	-3.40 ± 0.46	-2.91 ± 0.38	-2.57 ± 0.34
σ_8	0.8263 ± 0.0074	0.8151 ± 0.0066	0.8221 ± 0.0070	0.8149 ± 0.0063	0.8126 ± 0.0046
S_8	0.875 ± 0.023	0.836 ± 0.016	0.857 ± 0.020	0.830 ± 0.014	0.8169 ± 0.0087
Age [Gyr]	13.801 ± 0.023	13.800 ± 0.024	13.788 ± 0.019	13.789 ± 0.018	13.772 ± 0.015
$10^4\theta_\star$	104.075 ± 0.031	104.109 ± 0.031	104.085 ± 0.029	104.094 ± 0.025	104.107 ± 0.025
$10^4Y_{\rm He}$	2459.50 ± 0.71	2458.55 ± 0.64	2459.66 ± 0.51	2459.10 ± 0.48	2459.37 ± 0.46
$10^{10}\eta_b$	6.185 ± 0.046	6.124 ± 0.041	6.196 ± 0.033	6.159 ± 0.030	6.177 ± 0.029
$z_{\rm reio}$	$7.88^{+0.54}_{-0.61}$	$8.15^{+0.55}_{-0.62}$	$7.93^{+0.54}_{-0.61}$	8.23 ± 0.59	$8.47^{+0.54}_{-0.61}$
$\tau_{\rm rec}$ [Mpc]	593.6 ± 3.1	599.5 ± 2.0	596.2 ± 2.6	600.4 ± 1.8	602.4 ± 1.3
$z_\star$	1089.96 ± 0.30	1089.92 ± 0.29	1089.75 ± 0.24	1089.68 ± 0.21	1089.47 ± 0.18
$r_{s,\star}$ [Mpc]	143.32 ± 0.54	144.43 ± 0.31	143.74 ± 0.45	144.53 ± 0.29	144.85 ± 0.22
z_d	1060.72 ± 0.39	1059.94 ± 0.29	1060.67 ± 0.28	1060.17 ± 0.23	1060.21 ± 0.23
r_d [Mpc]	145.88 ± 0.56	147.09 ± 0.30	146.30 ± 0.46	147.14 ± 0.29	147.45 ± 0.23
$-2\ln\mathcal{L}^{\rm MAP}_{\rm posterior}$	1929.71	996.82	3934.93	2180.49	2216.71
$\chi^2_{\rm MFLike}$	1590.91 (1651)		1592.20 (1651)	1597.72 (1651)	1598.13 (1651)
$\chi^2_{\rm Planck-high\ell}$		583.16 (613)		221.51 (252)	221.02 (252)
$\chi^2_{\rm Planck-lowT}$		23.45 (28)		22.46 (28)	22.11 (28)
$\chi^2_{\rm WMAP}$			2017.02 (1945)		
$\chi^2_{\rm CMBlens}$					19.63 (19)
$\chi^2_{\rm DESI-BAO}$					15.48 (12)

Table 5. Marginalized constraints on the ΛCDM sampled and derived parameters from the ACT data (including the *Planck* Sroll2 large-scale EE data to constrain the optical depth), and its combination with *WMAP* (W-ACT), $\ell < 1000$ *Planck* data (P-ACT), and CMB lensing from ACT and Planck and BAO data from DESI Y1 (P-ACT-LB). Parameter definitions are given in Appendix G.1. The goodness of fit of the best-fitting model, with maxium posterior probability, is reported for the different datasets along with the total maximum a posteriori (MAP) value that includes contributions from the Sroll2 likelihood and informative priors. Numbers in parentheses indicate the number of data points used in the respective χ^2 calculations. For comparison, constraints are shown from the *Planck* PR3 (Planck Collaboration 2020d) TT/TE/EE data that we rerun with the Sroll2 large-scale polarization data for consistency. Parameter constraints using the *Planck* NPIPE maps in Rosenberg et al. (2022) and Tristram et al. (2024) are typically 10-20% tighter, with comparable errors to our P-ACT combination.

Measuring H0 from the CMB

Measuring the Hubble constant using the CMB

The angular size of the sound horizon is given as the ratio of the physical size of the sound horizon and the diameter angular distance of the last scattering surface

$$\theta_* = r_s^* / D_A^*$$

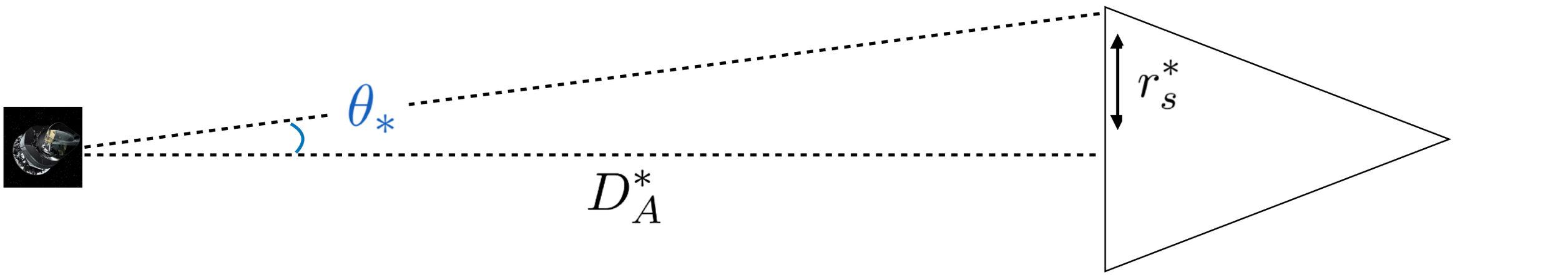

Measuring the Hubble constant using the CMB

The angular size of the sound horizon is given as the ratio of the physical size of the sound horizon and the diameter angular distance of the last scattering surface

$$\theta_* = r_s^*/D_A^*$$

$$r_s^* = \int_0^{t^*} \frac{dt}{a(t)} c_s(t) = \int_{z^*}^{\infty} \frac{dz}{H(z)} c_s(z)$$

r_s^* **is fully determined by the cosmological parameters we have measured**

$$c_s(z) = c\sqrt{\frac{1}{3\left[1 + 3\rho_b^0/4\rho_\gamma^0(1+z)^{-1}\right]}}$$

$$\left.\frac{3H^2(z)}{8\pi G}\right|_{\text{high z}} = \left[\rho_{\text{rad}}^0(1+z)^4 + (\rho_b^0 + \rho_{\text{CDM}}^0)(1+z)^3\right]$$

We know r_s^* **and** θ_* **this gives us** D_A^*

$$D_A^* = c\int_0^{z^*} \frac{dz}{H(z)}$$

$$\left.\frac{3H^2(z)}{8\pi G}\right|_{\text{low z}} = \left[(\rho_b^0 + \rho_{\text{CDM}}^0)(1+z)^3 + \rho_\Lambda\right]$$

Which gives us ρ_Λ

Once ρ_Λ **known, we get** H_0

PR3 and PR4

Comparison with Planck PR4 (NPIPE)

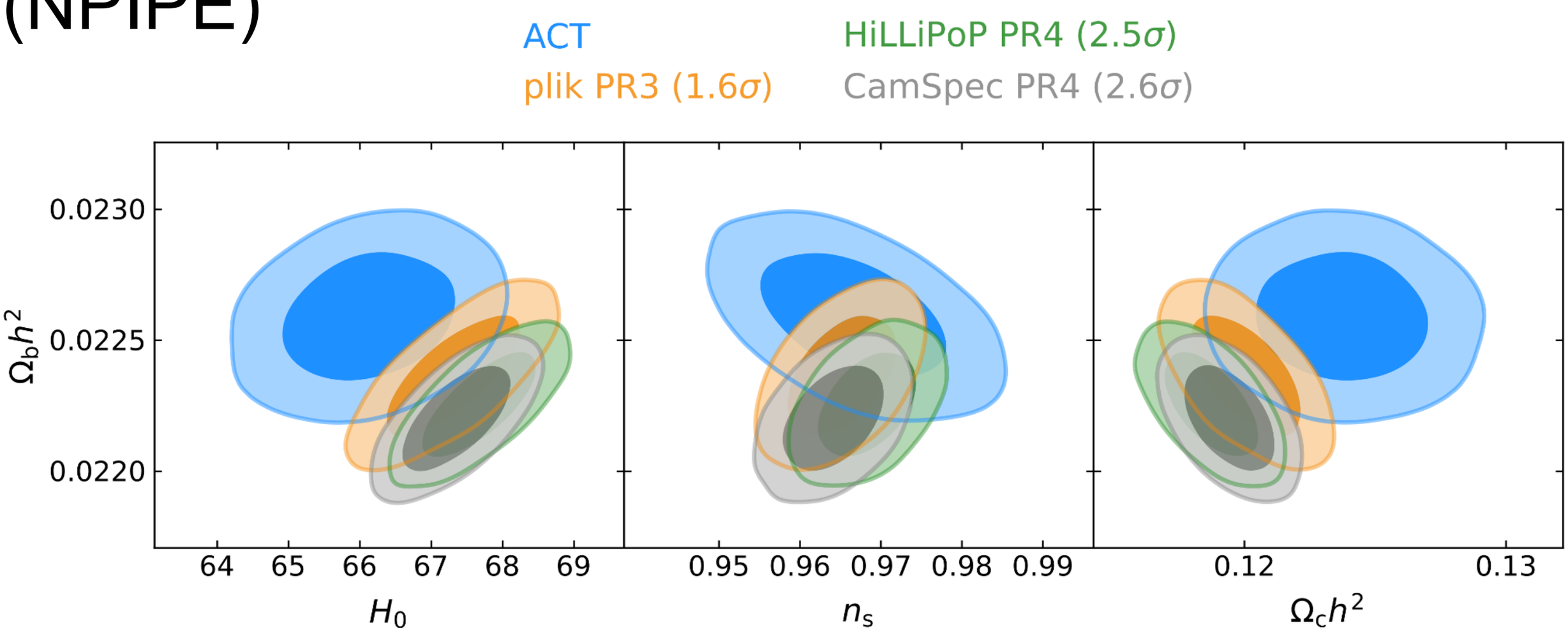

HiLLiPoP/NPIPE, curvature

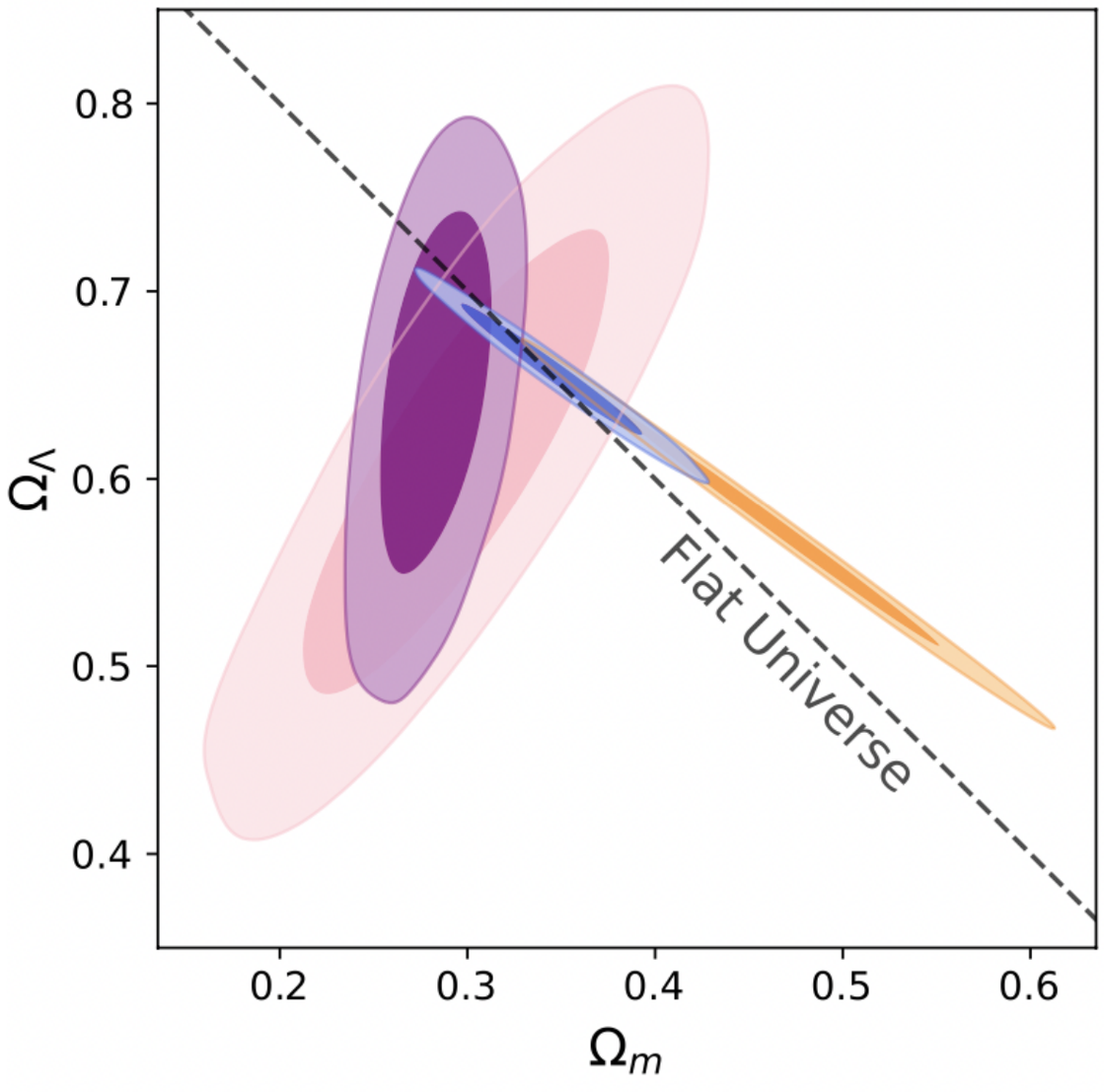

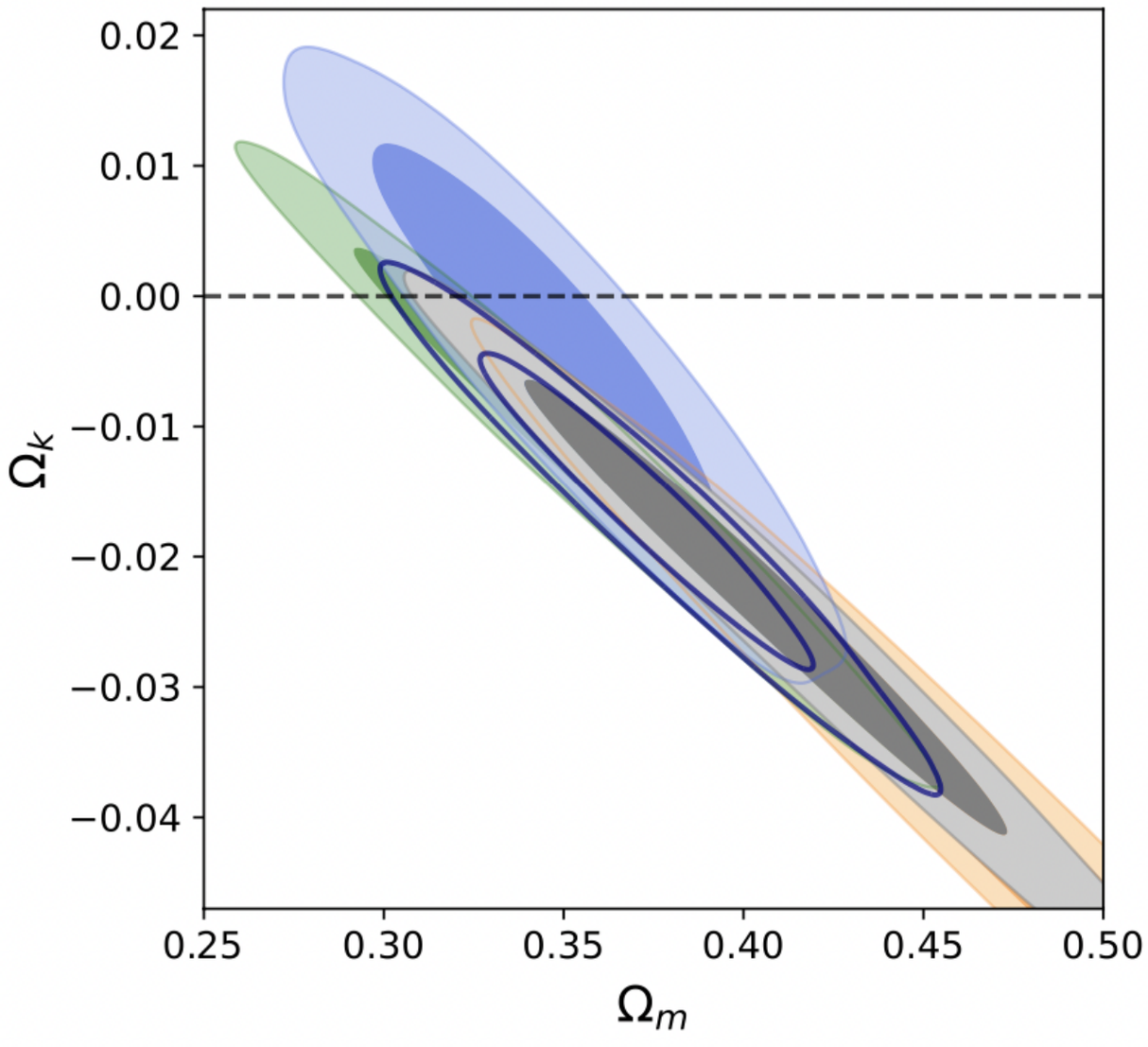

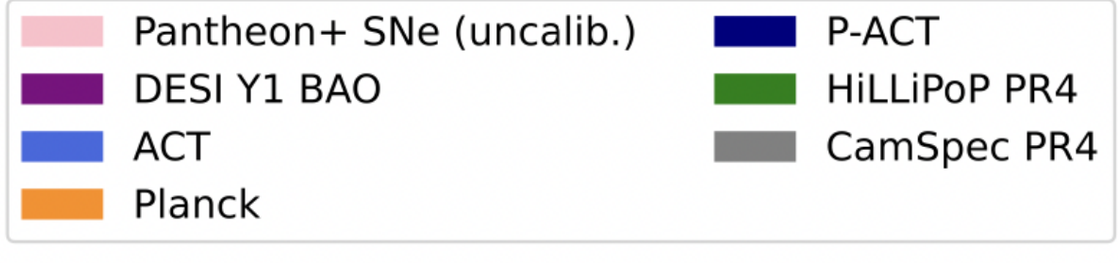

ACT and Planck on the same patch of the sky

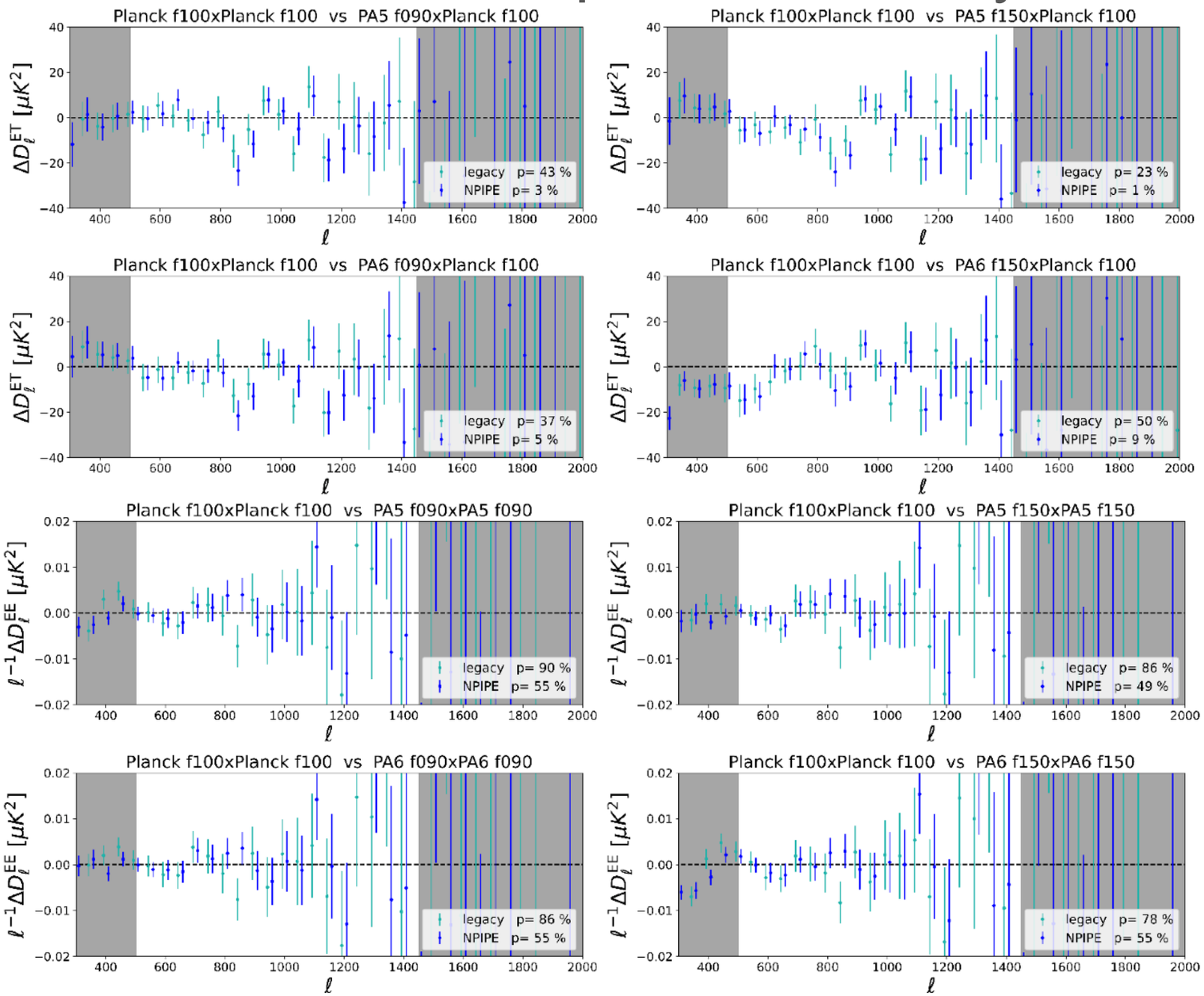

ACT and Planck on the same patch of the sky

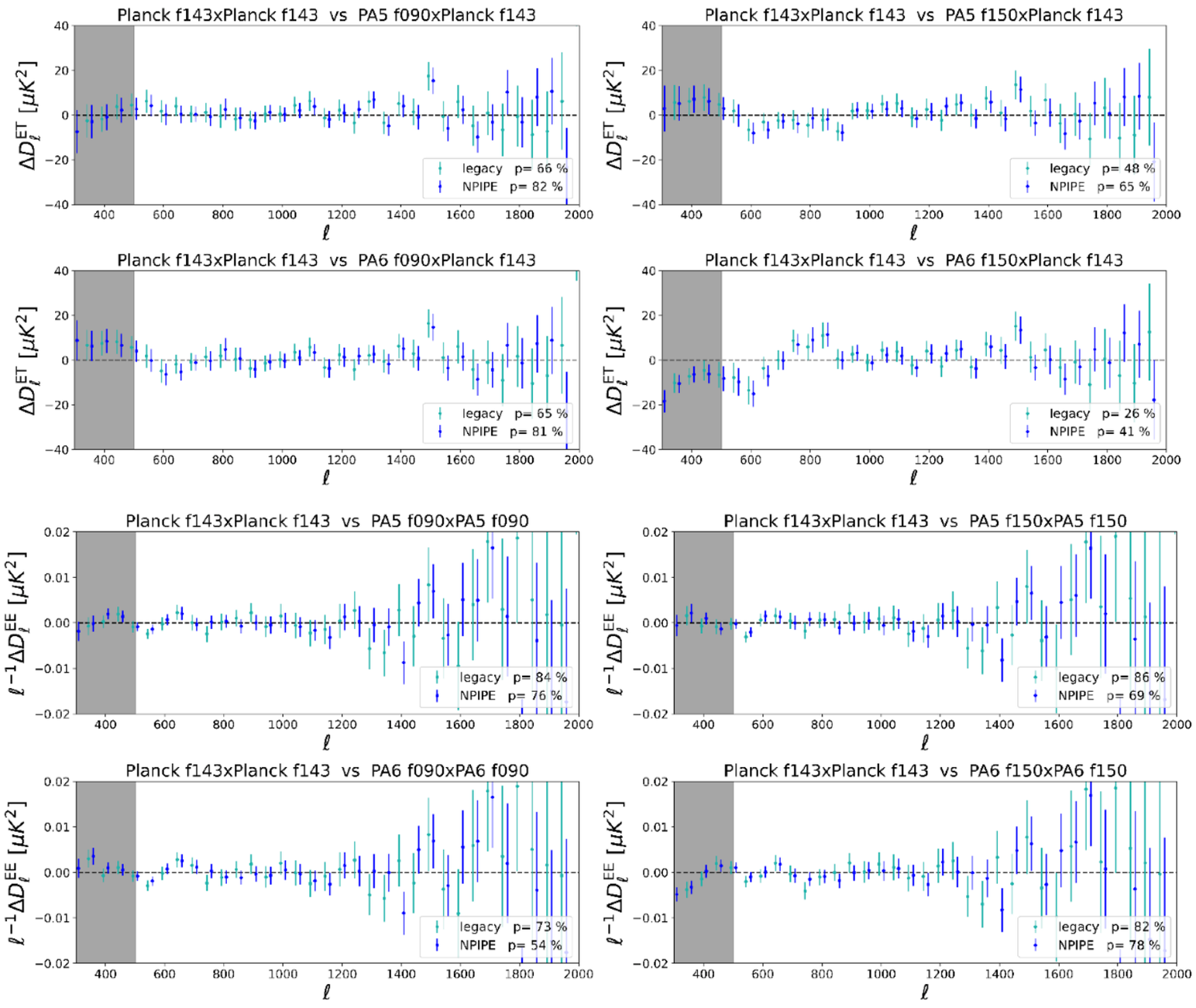

ACT and Planck on the same patch of the sky

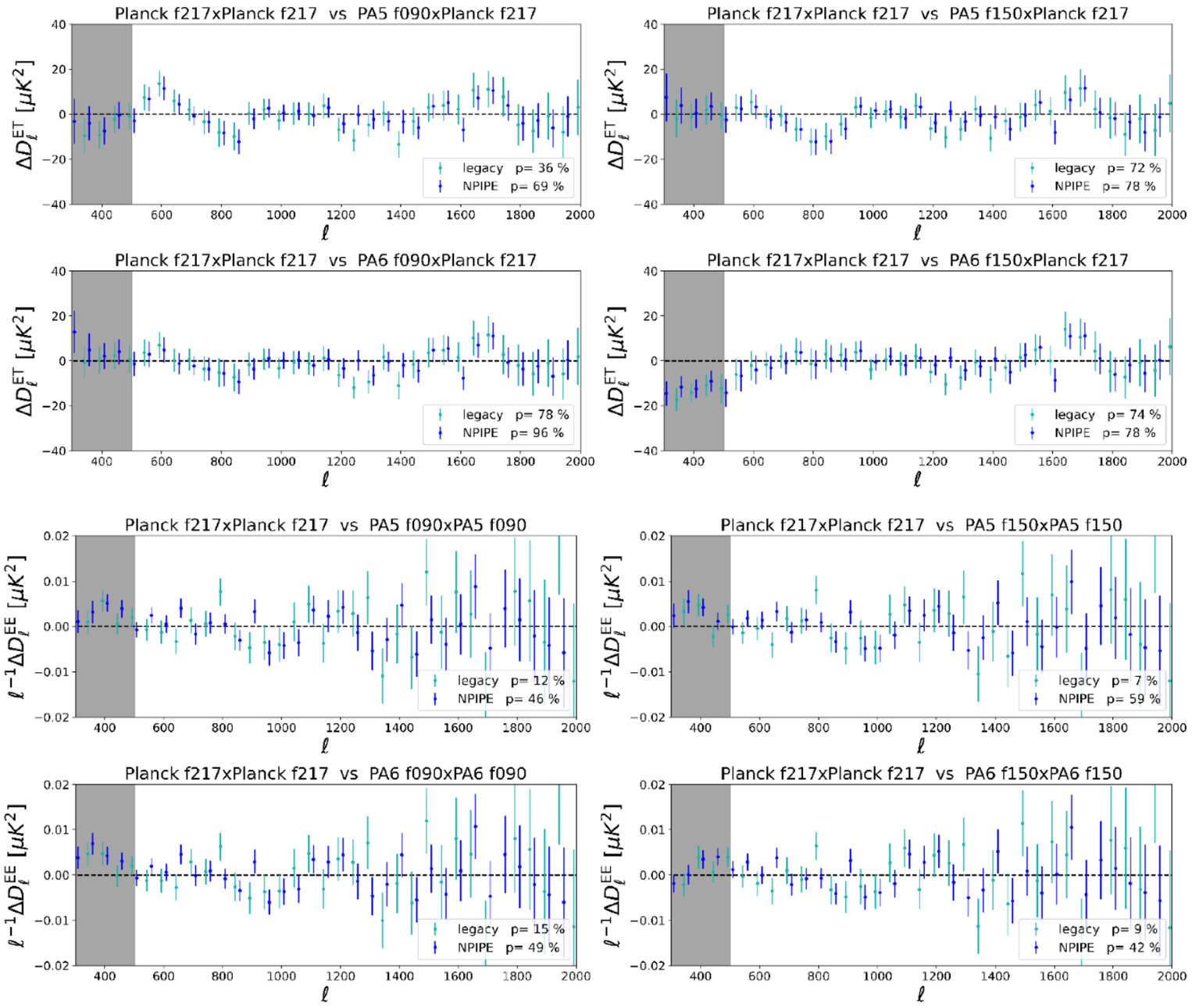

Comparison with Planck PR4 (NPIPE)

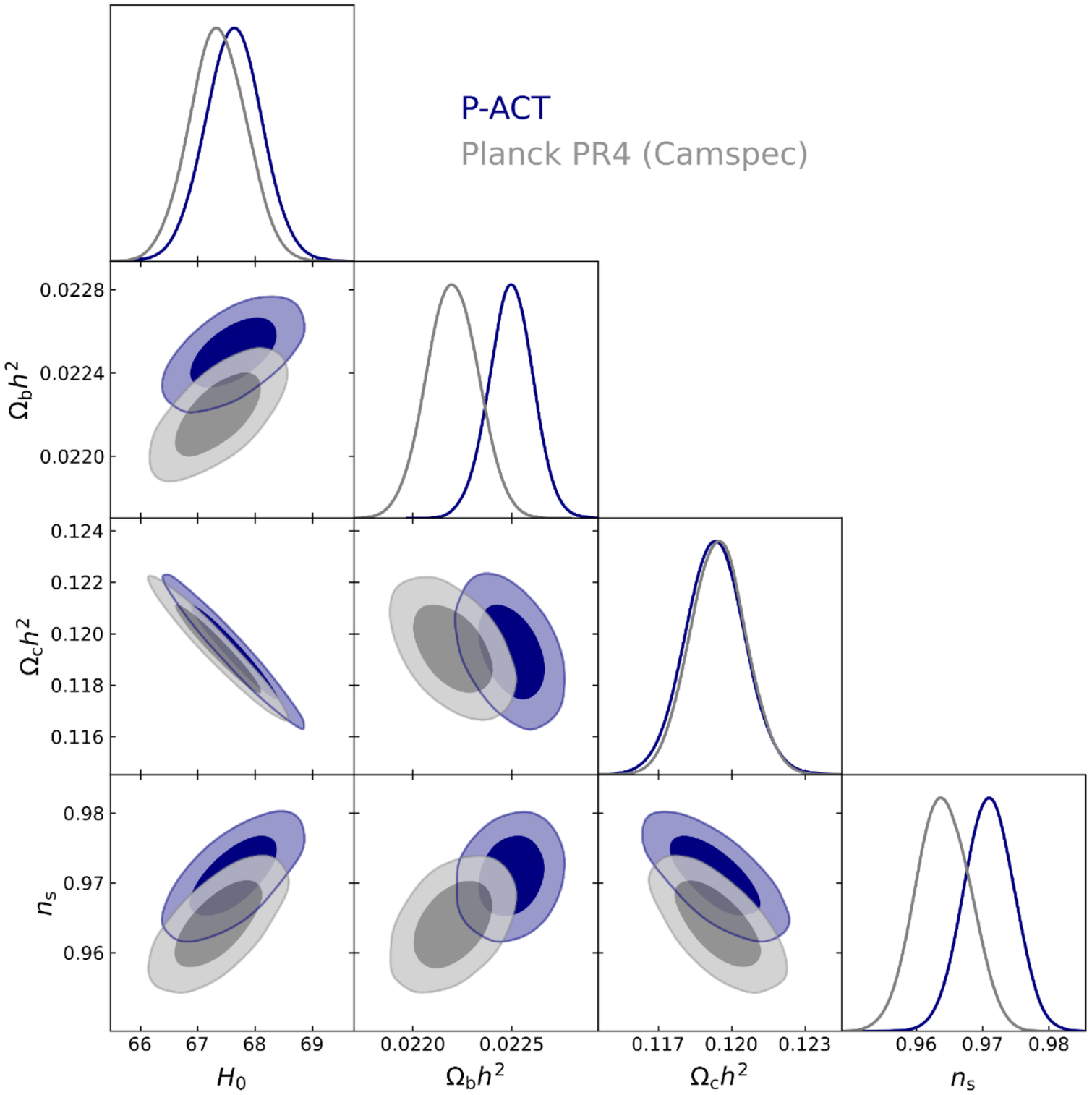

Birefringence

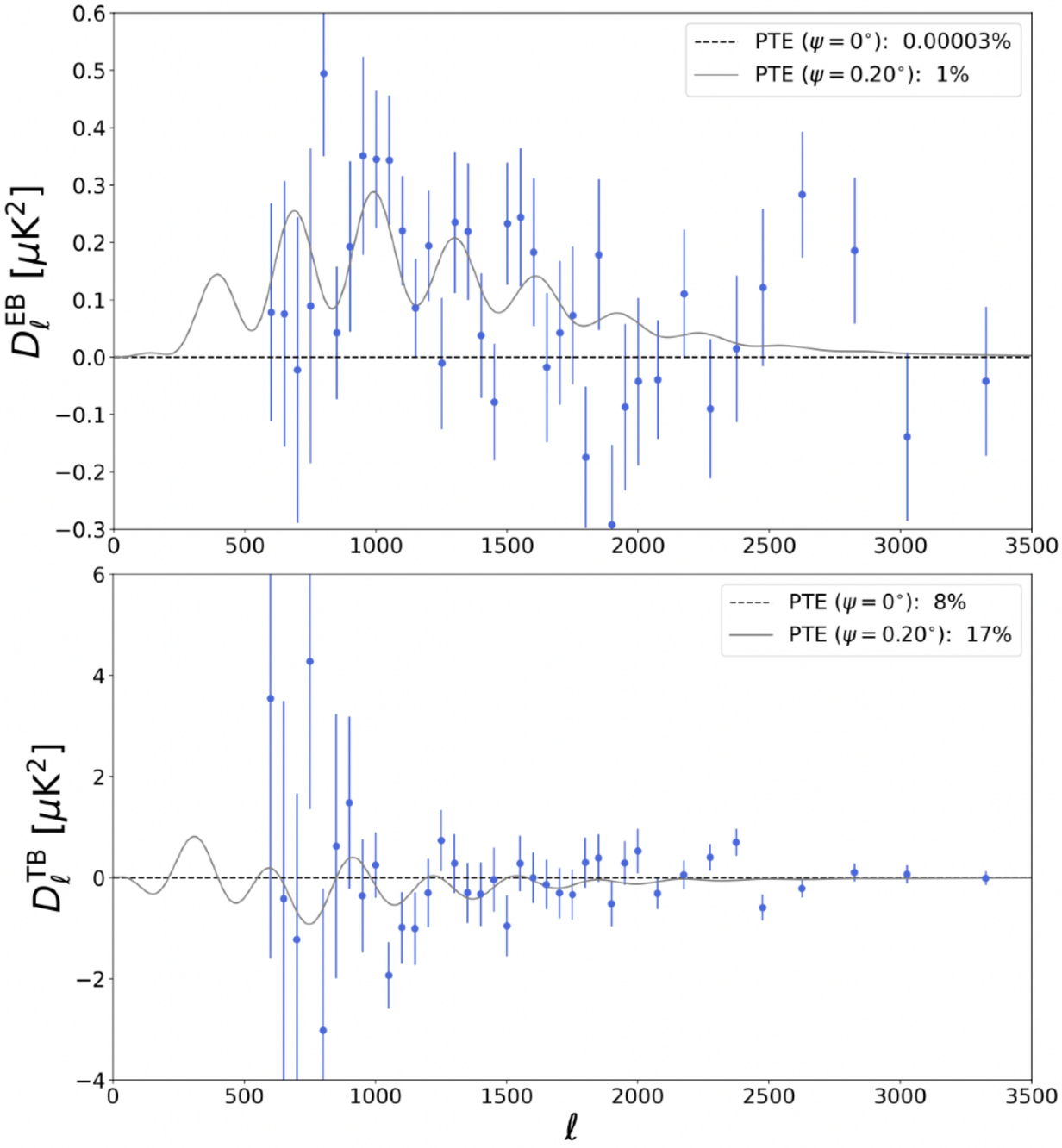
PTE ($\psi = 0°$): 0.00003%
PTE ($\psi = 0.20°$): 1%
D_ℓ^{EB} [μK^2]
PTE ($\psi = 0°$): 8%
PTE ($\psi = 0.20°$): 17%
D_ℓ^{TB} [μK^2]
ℓ

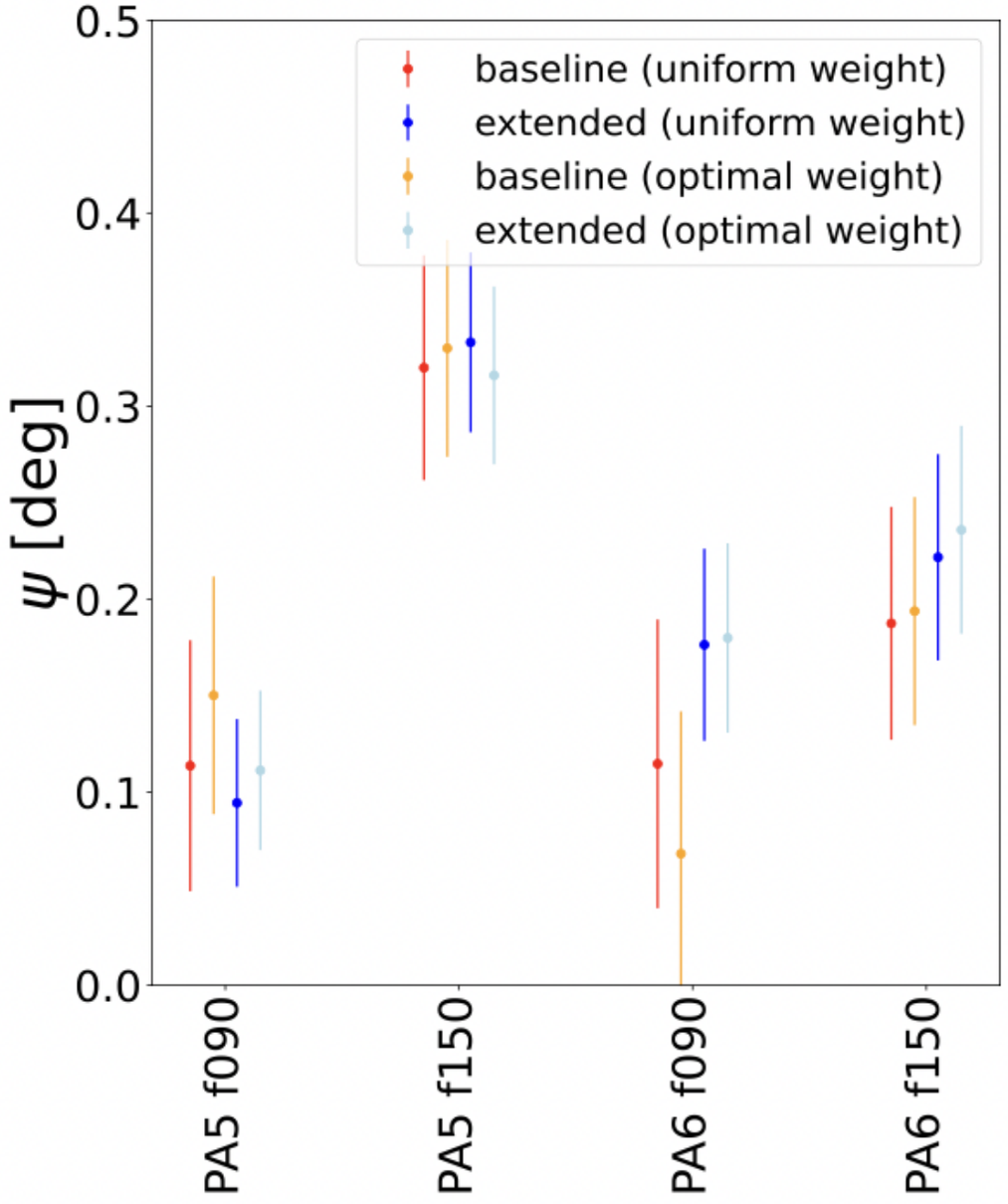
baseline (uniform weight)
extended (uniform weight)
baseline (optimal weight)
extended (optimal weight)
ψ [deg]
PA5 f090
PA5 f150
PA6 f090
PA6 f150

Post unblinding

Cosmo

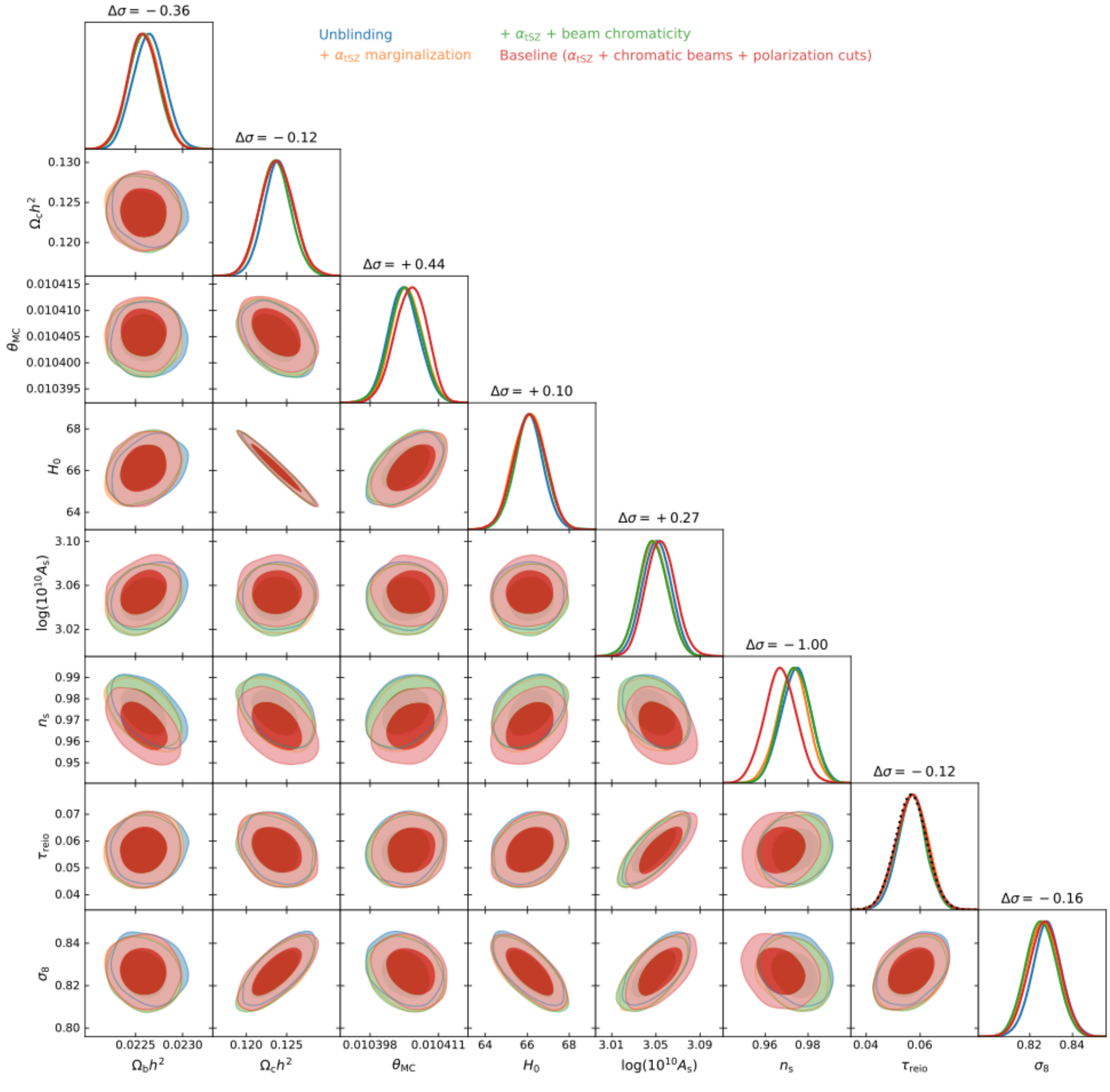
Unblinding
+ α_{tSZ} marginalization
+ α_{tSZ} + beam chromaticity
Baseline (α_{tSZ} + chromatic beams + polarization cuts)
$\Delta\sigma = -0.36$
$\Delta\sigma = -0.12$
$\Delta\sigma = +0.44$
$\Delta\sigma = +0.10$
$\Delta\sigma = +0.27$
$\Delta\sigma = -1.00$
$\Delta\sigma = -0.12$
$\Delta\sigma = -0.16$
$\Omega_c h^2$
θ_{MC}
H_0
$\log(10^{10}A_s)$
n_s
τ_{reio}
σ_8
$\Omega_b h^2$

Astrophysical foregrounds and instrument parameters

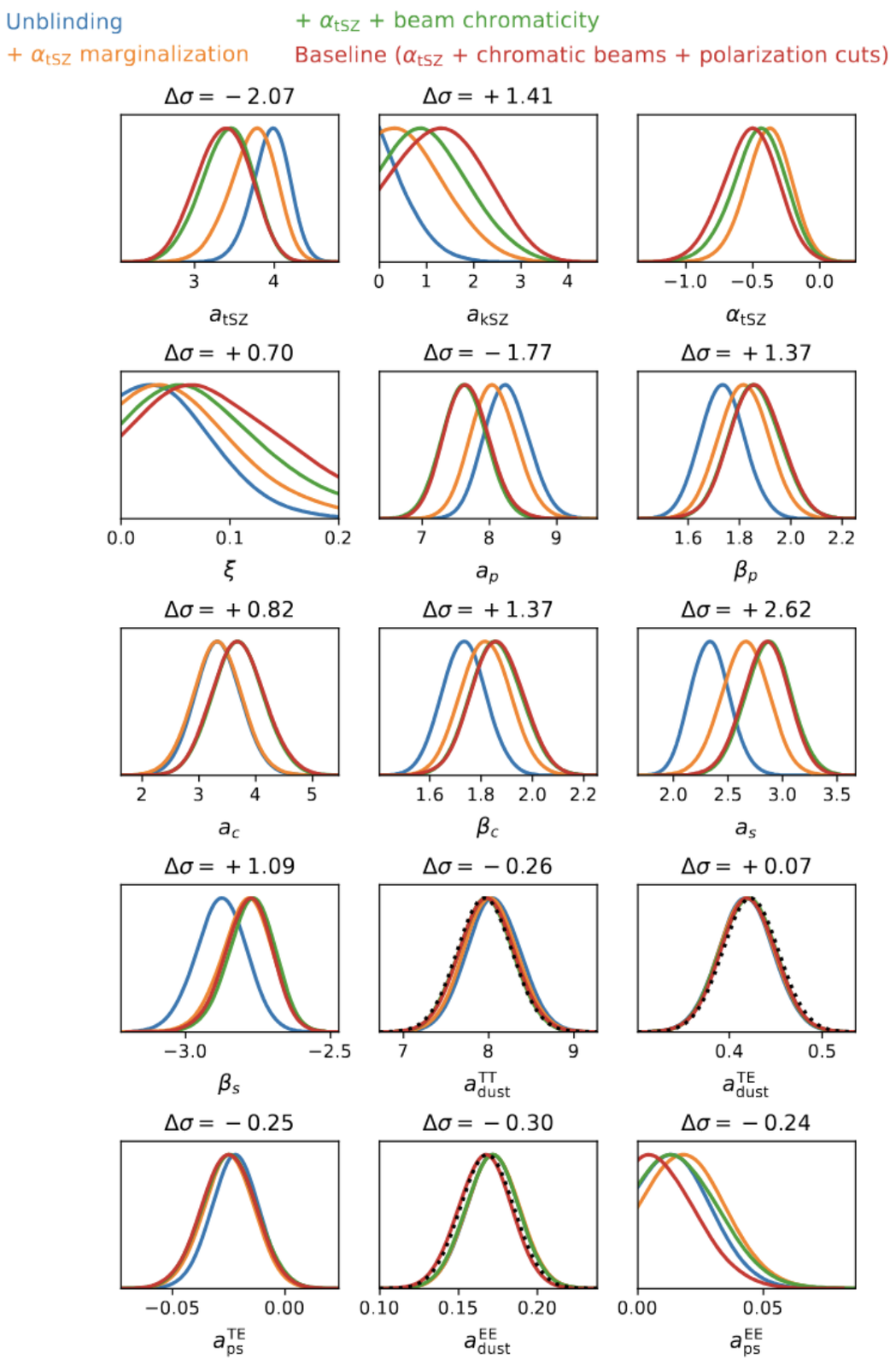

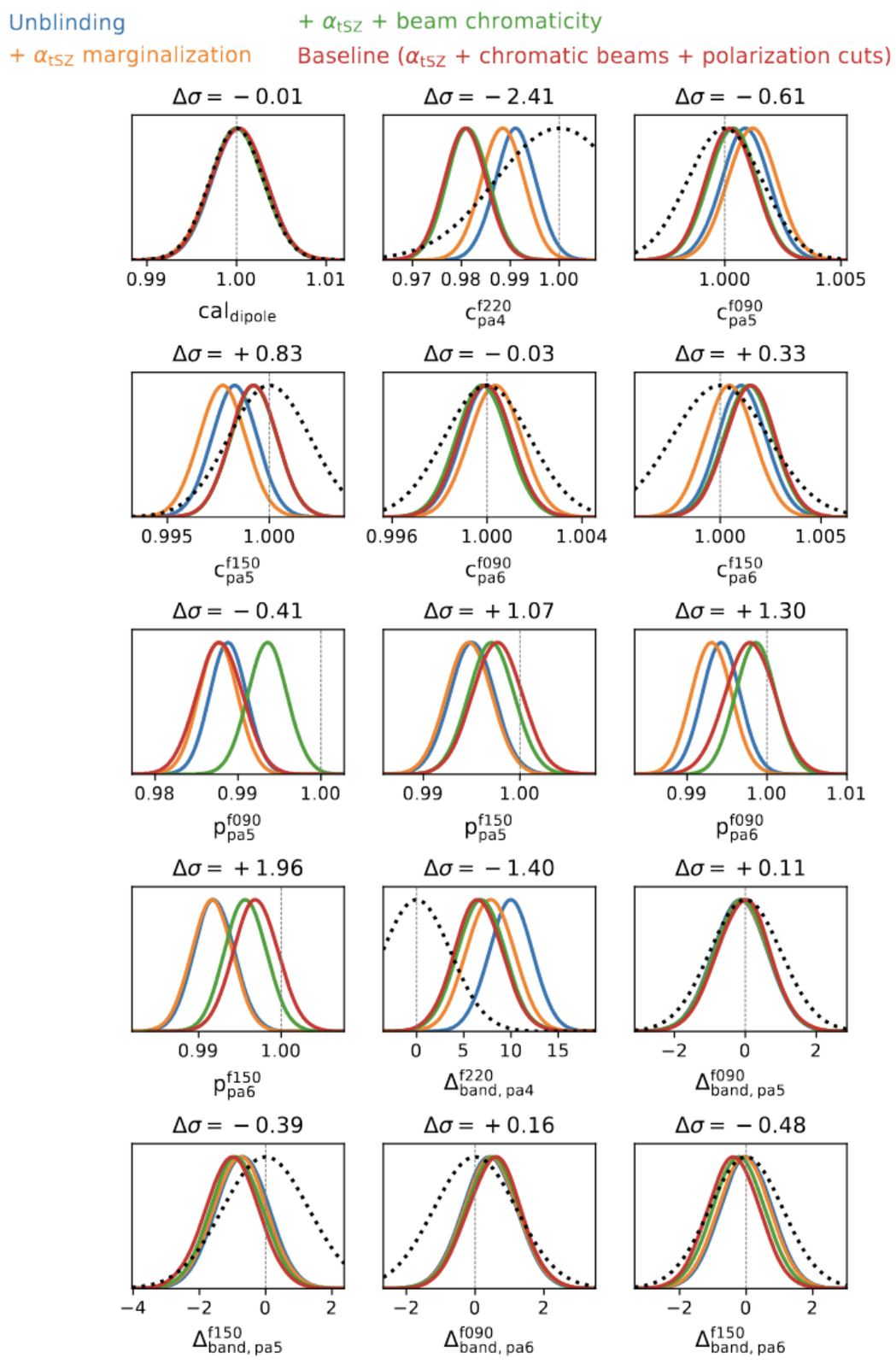

Baseline cuts

Extended cuts

PA5 f090 TE/EE
PA5 f150 TE/EE
PA6 f090 TE/EE
PA6 f150 TE/EE
ACT TE/EE
Planck TT/TE/EE

n_s

1.1
1.0
0.9

0.10
0.11
0.12
0.13
0.14

$\Omega_c h^2$

PA5 f090 Relative Multiplicative Systematic

Extended Multipole Cuts

Baseline Multipole Cuts

$m^{\delta E}_{\mathrm{PA5\ f090}}$

0.08
0.06
0.04
0.02
0.00
−0.02

0
1000
2000
3000
4000

ℓ

ΛCDM
ΛCDM + N_{eff}

4×10^{-5}
2×10^{-5}
0

0.022
0.023

$\Omega_b h^2$

0.93
1.00

n_s

0
2
4

$\times10^{-5}$

$m^{\delta E}_{\mathrm{PA5\ f090}}$

ΛCDM
ΛCDM + N_{eff}

5×10^{-5}
0
-5×10^{-5}

0.022
0.023

$\Omega_b h^2$

0.93
1.00

n_s

−5
0
5

$\times10^{-5}$

$m^{\delta E}_{\mathrm{PA5\ f090}}$

DR6 vs DR4

DR6 vs DR4 cosmology

- very good agreement between DR6 and DR4 baseline result obtained from ACT+WMAP
- some differences with DR4 ACT-alone cosmology
- mainly driven by TE data at multipoles <2000 (where residuals are mostly negative, disfavoring the DR6 LCDM cosmology)
- we speculate beam leakage modelling might be playing a role

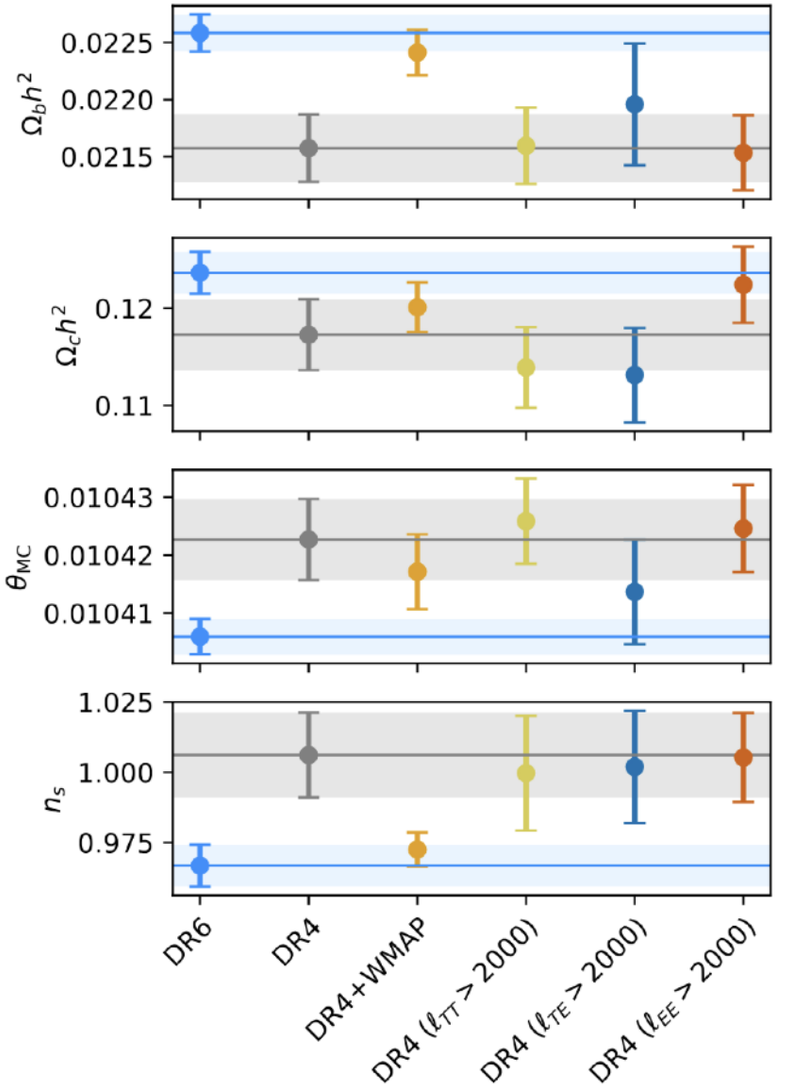

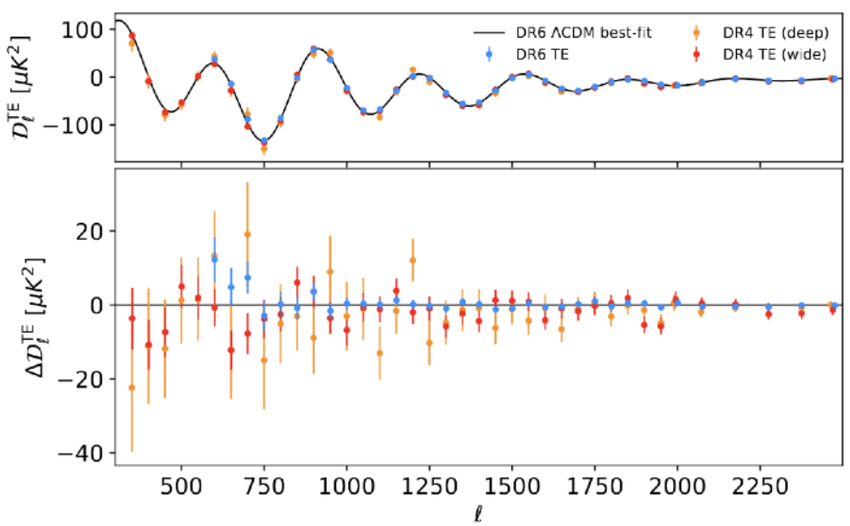

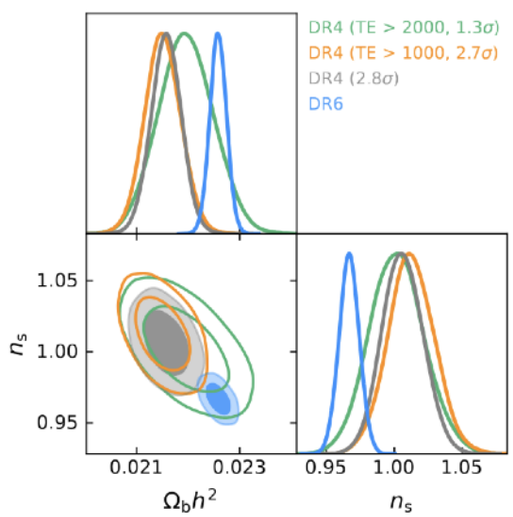

Pre- and modified recombination physics: DR4 vs. DR6 EDE constraints

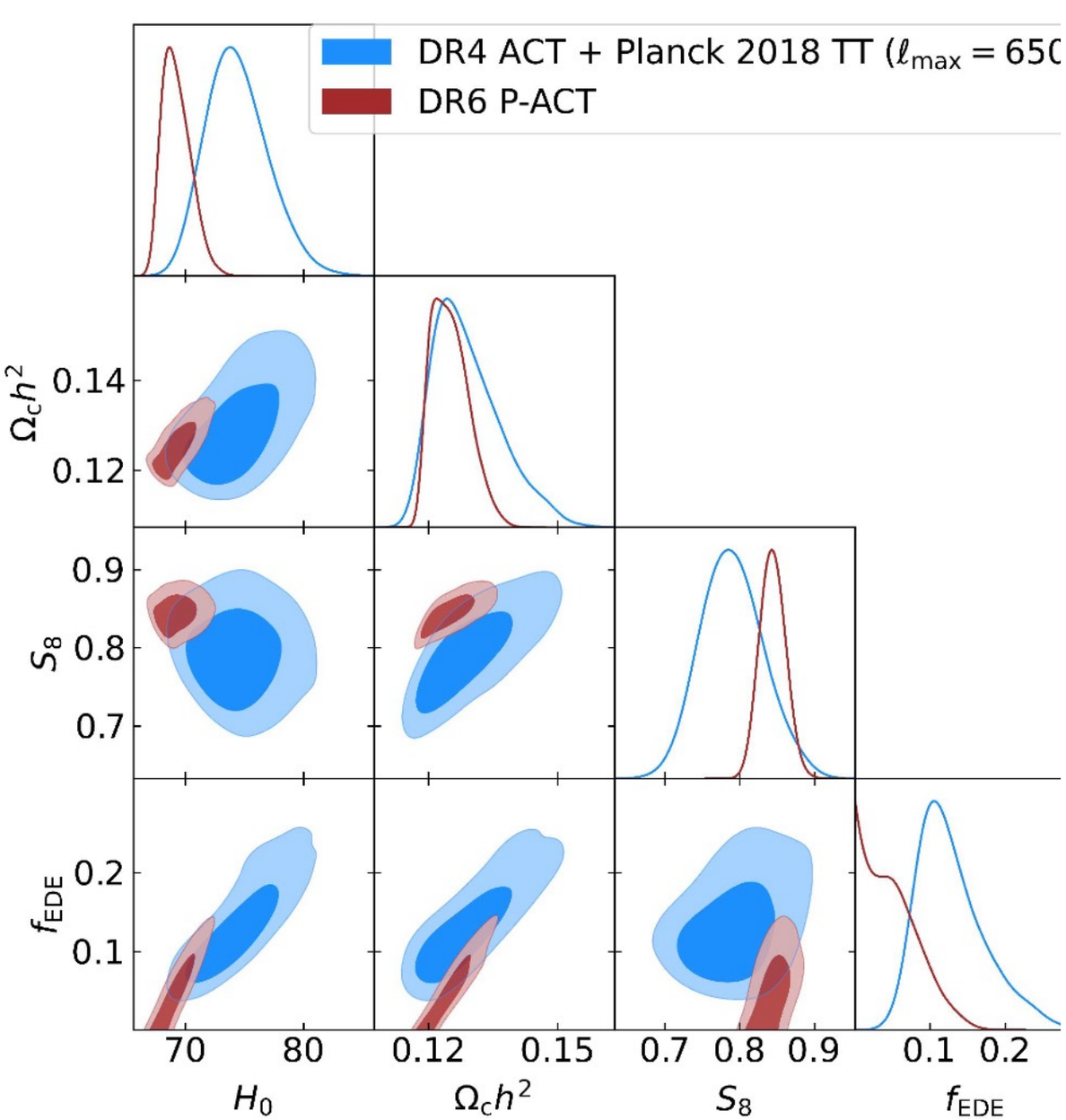

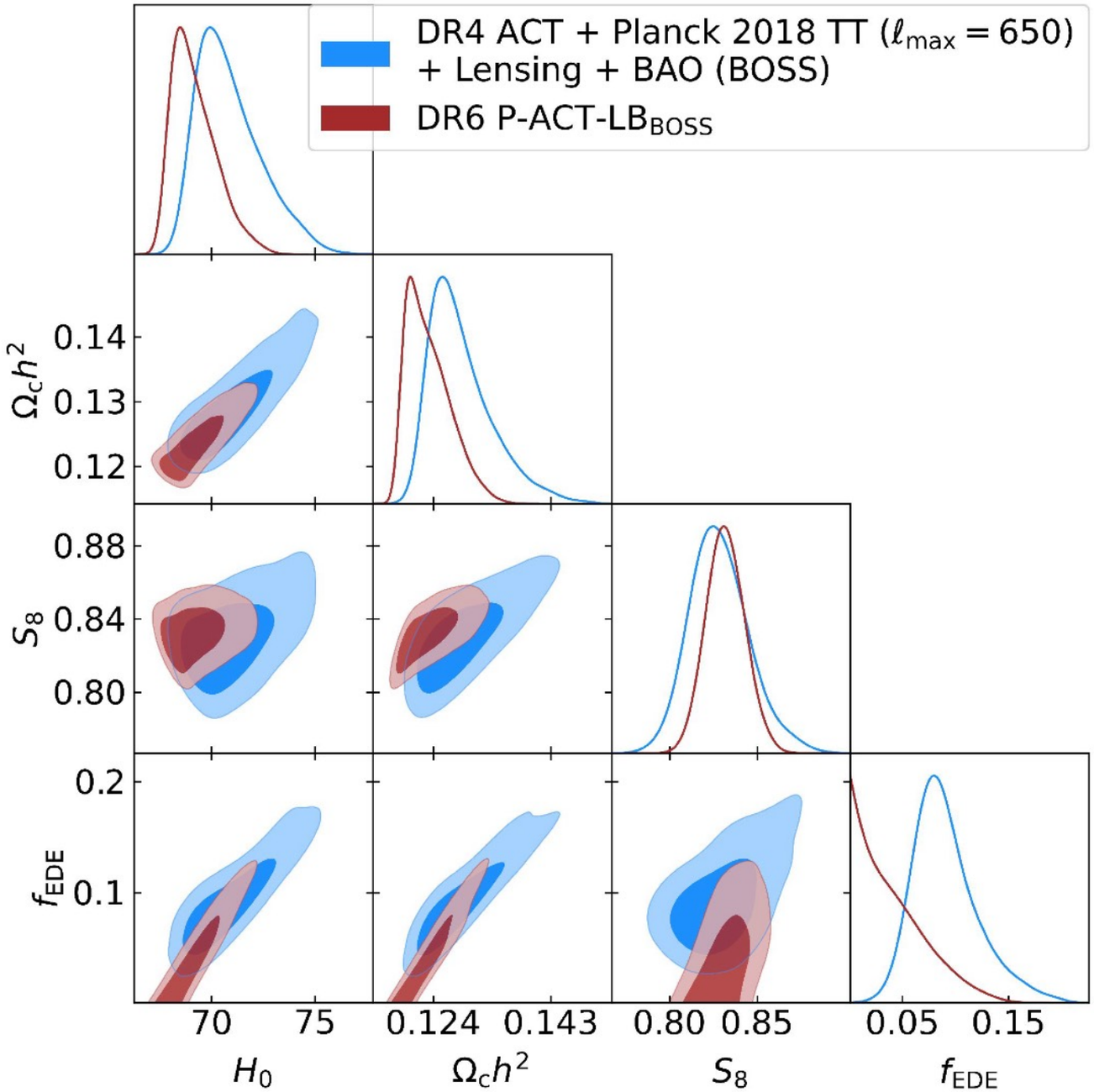

Dust in the DR6 patch

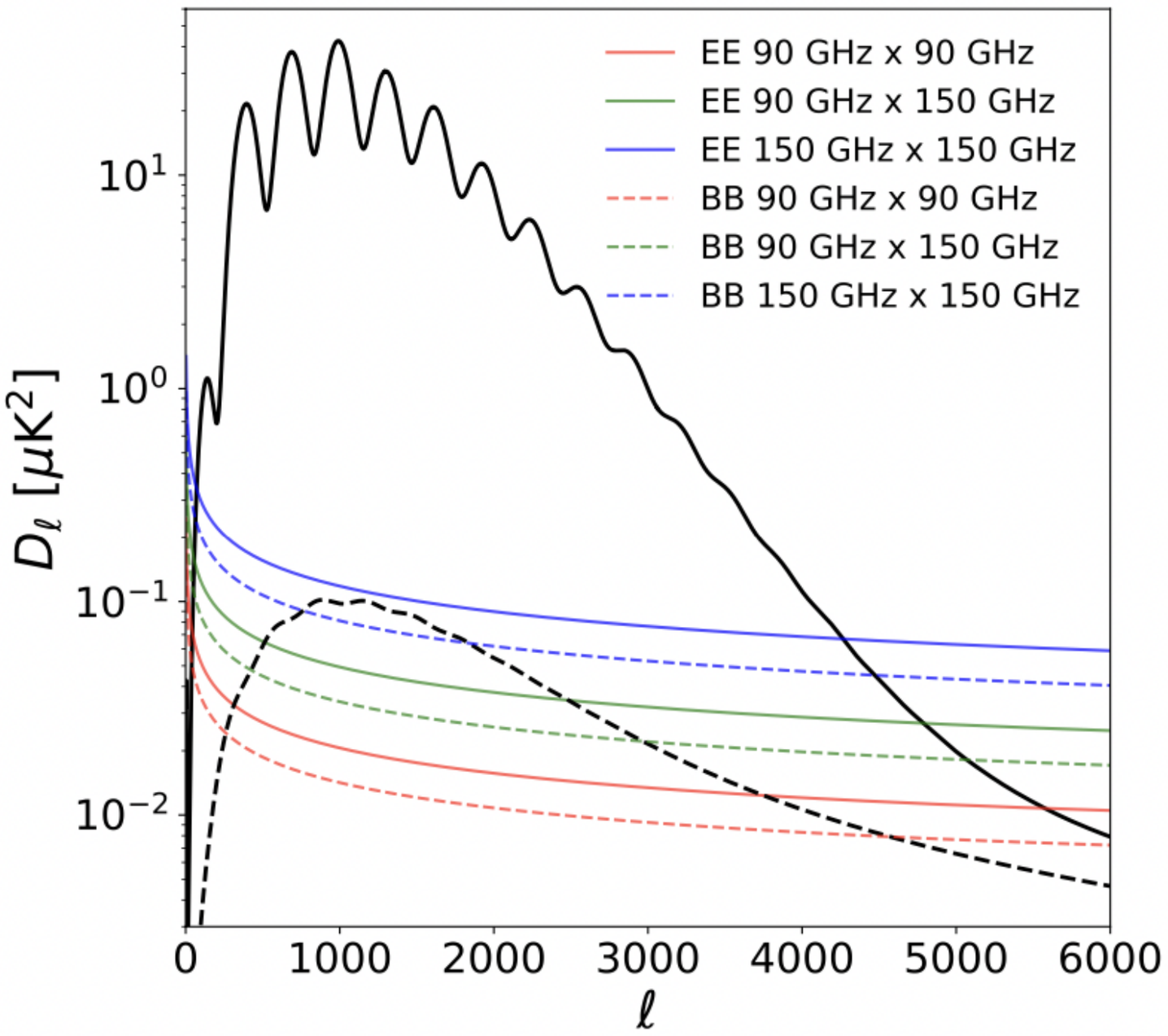

Independent constraints from ACT & WMAP

- Cosmological constraints from ACT DR6 and Planck are consistent (**1.6σ**)

- ACT + WMAP provides an independent and competitive dataset with e.g.

$\Omega_b h^2 = 0.02263 \pm 0.00012$

$H_0 = 66.78 \pm 0.68$ km/s/Mpc

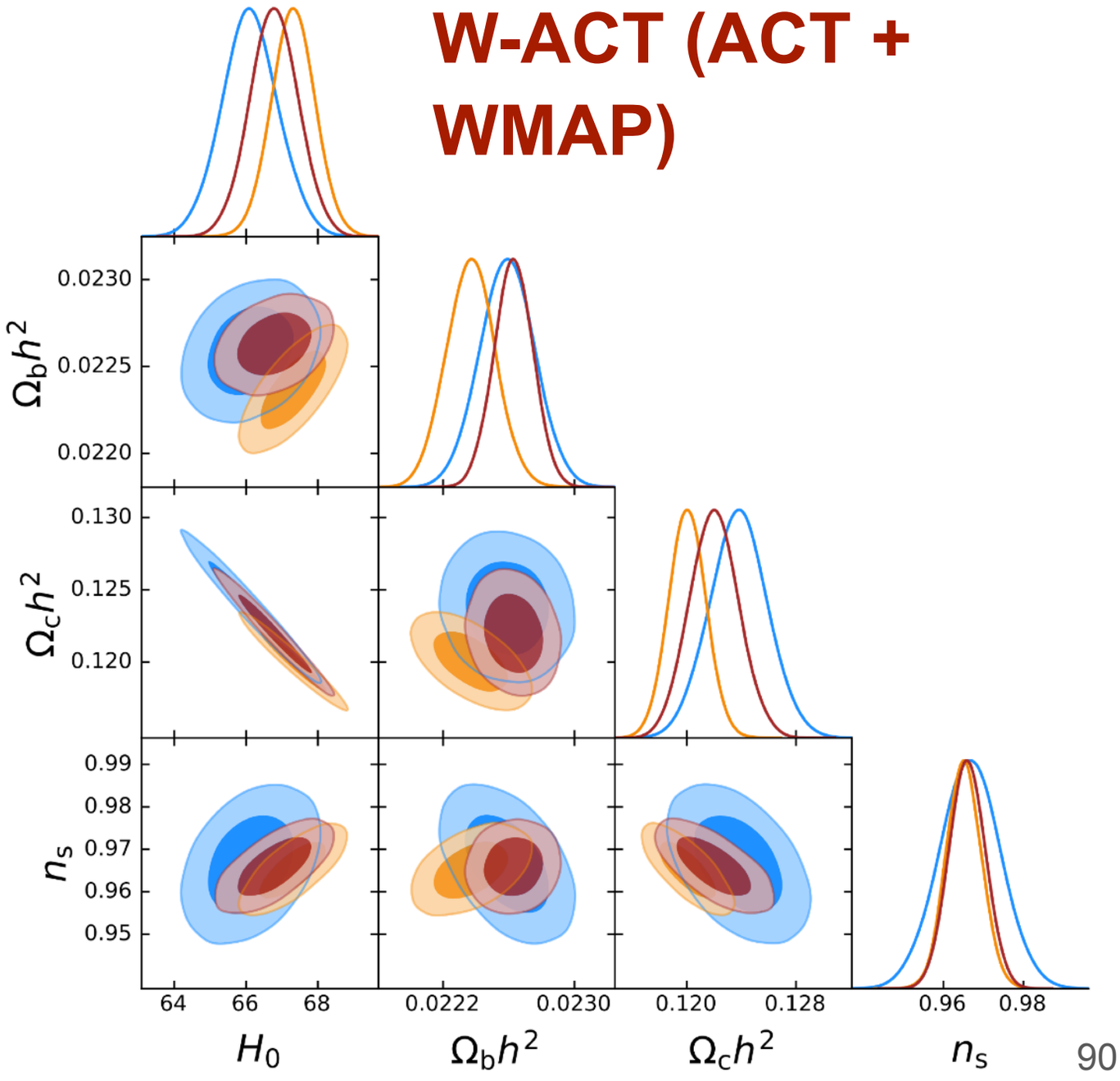

SPT post unblinding

https://arxiv.org/pdf/2411.06000 / SPT3G

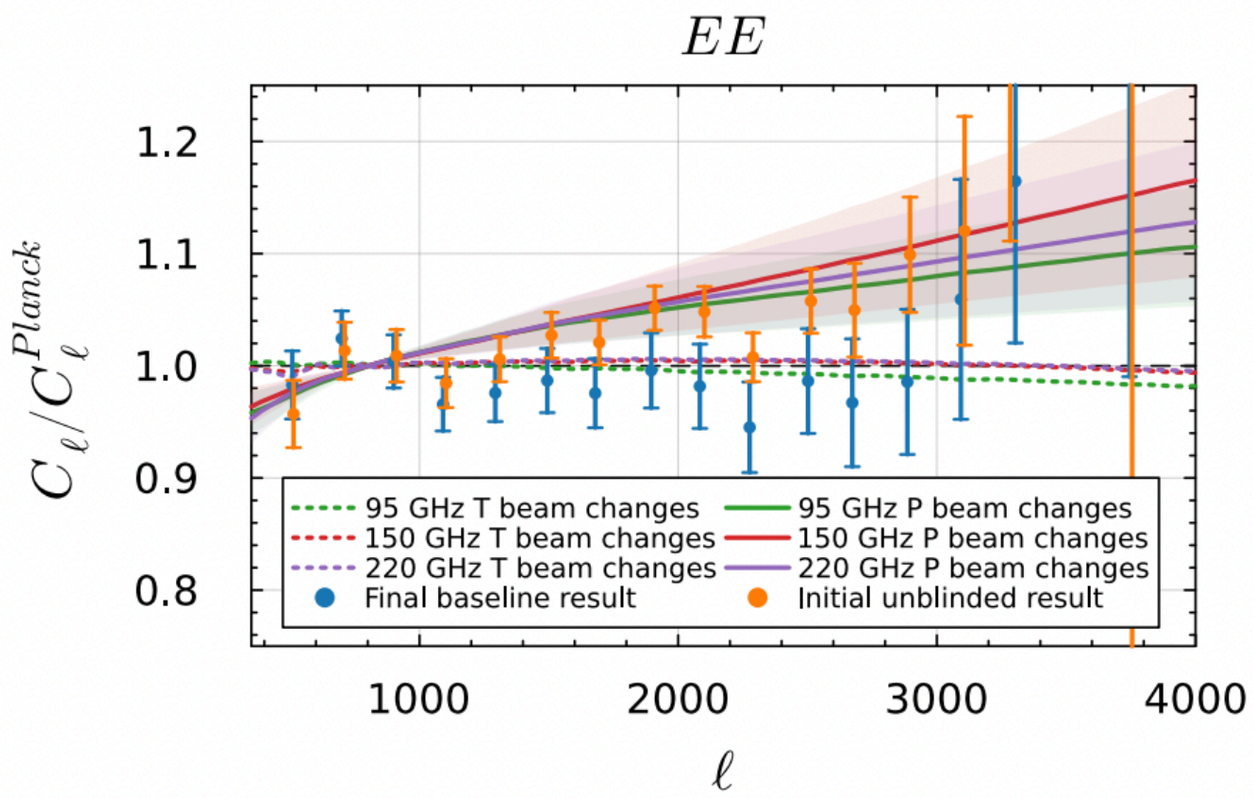

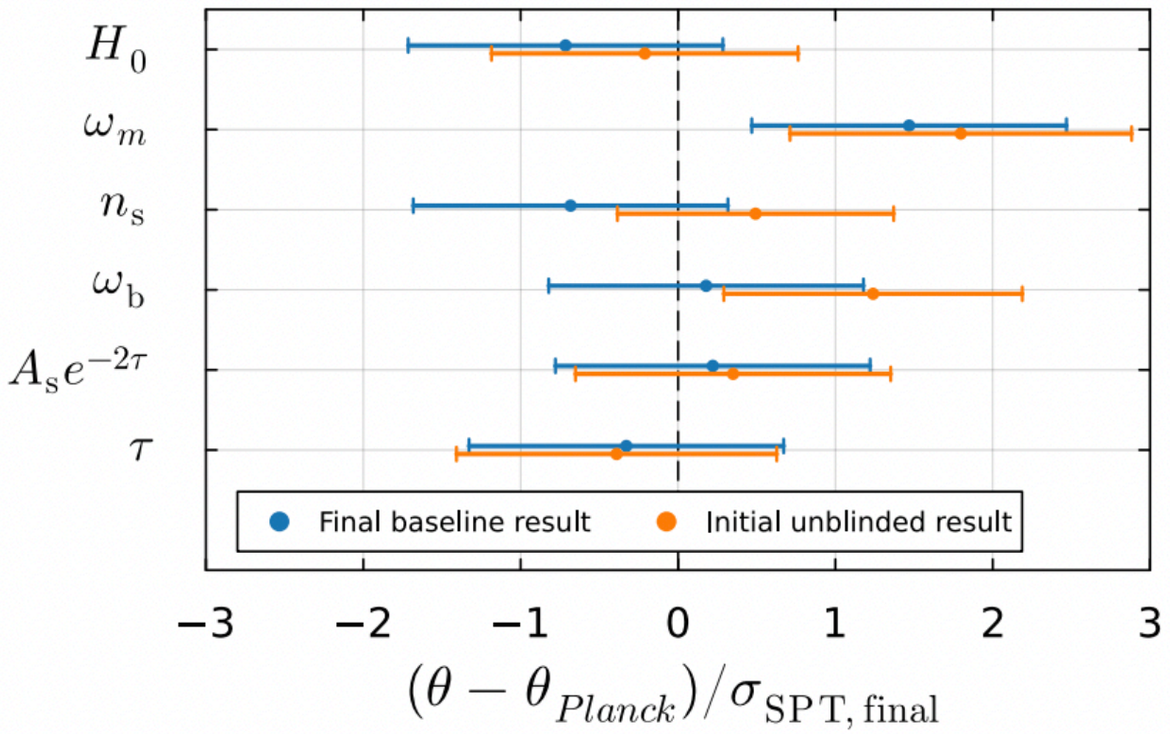

https://arxiv.org/pdf/2411.06000 / SPT3G

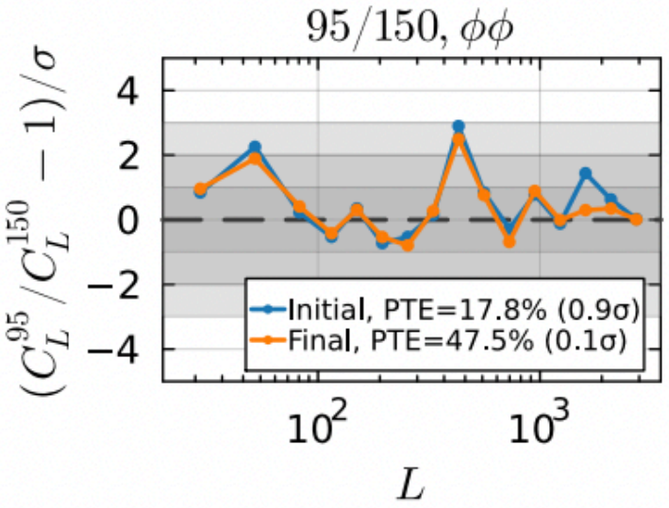

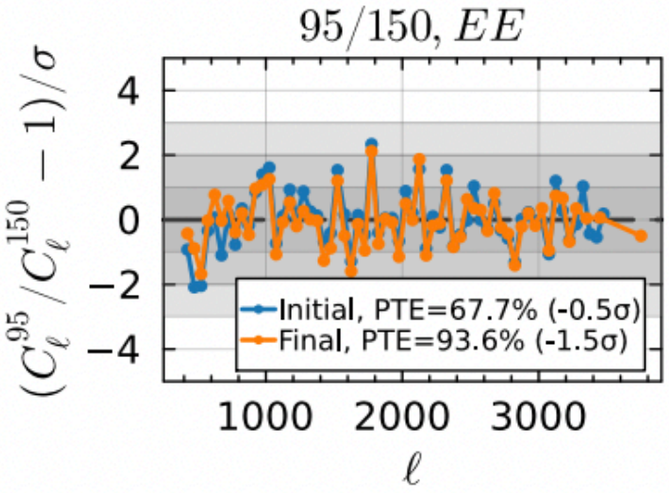

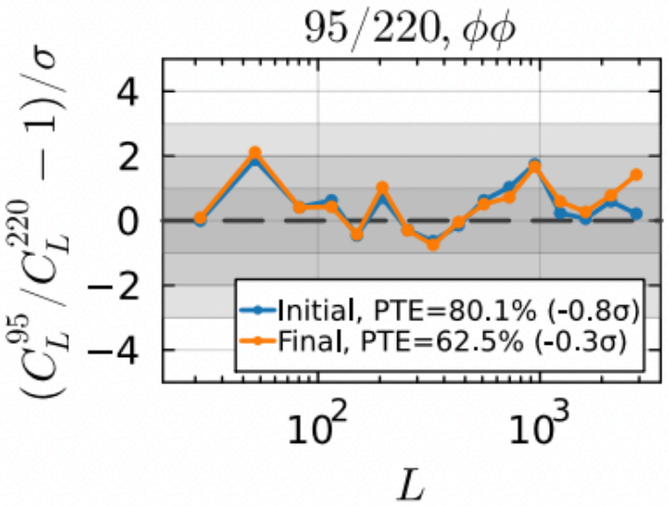

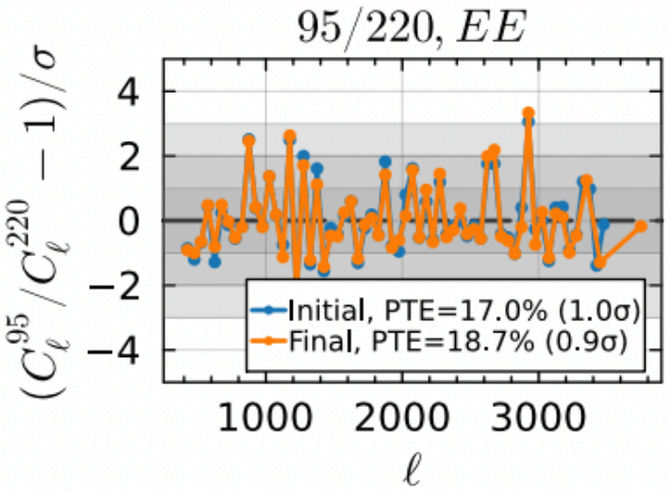

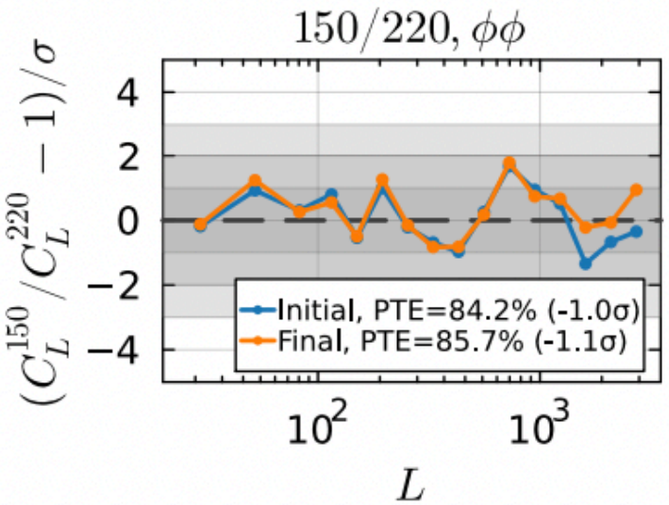

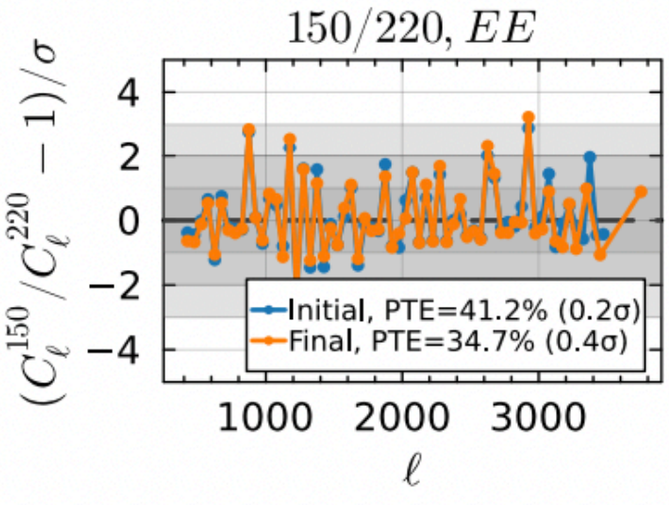

https://arxiv.org/pdf/2411.06000 / SPT3G

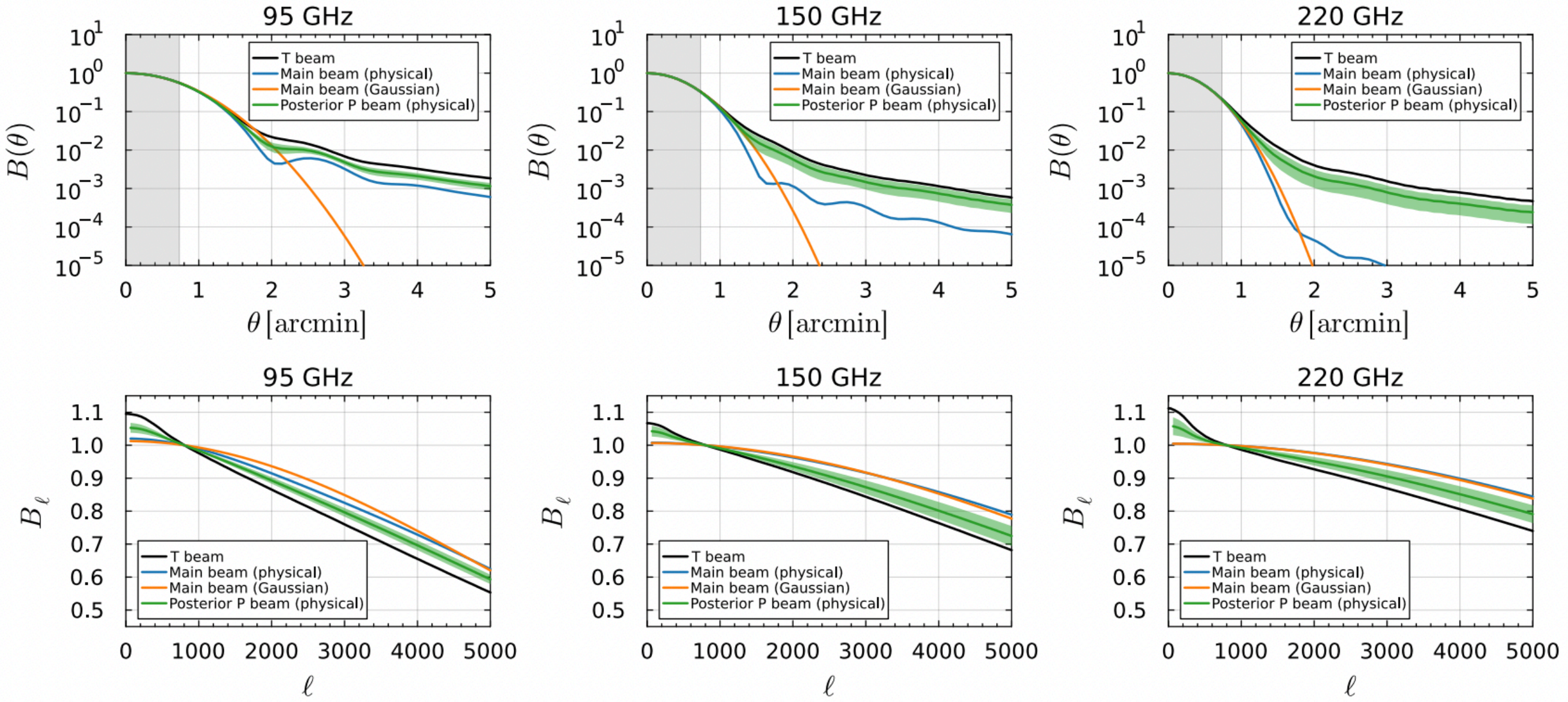

	Posterior		
	95 GHz	150 GHz	220 GHz
$A^1_{\rm cal}$	0.8977±0.0074	0.9276±0.0074	0.8612±0.0084
$A^2_{\rm cal}$	0.8928±0.0072	0.9133±0.0071	0.864±0.0079
$A^3_{\rm cal}$	0.8861±0.0073	0.9399±0.0075	0.849±0.0083
$A^4_{\rm cal}$	0.8775±0.008	0.9272±0.0081	0.8405±0.0097
$100\,\epsilon^1_{\rm Q}$	0.291±0.025	0.319±0.021	0.492±0.059
$100\,\epsilon^2_{\rm Q}$	0.402±0.024	0.39±0.022	0.418±0.06
$100\,\epsilon^3_{\rm Q}$	0.555±0.025	0.838±0.021	2.096±0.066
$100\,\epsilon^4_{\rm Q}$	0.603±0.033	0.912±0.03	2.221±0.084
$100\,\epsilon^1_{\rm U}$	0.584±0.027	0.74±0.025	0.735±0.064
$100\,\epsilon^2_{\rm U}$	0.648±0.025	0.748±0.023	0.642±0.058
$100\,\epsilon^3_{\rm U}$	0.851±0.027	1.238±0.023	1.33±0.063
$100\,\epsilon^4_{\rm U}$	0.83±0.035	1.174±0.03	1.121±0.092
$\psi_{\rm pol}\,[^\circ]$	0.393±0.024	0.419±0.021	-0.188±0.079
$\beta_{\rm pol}$	0.44±0.20	0.60±0.28	0.51±0.26

Polar efficiencies

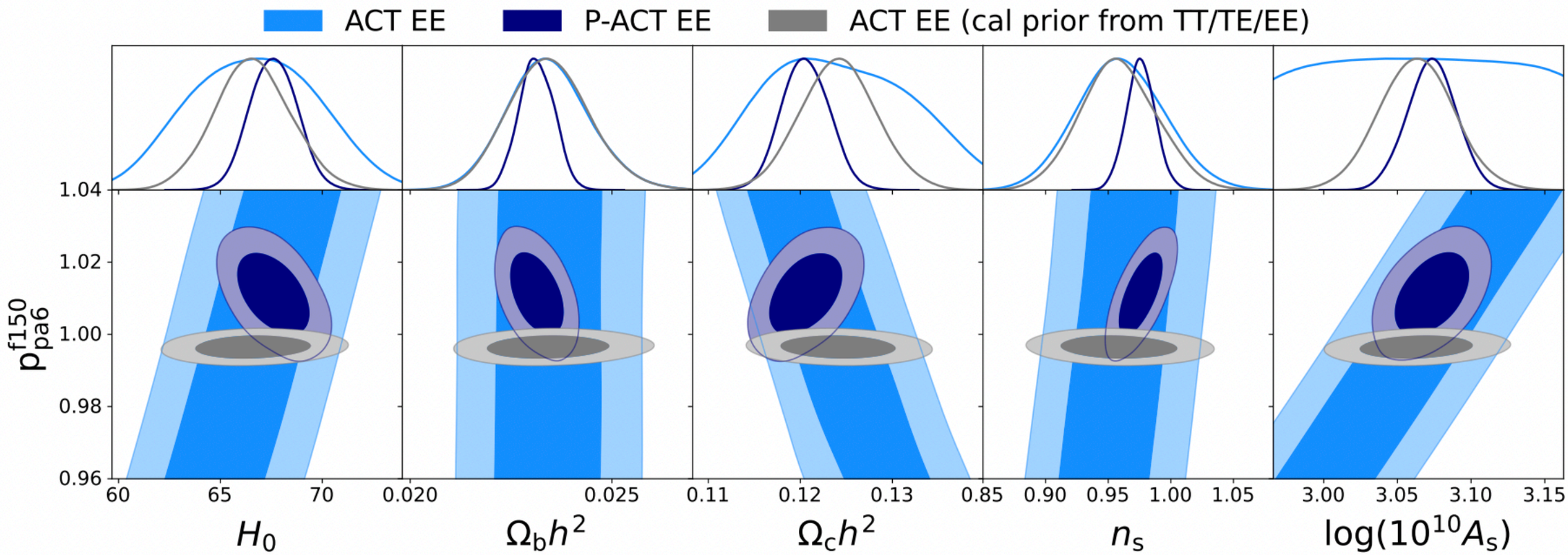

Figure 38. Marginalised posterior distributions of sampled parameters from EE, including the polarization efficiency for PA6 f150. We show constraints from ACT only (including the Sroll2 data to measure optical depth, light blue), P-ACT (dark blue) and ACT when using calibration and polarization efficiency priors from a full TT/TE/EE run (gray).

Telescopes

Telescope [edit]

The ACT is an off-axis Gregorian telescope. This off-axis configuration is beneficial to minimize artifacts in the point spread function. The telescope reflectors consist of a six-metre (236 in) primary mirror and a two-metre (79 in) secondary mirror. Both mirrors are composed of segments, consisting of 71 (primary) and 11 (secondary) aluminum panels. These panels follow the shape of an ellipsoid of revolution and are carefully aligned to form a joint surface.

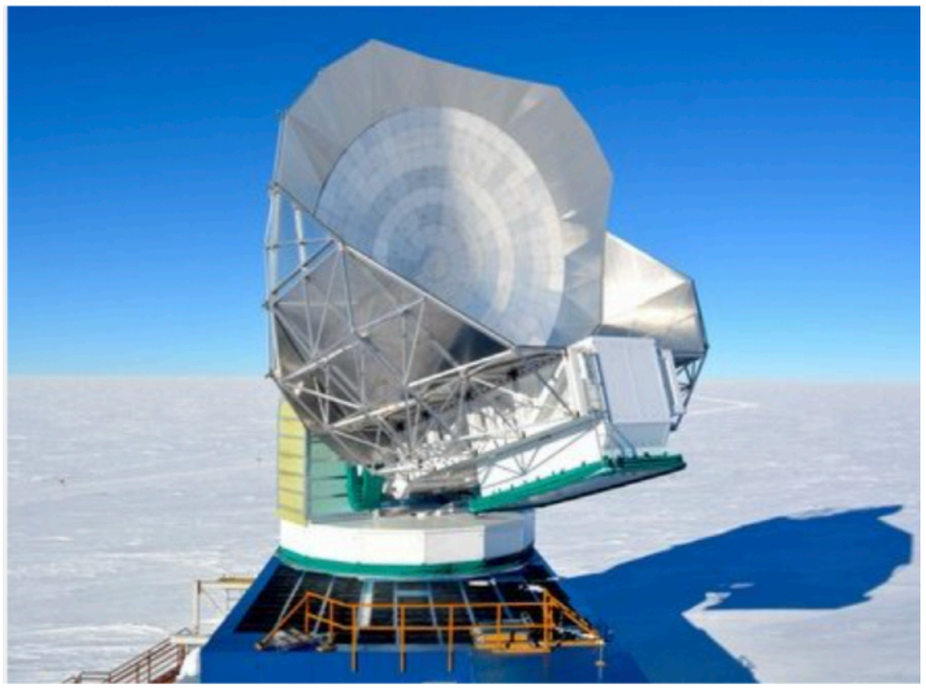

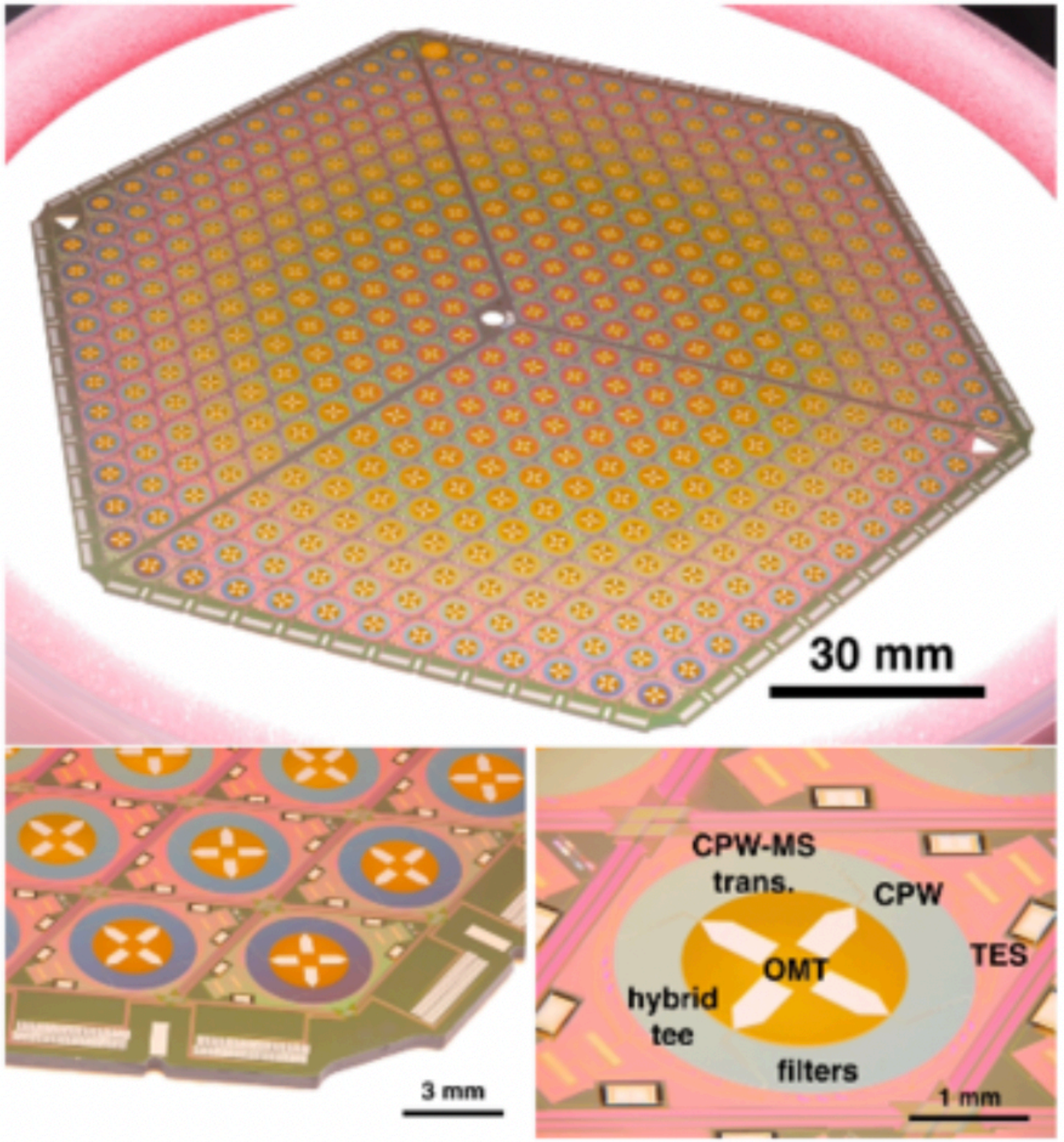

Figure 2.2: (Top): The full MF1 array showing high-density pixels. (Bottom left): The MF1 array partially zoomed at a corner to show a few pixels, and bond pads. (Bottom right): The MF1 array zoomed to show details of individual pixels including the OMT, CPW to microstrip (MS) transition, stub filters, hybrid tee, and the TES islands. The AdvACT detector arrays were fabricated by Shannon Duff at NIST. Base photos courtesy of Shannon Duff.

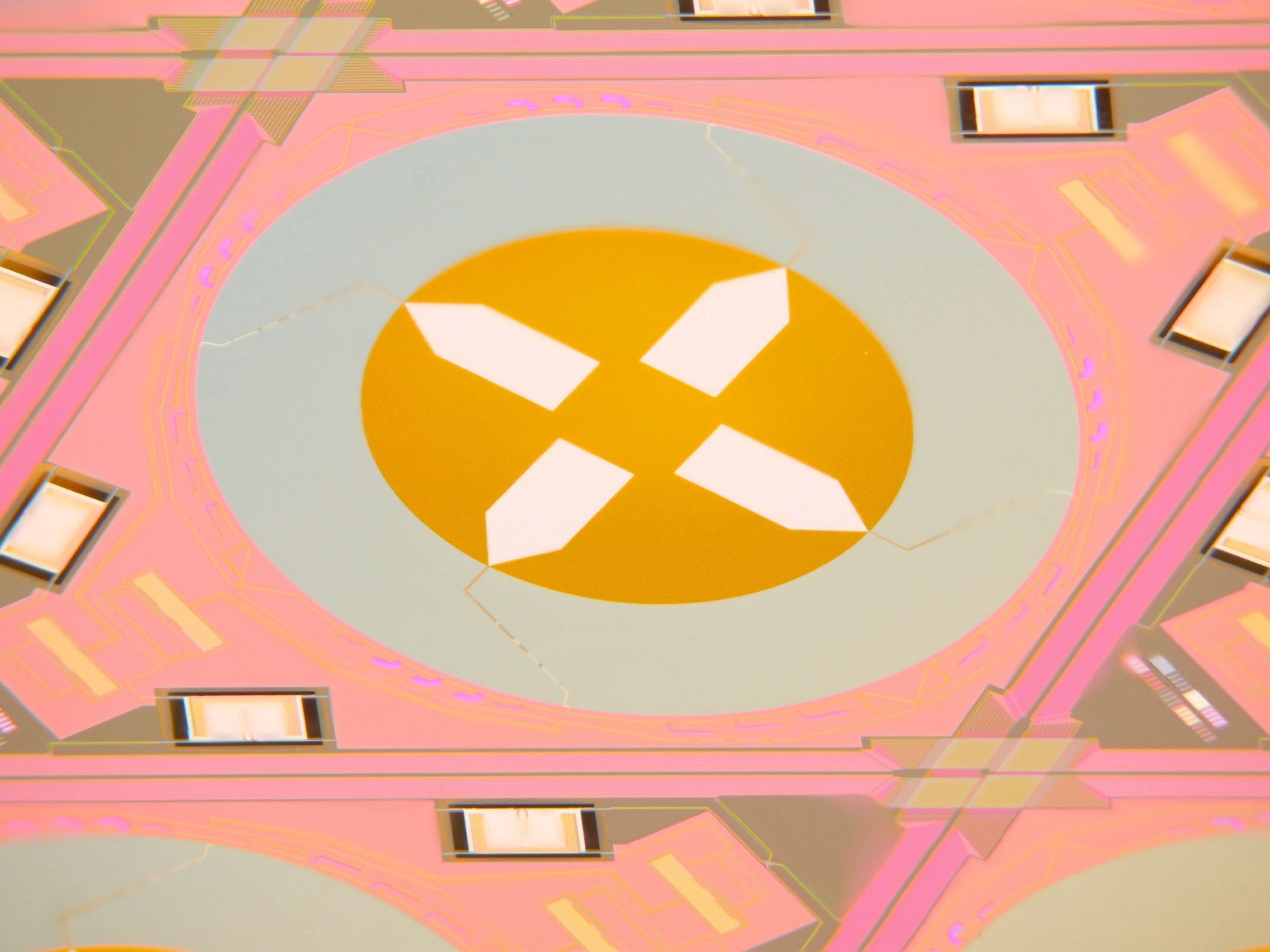

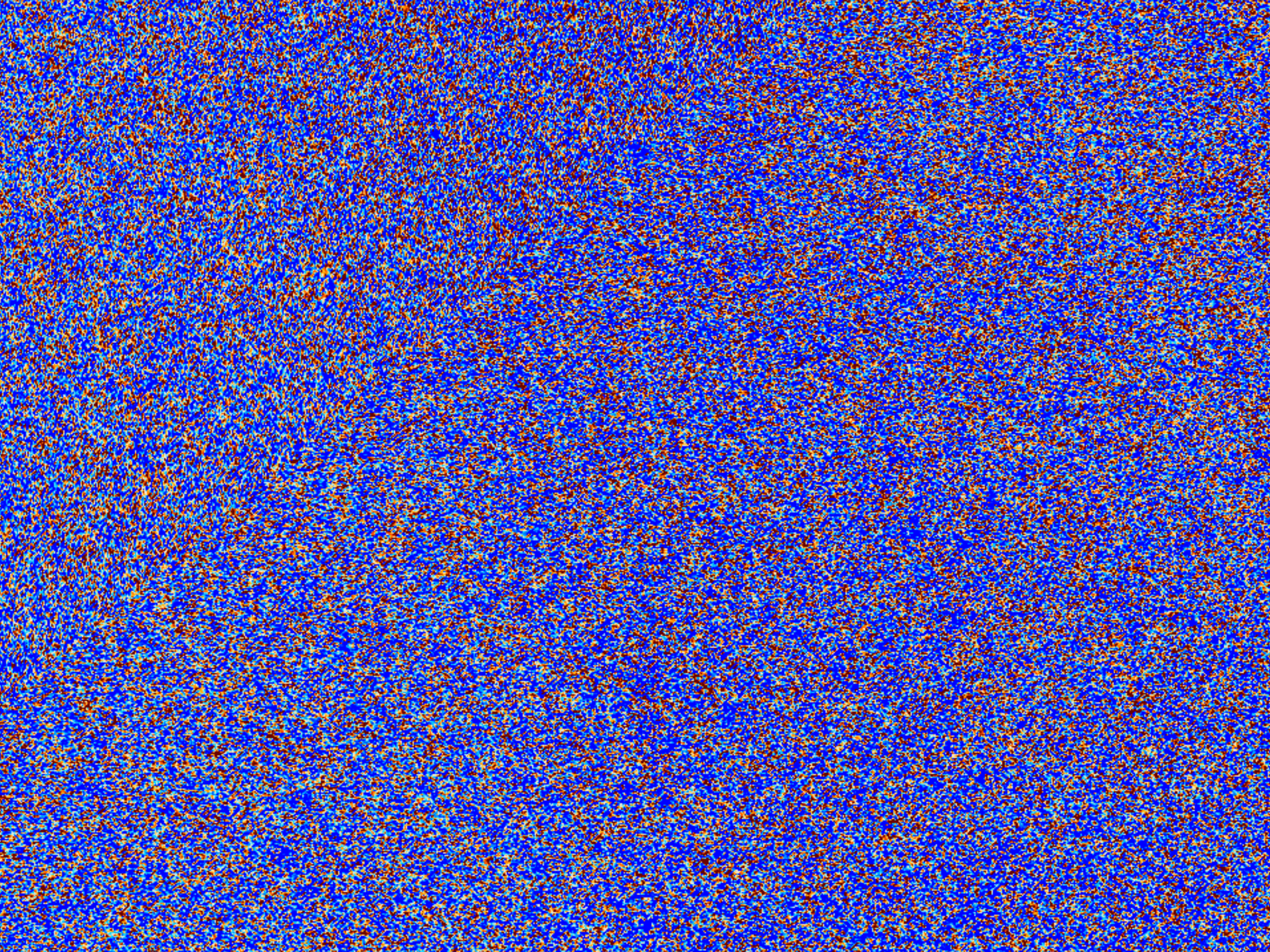

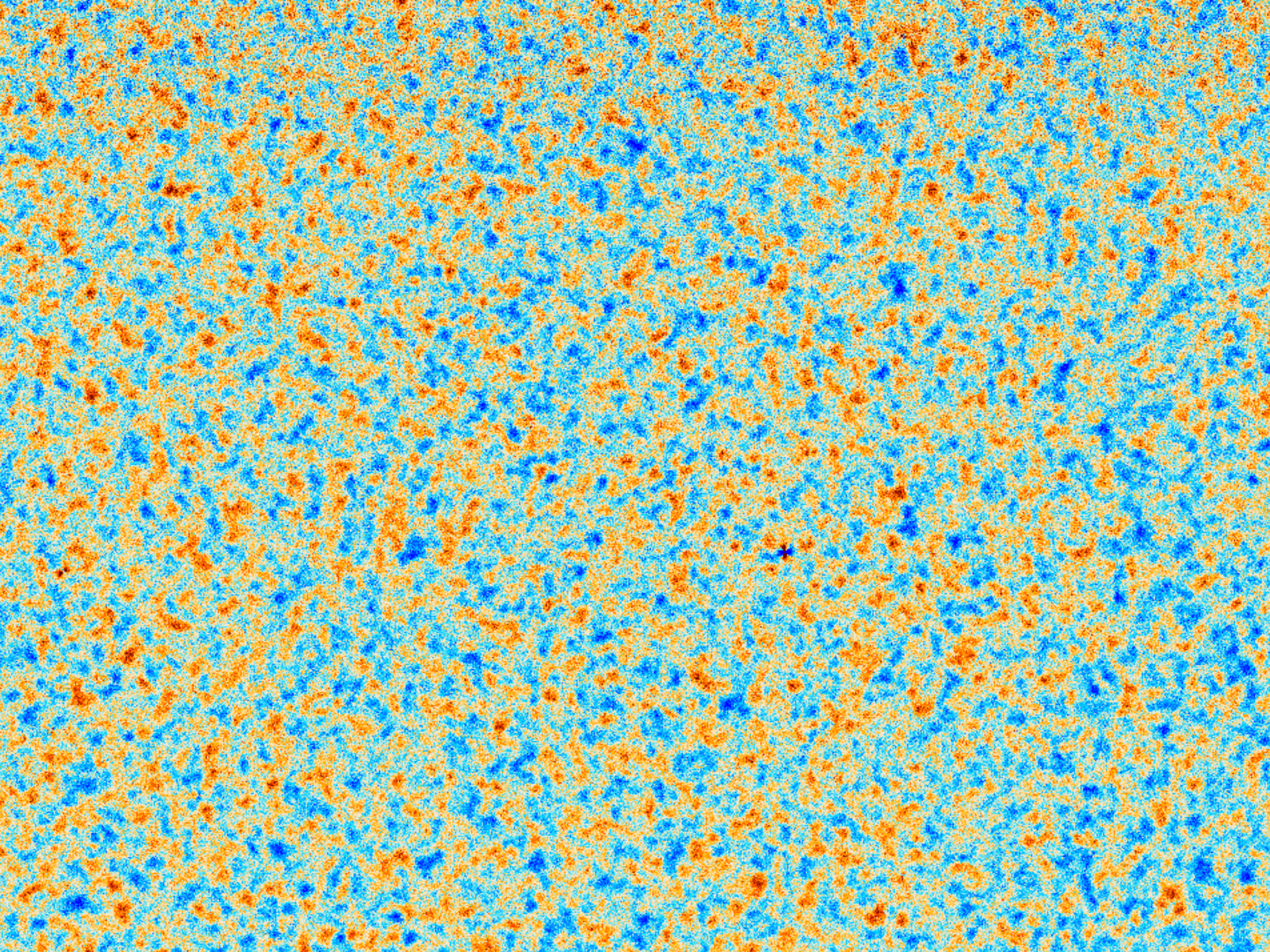

How does model change H0

Early dark energy : new field that accelerates the expansion prior to recombination, reduces sound horizon.

$$V(\phi) = m^2 f^2 (1 - \cos(\phi/f))^n \,, \qquad (10)$$

where m is the mass of the field, f is the axion decay constant, and n is a power-law index. While $n = 1$ is excluded on phenomenological grounds — as the EDE would act as an additional contribution to dark matter at late times — values of $n \geq 2$ constitute viable models. Here, we consider as baseline the $n = 3$ model, as in previous literature (e.g., Hill et al. 2020; Ivanov et al.

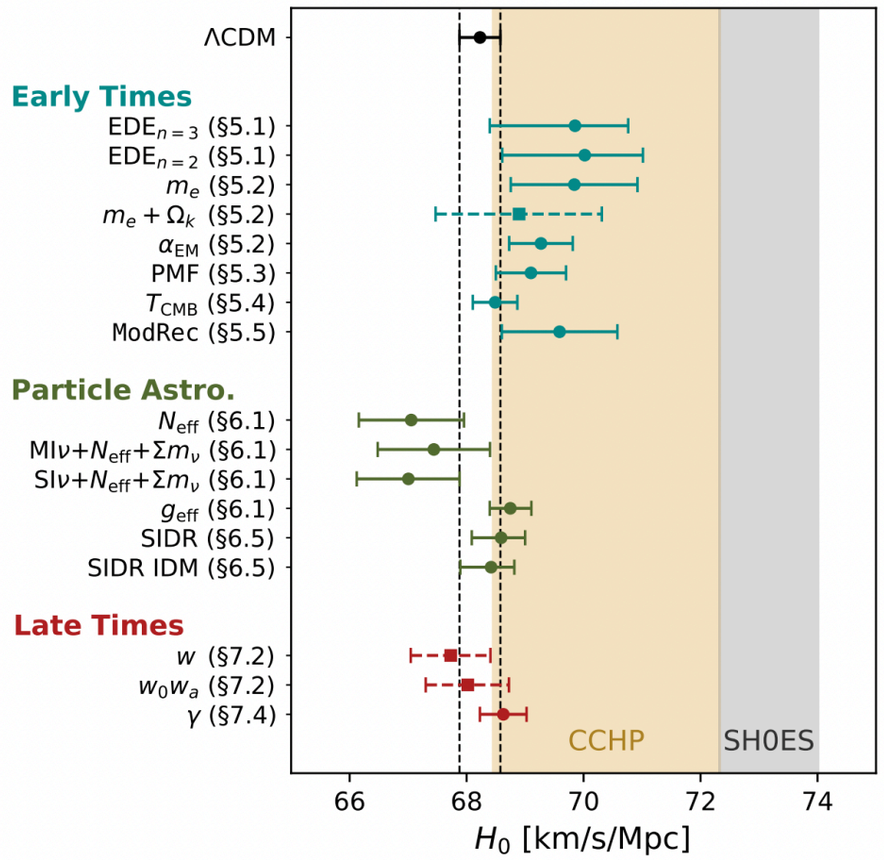

Fondamental constant

The dynamics of recombination depends critically on the values of fundamental constants during the decoupling epoch, including the fine-structure constant and the electron mass, we assume that the value of these parameters undergoes an instantaneous, step-function transition well after recombination is completed, but well before the reionization epoch (specifically, we choose z = 50 for the redshift of this transition).

these effects). The dominant physical effects are due to changes in the Thomson scattering cross-section, with $\sigma_T \propto \alpha_{EM}^2 m_e^{-2}$, and changes in the energy levels of atomic hydrogen, with $E \propto \alpha_{EM}^2 m_e$. Many additional, subtle effects arise due to the non-equilibrium nature of cosmological recombination — see, e.g., Hart & Chluba (2018); Chluba & Ali-Haïmoud (2016); Planck Collaboration (2015) for a thorough discussion. In general, variations of α_{EM} or m_e change the timing of recombination, with higher values of these constants associated with earlier recombination. Thus, such variations change the physical scales imprinted in the CMB power spectrum, including the damping scale. The new ACT DR6 spectra allow tests of these effects in a qualitatively new regime, deep into the damping tail in TT and across a wide range of scales in TE and EE.

How does model change H0

5.3. *Primordial magnetic fields*

The existence of primordial magnetic fields (PMFs) is a compelling possibility. Such PMFs could cause inhomogeneities in the baryon distribution around recombination. Thus, the PMF model is an example of a slightly more generic scenario known as "baryon clumping" (Jedamzik & Abel 2013; Jedamzik & Saveliev 2019). Primordial magnetic fields with a blue-tilted power spectrum can naturally have kpc-scale correlation lengths. Once the photon gas dynamically decouples from the baryon fluid on small scales, the magnetic force causes efficient growth of baryon density perturbations to potentially $\mathcal{O}(1)$ contrasts. These kpc-scale perturbations are not directly resolvable in CMB observations, but they cause accelerated recombination due to the quadratic source term in the equation describing the recombination rate (Peebles 1968). The corresponding decrease in the sound horizon could then partially reconcile CMB-based determinations of the Hubble constant with local universe measurements (Jedamzik & Pogosian 2020). As magnetic fields are part of the standard model and their generation during early-universe phase transitions is conceivable, PMFs (or baryon clumping models in general) are a well-motivated scenario to potentially increase the CMB-inferred Hubble constant.[17]

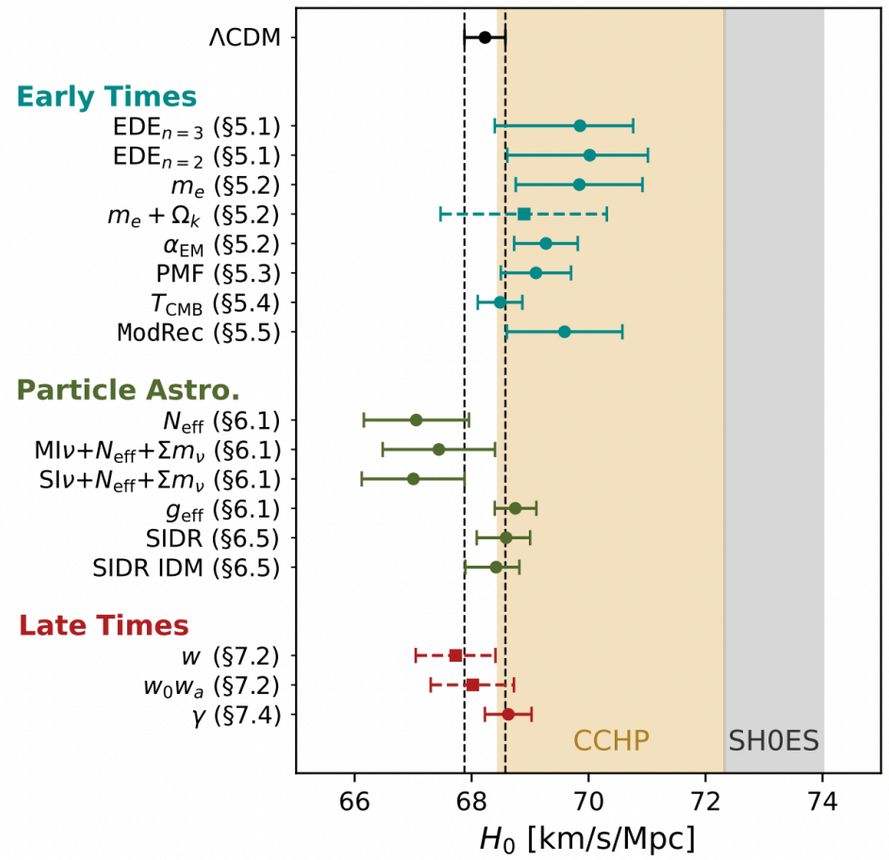

How does model change H0

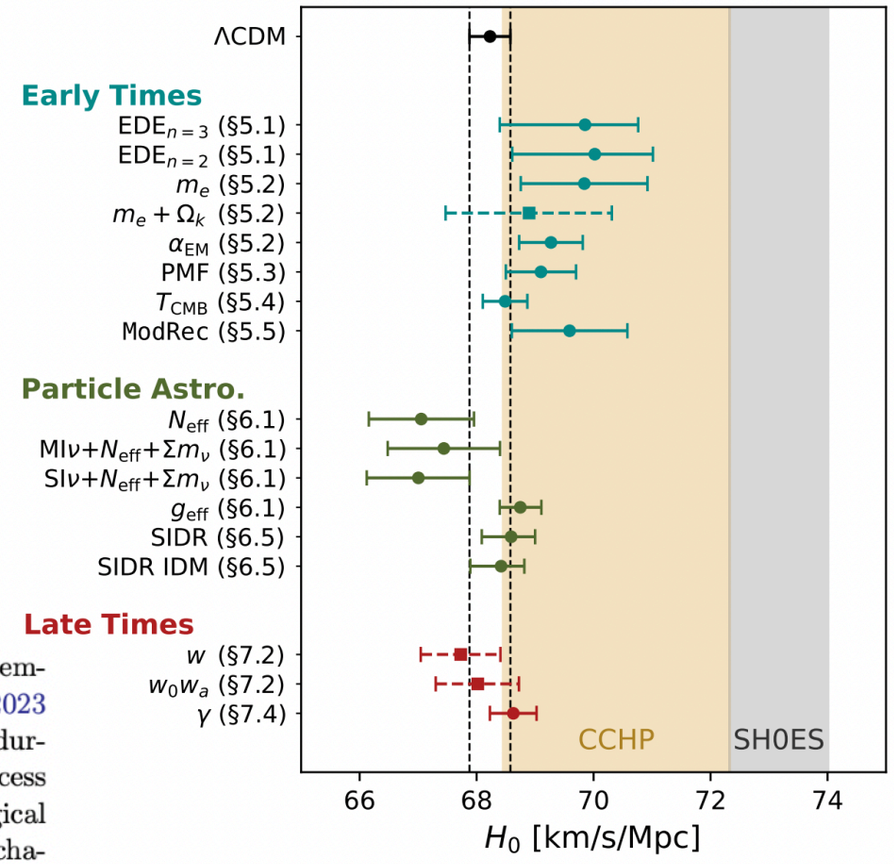

CMB temperature

Several studies (e.g., Ivanov et al. 2020a; Wen et al. 2021; Hill & Bolliet 2023) have explored the possibility of increasing the CMB-anisotropy-inferred value of the Hubble constant by changing the CMB monopole temperature, $T_{\rm CMB}$. In particular, Ivanov et al. (2020a) highlighted a strong negative degeneracy in the H_0-$T_{\rm CMB}$ plane when the monopole temperature is left free in analyses of *Planck* data. Setting a SH0ES prior on H_0 would then yield a temperature measurement 3σ lower than the combined measurement of $T_{\rm CMB} = 2.72548 \pm 0.00057$ K (Fixsen 2009) from *COBE/FIRAS* and other data.[18]

Obtaining a higher value of H_0 via a decrease in the monopole CMB temperature is difficult. Models with some level of post-recombination reheating can have an impact by allowing a lower value of the monopole temperature in the early universe (e.g., Hill & Bolliet 2023 propose to convert a fraction of DM into photons during the dark ages). However, although such a process is straightforward to implement in a phenomenological way, it is hard to find a well-grounded physical mechanism to motivate it such that the blackbody spectrum is preserved (see, e.g., Chluba 2014).

Nevertheless, these studies have led to the realization that current CMB anisotropy data in combination with BAO data provide, on their own, a powerful probe of the amount of radiation in the universe.[19] A single-parameter extension to the ΛCDM model, where $T_{\rm CMB}$ is left free, is well constrained. Ivanov et al. (2020a) combine *Planck* 2018 CMB anisotropy and lensing data with BOSS DR12 BAO data (eBOSS Collaboration 2018) and find $T_{\rm CMB} = 2.706^{+0.019}_{-0.020}$ K (68% CL). Updating this *Planck* result including BAO from DESI, we find a slightly tighter constraint, $T_{\rm CMB} = 2.696 \pm 0.017$ K. With the addition of the new ACT DR6 spectra, we find a similar constraint

$$T_{\rm CMB} = 2.698 \pm 0.016\,{\rm K}\ (68\%, \textsf{P-ACT-LB}). \quad (28)$$

How does model change H0

Neutrino number

The CMB is able to constrain $N_{\rm eff}$ because its value affects the expansion rate of the universe, especially during the radiation-dominated phase, thereby altering the expansion history just before recombination and the predicted abundances of primordial light elements (Bashinsky & Seljak 2004; Hou et al. 2013; Abazajian et al. 2015; Pan et al. 2016; Baumann et al. 2016a). At the perturbative level, $N_{\rm eff}$ alters the damping tail (high-ℓ region) of the TT/TE/EE spectra, both because the change to the expansion history alters the timescale for diffusion damping and because the free-streaming nature of the radiation damps the growth of perturbations, with the latter also inducing a characteristic phase shift in the acoustic peaks (Bashinsky & Seljak 2004). Combining the *Planck* legacy CMB with *Planck* CMB lensing and BOSS BAO, the neutrino number is measured to be $N_{\rm eff} = 2.99 \pm 0.17$ at 68% CL (Planck Collaboration 2020c), or $N_{\rm eff} = 3.06 \pm 0.17$ at 68% CL when we evaluate this estimate using Planck-LB.

With the new ACT DR6 spectra we find $N_{\rm eff} = 2.60^{+0.21}_{-0.29}$ at 68% CL, combining into

$$\begin{aligned} N_{\rm eff} &= 2.73 \pm 0.14 \quad (68\%, \text{P-ACT}), \\ &= 2.86 \pm 0.13 \quad (68\%, \text{P-ACT-LB}), \end{aligned} \tag{30}$$

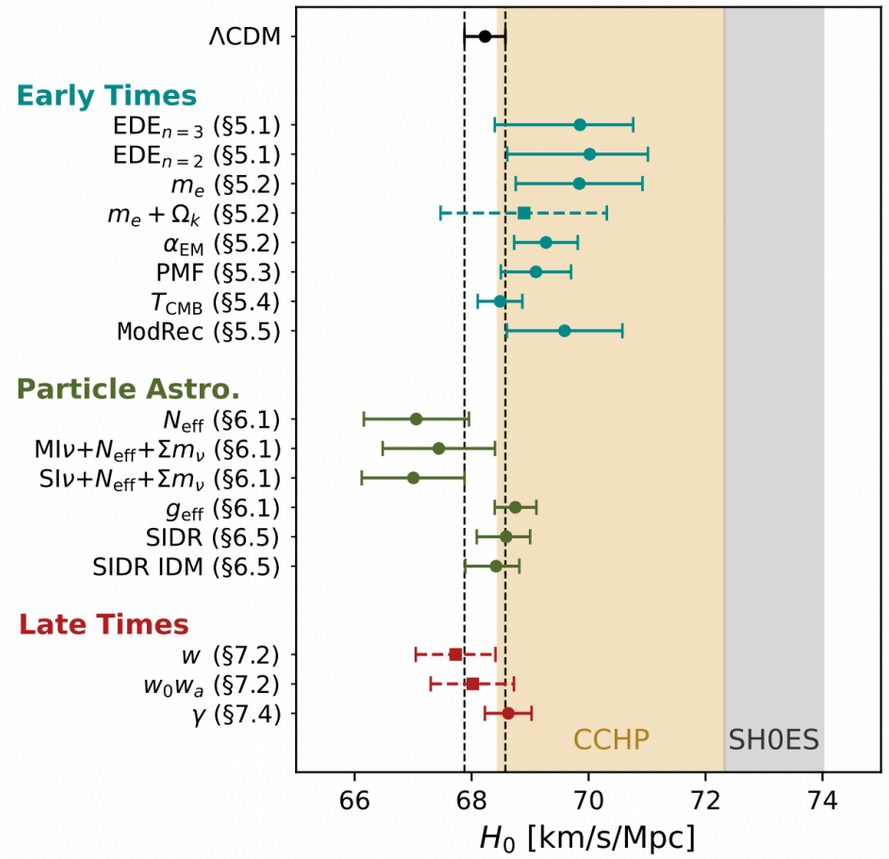

How does model change H0

Neutrino self-interactions: heavy mediator

We consider first the case where the mass m_ϕ of the mediator is much larger than the neutrino temperature at all times directly probed by CMB anisotropies (Cyr-Racine & Sigurdson 2014). In this case, the neutrino interaction is effectively a four-fermion vertex controlled by a dimensional coupling constant $G_{\rm eff} = g^2/m_\phi^2$, i.e., the effective low-energy Lagrangian is $\mathcal{L}_{\rm eff} = G_{\rm eff}\bar{\nu}\nu\bar{\nu}\nu$. This is analogous to the low-energy behavior of standard weak interactions, just with $G_{\rm eff}$ taking the place of the Fermi constant $G_{\rm F} \simeq 1.17 \times 10^{-5}\ {\rm GeV}^{-2}$. This low-energy limit does not depend on the nature of the mediator, so the analysis here naturally encompasses both the scalar and vector cases. The Boltzmann hierarchy for neutrino perturbations including the collision term $\mathcal{L}_{\rm eff}$ generated by the interaction has been derived by Kreisch et al. (2020).

In this scenario, neutrino free-streaming does not start at the time of weak decoupling, but is instead delayed until $T_{\rm fs} = T_{\nu,{\rm dec}}(G_F/G_{\rm eff})^{2/3}$, where $T_{\nu,{\rm dec}} \simeq 1\,{\rm MeV}$ is the neutrino decoupling temperature. Neutrino self-interactions through a heavy mediator leave an imprint at angular scales $\theta \lesssim \theta_{\rm fs}$ (assuming $\theta_{\rm fs} < \theta_{\rm eq}$), where $\theta_{\rm fs}$ is the scale entering the horizon at $T = T_{\rm fs}$.

Previous analyses have shown that CMB and BAO data are compatible with, and in some cases prefer, neutrino self-interactions with $G_{\rm eff} \gg G_F$ (Cyr-Racine & Sigurdson 2014; Archidiacono & Hannestad 2014; Lancaster et al. 2017; Oldengott et al. 2017; Park et al. 2019; Kreisch et al. 2020; Barenboim et al. 2019; Brinckmann et al. 2021; Das & Ghosh 2021; Mazumdar et al. 2022; Roy Choudhury et al. 2021; Poudou et al. 2025). In fact, the posterior for $G_{\rm eff}$ has been found to be bimodal, with probability being concentrated in two distinct regions: a moderately interacting (MIν) mode, compatible with no self-interactions, and a strongly interacting (SIν) mode. The analysis of ACT DR4 data showed a slight preference for neutrino self-interactions at the $2-3\sigma$ level, finding $G_{\rm eff} \lesssim 10^{-3}\,{\rm MeV}^{-2}$ for MIν, and $G_{\rm eff} \simeq 10^{-1.5}\,{\rm MeV}^{-2}$ for SIν (Kreisch et al. 2024).

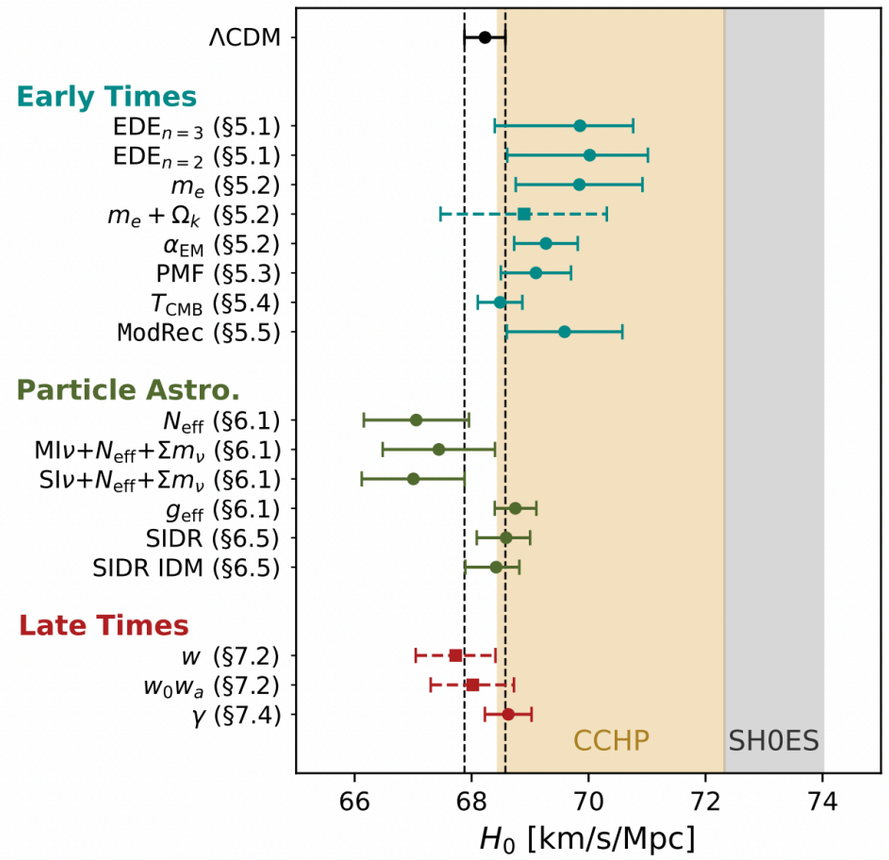

	ACT	P-ACT	P-ACT-LB
$\Delta\chi^2_{\rm MI\nu}$	−0.2	2.9	3.1
$\Delta\chi^2_{\rm SI\nu}$	−3.2	−10.6	−7.3
$\sigma_{\rm MI\nu}$	–	1.7	1.8
$\sigma_{\rm SI\nu}$	–	–	–

Table 3. $\Delta\chi^2 \equiv \chi^2_{\Lambda{\rm CDM}} - \chi^2_{\Lambda{\rm CDM}+G_{\rm eff}}$ from the MAP points of the MIν and SIν regions for different data combinations. When self-interacting neutrino models yield an improvement of the fit over ΛCDM we also report the preference for the model in units of σ. We find no statistically significant preference for neutrino self-interactions.

We start by considering a one-parameter extension of ΛCDM, including $G_{\rm eff}$ as an extra parameter and keeping fixed $\sum m_\nu = 0.06\,{\rm eV}$ and $N_{\rm eff} = 3.044$. To check if the bimodal behavior persists

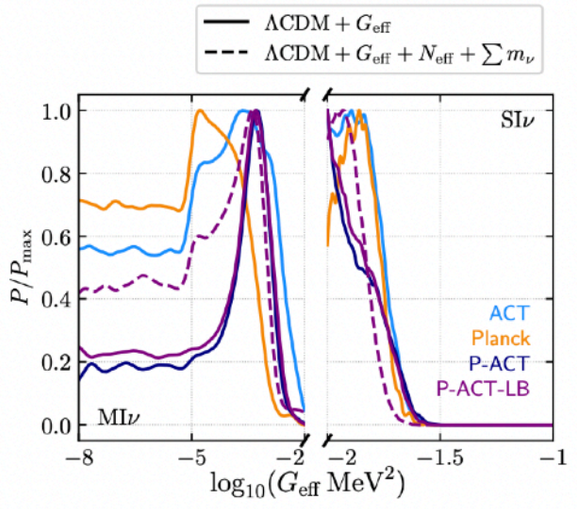

How does model change H0

Neutrino self-interactions: light mediator

In this scenario the mediator mass is much smaller than the average neutrino momentum at all times of interest and the scattering rate $\Gamma \propto g^4 T$, so that the ratio between the scattering and Hubble rates increases with time. Neutrinos will then start free streaming at weak decoupling as usual, and become collisional again at later times (Archidiacono & Hannestad 2014; Forastieri et al. 2015, 2019). The effects of collisions are confined to scales between $\theta_{\rm coll}$, the scale entering the horizon when neutrinos stop free streaming at late times, and $\theta_{\rm eq}$. These correspond to intermediate angular scales in the CMB power spectra (larger scales compared to those affected by a heavy mediator) and so we expect less contribution to this limit from ACT DR6.

From *Planck* CMB data, we find $g^4_{\rm eff} < 1.5 \times 10^{-27}$ at 95% CL. The new ACT DR6 spectra alone give a limit about three times weaker, with $g^4_{\rm eff} < 5.2 \times 10^{-27}$ at 95% CL. Combining the two datasets gives a $\sim$ 20% improvement on *Planck* alone, with

$$\begin{aligned} g^4_{\rm eff} &< 1.2 \times 10^{-27} \quad (95\%, \text{P-ACT}), \\ &< 1.3 \times 10^{-27} \quad (95\%, \text{P-ACT-LB}), \end{aligned} \tag{38}$$

or $|g_{\rm eff}| < 1.1 \times 10^{-7}$.

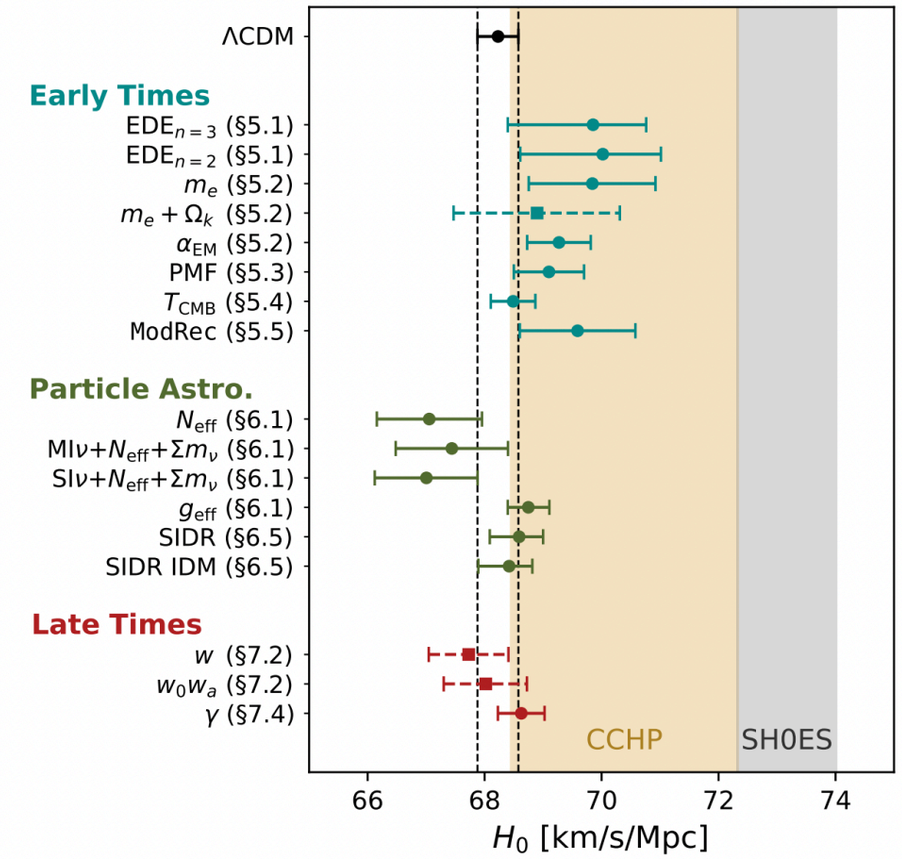

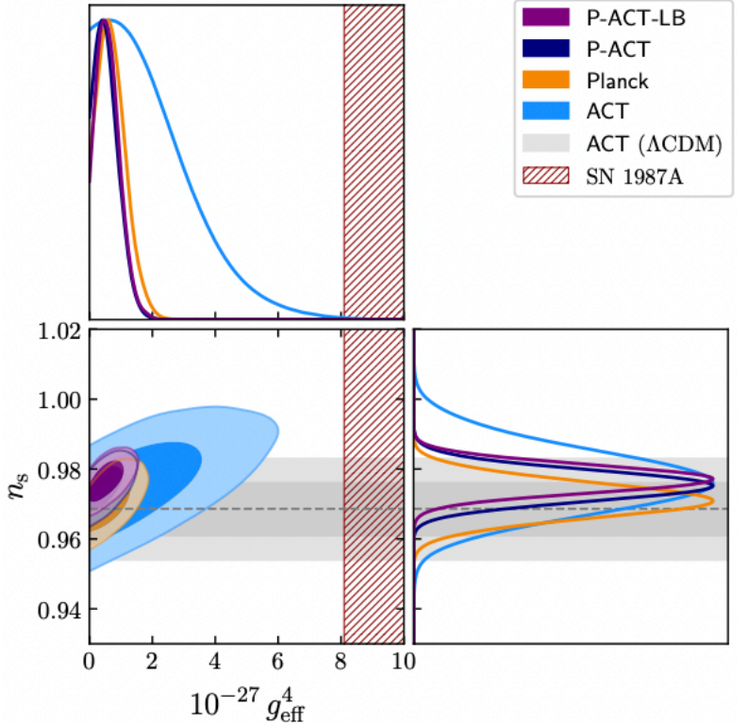

How does model change H0

Interacting DR-DM

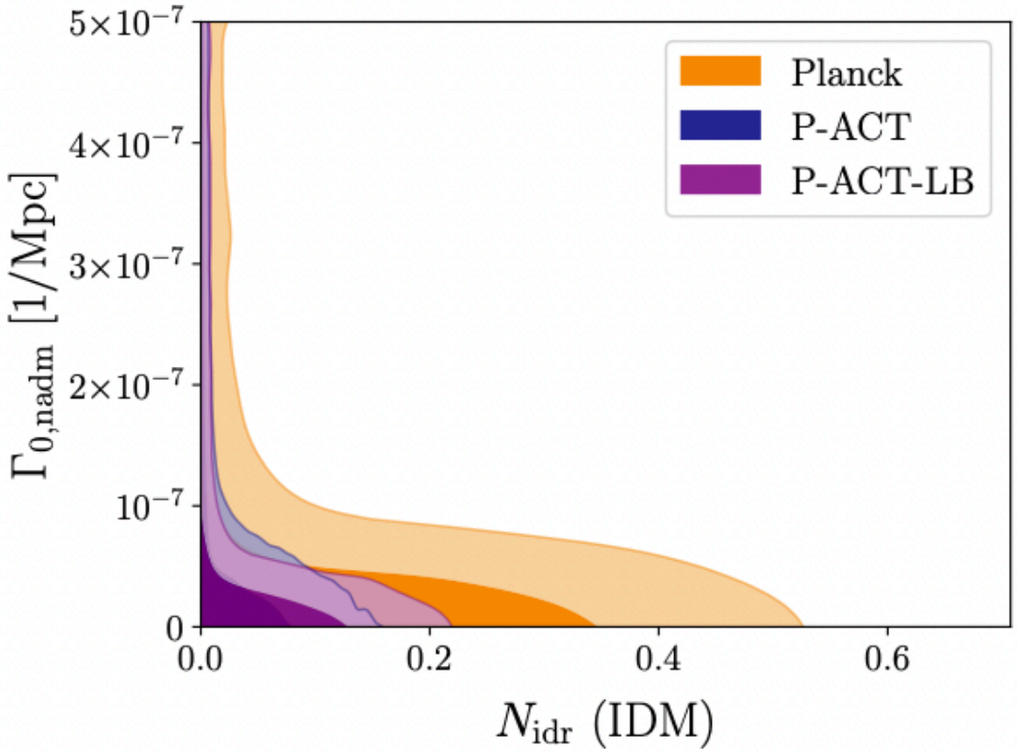

Figure 35. Constraints on the IDR-IDM model. Here the interaction strength $\Gamma_{0,\mathrm{nadm}}$ is given in 1/Mpc. The inclusion of ACT DR6 spectra (navy) significantly improves the constraints from *Planck* alone (orange). Inclusion of CMB lensing and DESI BAO data (purple) slightly weakens the N_{idr} upper limit due to small shifts in the best-fit model parameters, but further tightens the constraint on $\Gamma_{0,\mathrm{nadm}}$. The notation N_{idr} (IDM) indicates that the IDR in the model constrained here is interacting with the DM, unlike that in Fig. 34.

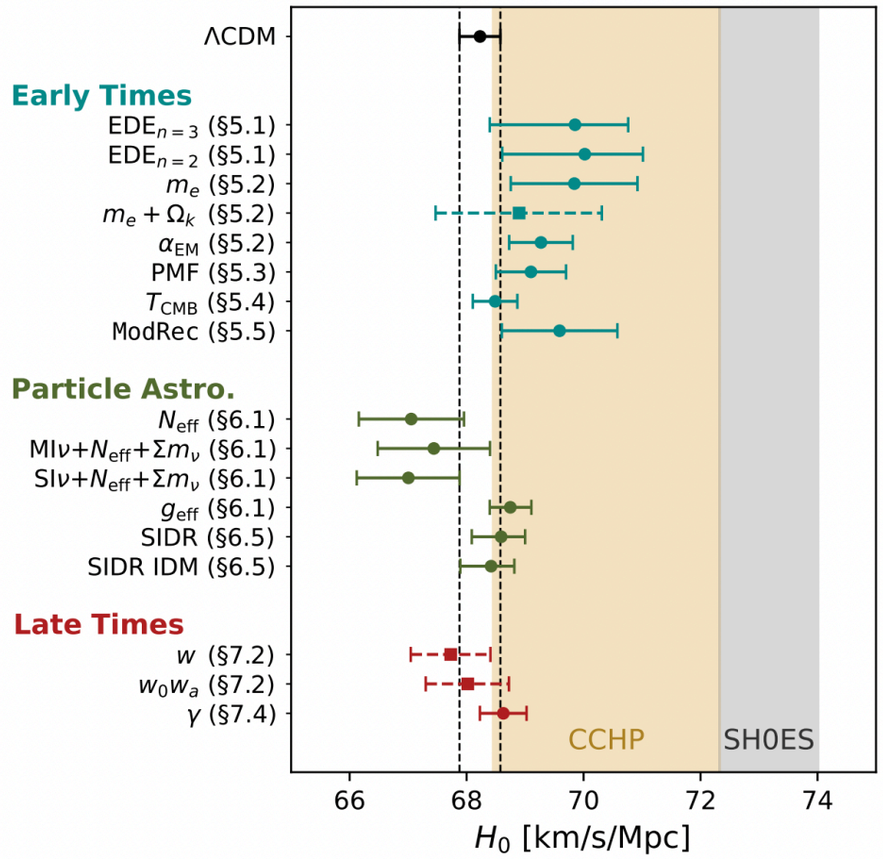

How does model change H0

Self-interacting dark radiation

A wide range of dark radiation (DR) models have been constructed, beyond the simple free-streaming case parameterized by $N_{\rm eff}$ (e.g., Jeong & Takahashi 2013; Buen-Abad et al. 2015; Cyr-Racine et al. 2016; Lesgourgues et al. 2016; Aloni et al. 2022; Joseph et al. 2023; Buen-Abad et al. 2023; Rubira et al. 2023; Schöneberg et al. 2023; Zhou & Weiner 2024). These models generically involve self-interactions amongst the DR, interactions between the DR and (a subset of) the DM, or combinations thereof, potentially with non-trivial time-dependence (e.g., due to the temperature of the DR-DM sector falling below the mass of a massive mediator particle). As a first step toward investigating these scenarios, we consider a simple model of (strongly) self-interacting DR (SIDR), for example due to a new gauge interaction in the dark sector. At the background level, this model is identical to $N_{\rm eff}$, with a free parameter $N_{\rm idr} \geq 0$ describing the number of additional relativistic species (and hence the additional DR energy density). However, the SIDR and free-streaming DR models differ at the perturbative level: the SIDR forms a perfect relativistic fluid with $w = 1/3 = c_s^2$, with interactions sufficiently strong that no anisotropic stress (or higher-order Boltzmann moments) can be supported. Thus, the perturbative dynamics are characterized fully by the continuity and Euler equations. Unlike free-streaming DR, SIDR can cluster on small scales, thus reducing the impact of Silk damping on the high-ℓ power spectra (at fixed DR energy density). In addition, SIDR generates a smaller phase shift in the power spectra. Thus, CMB fits to the SIDR model can accommodate larger amounts of DR than the free-streaming DR model, which can thus allow higher values of H_0 (e.g., Aloni et al. 2022; Schöneberg et al. 2022; Allali et al. 2024).

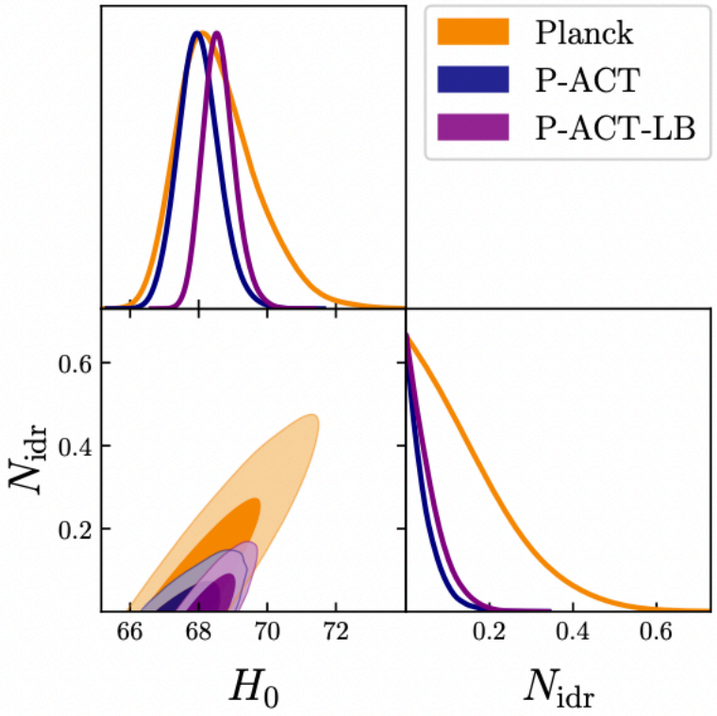

Figure 34. Constraints on the number of strongly self-interacting dark relativistic species, $N_{\rm idr}$. The addition of ACT DR6 spectra improves the constraint from *Planck* by more than a factor of three (navy versus orange) and notably disfavors values of H_0 above 70 km/s/Mpc that are allowed by *Planck* alone. Inclusion of CMB lensing and DESI BAO data (purple) slightly weakens the SIDR upper limit due to small shifts in the best-fit model parameters, but nevertheless further tightens the H_0 posterior. These are the tightest bounds on SIDR obtained to date.